S.I.C.S.
School of Industrial Complex Systems
Università Roma Tre
Department of Industrial Engineering

CGSI
Center for colloid and surface science
Department of Chemistry
University of Florence

PH.D. THESIS

Development of a new methodology for Flame Spraying of colloidal suspension process for nanostructured coating production

SUPERVISOR
Prof. Edoardo Bemporad

CANDIDATE
Martina Dinelli

TUTOR
Prof. Piero Baglioni

DOCTORATE COORDINATOR
Prof. Fabio Carassiti

TABLE OF CONTENTS

Introduction

During last years surface treatments become an interesting research subject to assist the industrial application changes. Starting from traditional electroplating, several alternative processes were developed because of the environmental problems strongly connected with this class of process but also because of the innovative performances. The most sophisticated and demanding approaches are required for application in high technology such as advanced microelectronic device fabrication, but several examples could be set regarding other fields. Some of these processes and techniques have been studied for a long time and several researches are going on in this field.

The results presented in this work are referred to nanostructured coatings from a Flame Spraying of colloidal suspensions, patented by CSGI, Center for Colloid and Surface Science of Chemical Department of University of Florence.

It is a new way to prepare thin films of nanoparticles. The most interesting aspect is the possibility to spray a nanoparticles suspension instead of the powders, avoiding the nanoparticle agglomerations with the related handling and processing critical situations, with consequences on the coating structure.

Studies were directed to develop the equipment to find the limiting application conditions. The goal was to extend the applications field of this deposition technique. Thus the work was directed to develop the process thanks to changes in the experimental equipment and to analyze different substrate-coating combinations, to explore how many unexpected possibilities can be

realized. Since this research is connected to possible future industrial applications, the combinations that better emphasizes the peculiarity of the obtainable sprayed material were more deeply analyzed.

The staring point is the consideration of two key characteristics of the equipment:

- the possibility of very small film thickness
- the high purity of the deposited materials

The consequence of these features was the choice of depositing nanoparticles with particular properties that needs to be very small quantities. Also the choice of the substrates can be relevant to obtain special product. An example of a possible application is TiO_2 deposited onto glass for producing antifogging and self-cleaning glasses.

The present work want to be of assistance to develop the possible industrial applications for future productions with the extension of the scenario of choices: in this broad field of different options became important giving a direction to these choices to take advantage of the characteristics of this technique, underlining application areas where this technique is better performing than others.

The thesis is organized as follows. First chapters concern the deposition process description. Also a brief description of the most important techniques to produce nanostructured coating is added in chapter one to better understand the differences with the process of interest used, Flame spraying of colloidal suspension, deeply described in the third chapters. Some parts were added in chapter two to explain the complete functions of the system, patented by CSGI, Center for Colloid and Surface Science of Chemical Department of University of Florence. Next chapters are focused to the characterization of the nanostructured materials obtained during experimentations. A differentiation between mechanical properties and specific properties of the sprayed thin films is underlined by distinguishing in two different chapters (chapter 4 and chapter 5). It helps to underline the peculiarities of the nanostructured materials obtainable from flame spraying of colloidal suspension.

Chapter 1

Nanostructured materials

Nanostructured materials, especially coatings and thin films, have mechanical, optic and magnetic exclusive properties: this is the reason of their great importance in the industrial area.

Nowadays few techniques allow realizing thin film. For example, nanostructured coating can be obtained by CVD (Chemical Vapour Deposition) but this method is very slow and expensive so its applications are limited to extremely exclusive products, with a high value to justify their fabrication costs. Thermal Spraying, with Plasma Spraying and other related methods are able to produce coating with reasonable costs; the limit of these techniques is connected with the dimension of the particles used, usually in the range of some micrometers: obviously the resulting films cannot be considered nanosized.

Thin film deposition is useful in the manufacture of optics (for reflective or anti-reflective coatings, for instance), electronics (layers of insulators, semiconductors, and conductors form integrated circuits), packaging (i.e., aluminium-coated PET film). Similar processes are sometimes used where thickness is not important: this is the field of photocatalytic or antibacterial activities, discussed in the chapter 5, concerning with TiO_2 or Ag thin films.

Another area recently object of interesting study is connected with the change in the surface roughness of the substrate with the controlled deposition of thin

films; interface phenomena like wetting behaviour are enhanced with suitable consequences (see Appendix A).

1.1 Introduction of Nanotechnologies

Prediction about the promise of nanotechnology can be traced back to Richard Feynmann's classic 1959 talk[1], where he stated "*The principles of physics, as far as I can see, do not speak against the possibility of maneuvering things atom by atom*". Feynman proceeded to describe building with atomic precision, and outlined a pathway involving a series of increasingly smaller machines.

Nanotechnology arise from these complex system concepts, starting from nanosized systems that are too large to be considered molecules but not large enough to be described by macroscopic world rules.

In 1972, Phillip W. Anderson explained the concept of *emergent properties* in the article "More is different"[2]: the sum of the properties of single parts of a system is different from the properties of the sum of the same parts against the reductionism theory and superposition principle based on reducing every complex system to a set of simpler components.

Nanoscale allows taking in evidence characteristics and properties impossible to observe with traditional materials. It is well known how interface properties are dramatically different from the ones of each phase alone. For example, considering some water in contact with air, the molecules located at the interface are settled to minimize the surface free energy, while the inside molecules move randomly with a completely different behaviour. This is a phenomenon that happens between the phases of several different materials, but usually it is not observable because of the low surface energy at the interface. Of course interface phenomena are deeply highlighted in nanostructured coating since those are composed by nanosized particles with the consequently strong increment of the ratio between surface and volume. It is understandable the innovation connected to these coatings: it is possible not only planning functional

characteristics for special applications, but also overcoming the limits of the traditional materials.

In parallel with the enthalpic and entropic interface effects, there are some properties distinguishing nanomaterials connected with the significant fraction of material governed by atomic scale forces. We are talking about photovoltaic effects, characteristic non linear optics, phenomena connected with the semiconductor nature of these materials, like the "electron-hole formation" with a strong importance in several application fields.

1.2 Nanoparticle deposition techniques

There is a really wide range of deposition techniques, differentiable according with the results to obtain and with the process characteristics.

Depending on the deposition techniques, the resulting nanostructured materials will be characterized by different properties and their performances can be very dissimilar.

A rough classification regards the resulting coating thickness: so it is usually distinguished between thin film and thick film deposition techniques.

While thick film are layers ranging from some micrometers to millimetres mostly applied against corrosion and wear phenomena, thin films are thin material layers ranging from fractions of a nanometre to several micrometers in thickness. The results discussed in the present work are focused on the second subject.
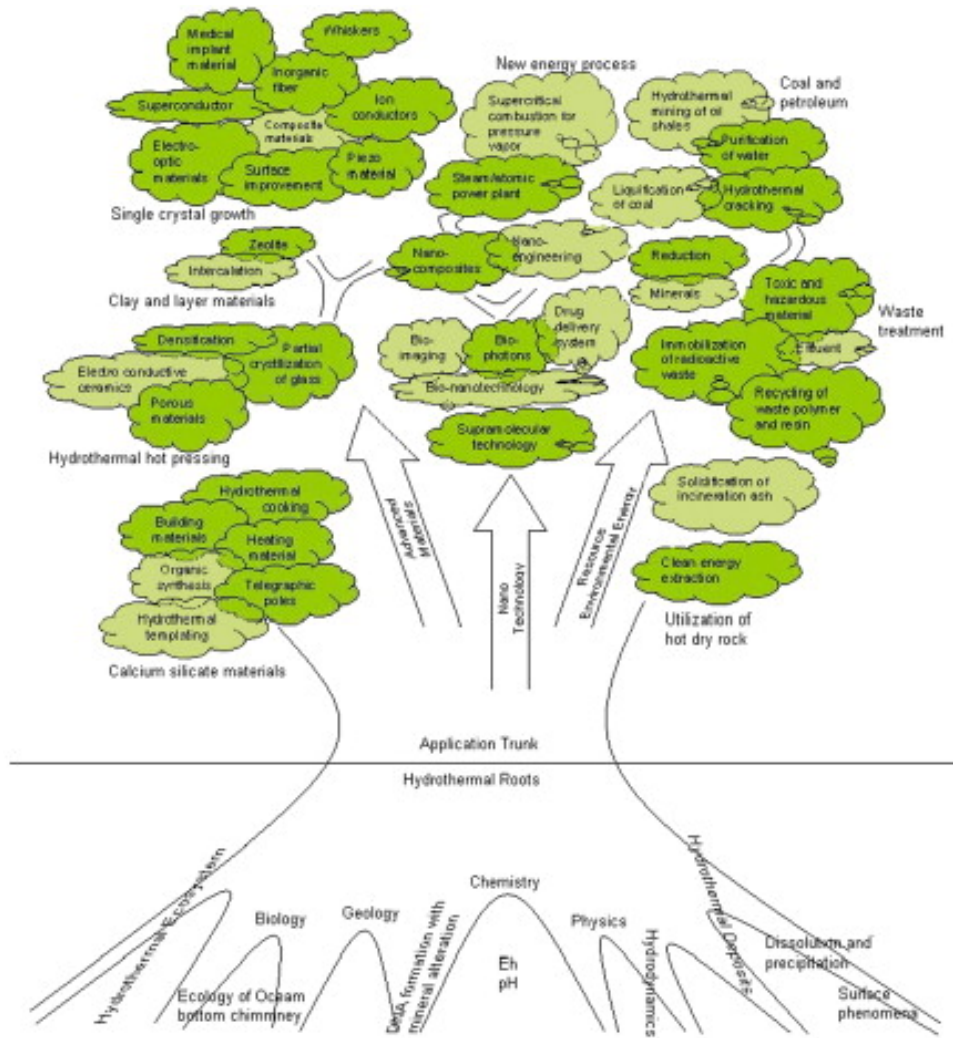
Medical implant material

Whiskers

Inorganic fiber

New energy process

Coal and petroleum

Superconductor

Ion conductors

Supercritical combustion for pressure vapor

Hydrothermal mining of oil shales

Composite materials

Purification of water

Electro-optic materials

Piezo material

Steam/atomic power plant

Liquification of coal

Hydrothermal cracking

Surface improvement

Single crystal growth

Zeolite

Nano-composites

Nano-engineering

Reduction

Intercalation

Minerals

Toxic and hazardous material

Clay and layer materials

Waste treatment

Densification

Partial crystillization of glass

Drug delivery system

Bio-imaging

Bio-photons

Immobilization of radioactive waste

Effluent

Electro conductive ceramics

Porous materials

Bio-nanotechnology

Recycling of waste polymer and resin

Hydrothermal hot pressing

Supramolecular technology

Hydrothermal cooking

Solidification of incineration ash

Building materials

Heating material

Organic synthesis

Telegraphic poles

Clean energy extraction

Hydrothermal templating

Calcium silicate materials

Advanced materials

Nano Technology

Resource Environmental Energy

Utilization of hot dry rock

Application Trunk

Hydrothermal Roots

Hydrothermal Ecosystem

Biology

Geology

Chemistry

Physics

Hydrothermal Deposits

Dissolution and precipitation

Ecology of Ocean bottom chimney

Delta formation with mineral alteration

Eh pH

Hydrodynamics

Surface phenomena

Fig. 1.1 Nanoparticle deposition techniques

Table 1.1   Characteristics of deposition processes and of resulting materials

Technique	Film characteristics		Process features	
	Microstructure	Deposition rate or thickness	Cost	Characteristics and limitations
Vapor phase				
Thermal spray technologies		$100–500 \ \mu m \ h^{-1}$		High deposition rates, various compositions possible, thick and porous coatings, high temperatures necessary
EVD	Columnar structures	$3–50 \ \mu m \ h^{-1}$	Expensive equipment and processing costs	High reaction temperatures necessary, corrosive gases
CVD	Columnar structures	$1–10 \ \mu m \ h^{-1}$	Expensive equipment	Various precursor materials possible, high reaction temperatures necessary, corrosive gases
PVD (RF and magnetron sputtering)	Columnar structures	$0.25–2.5 \ \mu m \ h^{-1}$	Expensive equipment	Tailor-made films, dense and crack-free films, low deposition temperatures, multipurpose technique, relatively small deposition rate
Laser ablation			Expensive equipment (laser)	Intermediate deposition temperatures, difficult upscaling, time-sharing of laser, relatively small deposition rate
Spray pyrolysis	Amorphous to polycrystalline	$5–60 \ \mu m \ h^{-1}$	Economical	Robust technology, upsealing possible, easy control of parameters, corrosive salts, post-thermal treatment usually necessary
Liquid phase				
Sol-gel, Liquid precursor route	Polycrystalline	$0.5–1 \ \mu m$ for each coating	Economical	Various precursors possible, very thin films, low temperature sintering, coating and drying/heating processes have to be repeated 5–10 times, crack formation during drying, many process parameters
Solid phase				
Tape casting	Polycrystalline slightly textured	$25–200 \ \mu m$		Robust technology, upscaling possible, crack formation
Slip casting and slurry coating	Polycrystalline	$25–200 \ \mu m$	Economical	Robust technology, crack formation, slow
Tape calendering	Polycrystalline	$5–200 \ \mu m$		Upscaling possible, co-calendering possible
EPD	Polycrystalline	$1–200 \ \mu m$		Short formation time, little restriction to shape of substrate, suitable for mass production, high deposition rates, inhomogeneous thickness
Transfer printing	Polycrystalline	$5–100 \ \mu m$	Economical	Robust technology, rough substrate surfaces possible, adhesion on smooth substrates difficult
Screen printing	Polycrystalline	$10–100 \ \mu m$	Economical	Robust technology, upscaling possible, crack formation

Basically, thin-film deposition technologies are either purely physical, such as evaporative methods, or purely chemical, such as gas- and liquid-phase chemical processes. A considerable number of processes that are based on glow discharges and reactive sputtering combine both physical and chemical reactions; these overlapping processes can be categorized as physical-chemical methods.
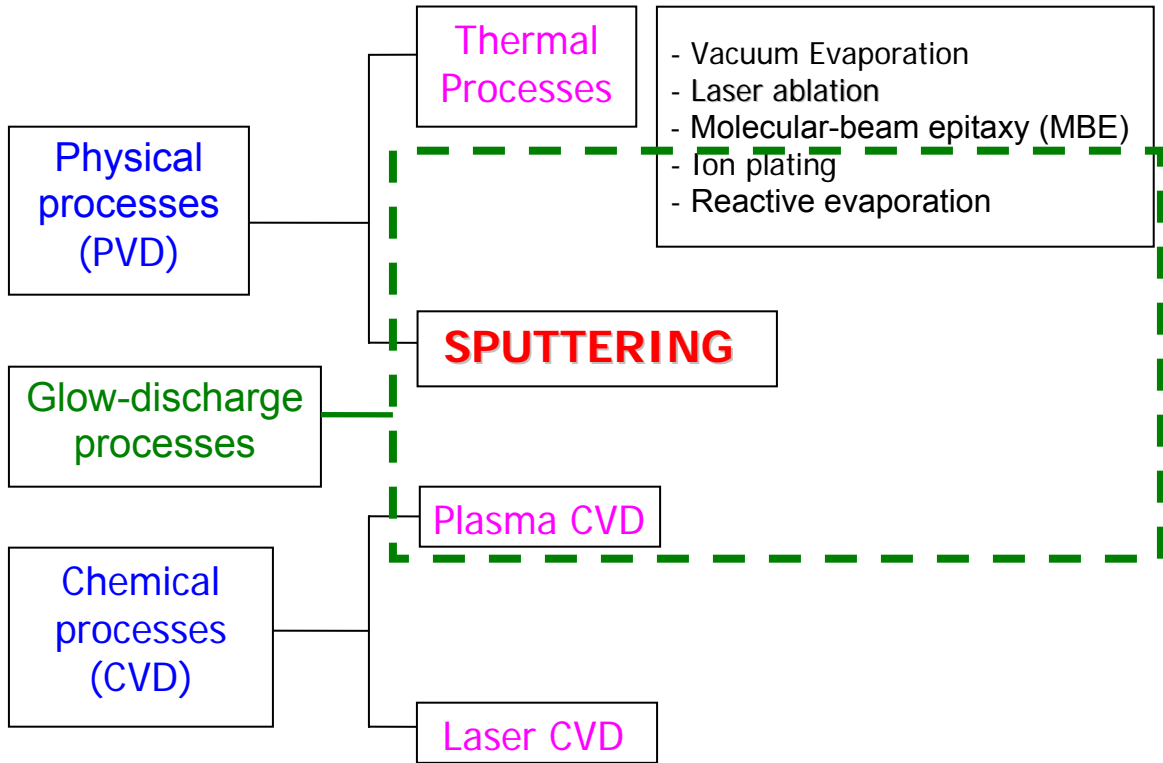
Fig. 1.2   Classification of thin film processes

A classification scheme is presented in Table 1.2 where we have grouped thin-film deposition technologies according to evaporative glow discharge, gas-phase chemical, and liquid-phase chemical processes.

Table 1.2   Classification of Thin-Film Deposition Technologies[3]

EVAPORATIVE METHODS
• Vacuum Evaporation
Conventional vacuum evaporation Molecular-beam epitaxy (MBE)
Electron-beam evaporation Reactive evaporation

GLOW-DISCHARGE PROCESSES
• Sputtering • Plasma Processes
Diode sputtering Plasma-enhanced CVD
Reactive sputtering Plasma oxidation
Bias sputtering (ion plating) Plasma anodization
Magnetron sputtering Plasma polymerization
Ion beam deposition Plasma nitridation
Ion beam sputter deposition Plasma reduction
Reactive ion plating Microwave ECR plasma CVD
Cluster beam deposition (CBD) Cathodic arc deposition

GAS-PHASE CHEMICAL PROCESSES
• Chemical Vapor Deposition (CVD) • Thermal Forming Processes
CVD epitaxy Thermal oxidation
Atmospheric-pressure CVD (APCVD) Thermal nitridation
Low-pressure CVD (LPCVD) Thermal polymerization
Metalorgainc CVD (MOCVD)
Photo-enhanced CVD (PHCVD)
Laser-induced CVD (PCVD)
Electron-enhanced CVD Ion implantation

LIQUID-PHASE CHEMICAL TECHNIQUES
• Electro Processes • Mechanical Techniques
Electroplating Spary pyrolysis
Electroless plating Spray-on techniques
Electrolytic anodization Spin-on techniques
Chemical reduction plating
Chemical displacement plating
Electrophoretic deposition Liquid phase epitaxy

1.3   Thin film deposition technologies

Thin-film deposition is any technique for depositing a thin film of material onto a substrate or onto previously deposited layers. "Thin" is a relative term, but most deposition techniques allow layer thickness to be controlled within a few tens of nanometers, and some (molecular beam epitaxy) allow single layers of atoms to be deposited at a time.

Deposition techniques fall into two broad categories, depending on whether the process is primarily chemical or physical.

Electronic semiconductor devices and optical coatings are the main applications benefiting from thin film construction. Some work is being done with ferromagnetic thin films as well for use as computer memory.

Ceramic thin films are also in wide use. The relatively high hardness and inertness of ceramic materials make this type of thin coating of interest for protection of substrate materials against corrosion, oxidation and wear. In particular, the use of such coatings on cutting tools may extend the life of these items by several orders of magnitude.

Thin-film technologies are also being developed as a means of substantially reducing the cost of photovoltaic (PV) systems. The rationale for this is that thin-film modules are expected to be cheaper to manufacture owing to their reduced material costs, energy costs, handling costs and capital costs. However, thin films have had to be developed using new semiconductor materials, including amorphous silicon, copper indium diselenide, cadmium telluride and film crystalline silicon. In all cases, these technologies face major technical and financial hurdles.

The engineering of thin films is complicated by the fact that their physics is in some cases not well understood. In particular, the problem of dewetting may be hard to solve, as there is ongoing debate and research into some processes by which this may occur.

It is out of the goals of the present work be interested in all the deposition thin films techniques so it will be briefly talked about the most common techniques or

the mostly interesting because of comparison with the process analyzed in the present work, flame spraying of colloidal suspension.

1.3.1   Physical Vapor Deposition

Physical deposition uses mechanical or thermodynamic means to produce a thin film of solid. Since most engineering materials are held together by relatively high energies, and chemical reactions are not used to store these energies, commercial physical deposition systems tend to require a low-pressure vapor environment to function properly; most can be classified as Physical vapor deposition or PVD.

The material to be deposited is placed in an energetic, entropic environment, so that particles of material escape its surface. Facing this source is a cooler surface which draws energy from these particles as they arrive, allowing them to form a solid layer. The whole system is kept in a vacuum deposition chamber, to allow the particles to travel as freely as possible. Since particles tend to follow a straight path, films deposited by physical means are commonly *directional*, rather than *conformal*.

Although one of the oldest techniques used for depositing thin films, thermal evaporation or vacuum evaporation[4,5,6] is still widely used in the laboratory and in industry for depositing metal and metal alloys. The following sequential basic steps take place: (*i*) a vapor is generated by boiling or subliming a source material, (*ii*) the vapor is transported from the source to the substrate, and (*iii*) the vapor is condensed to a solid film on the substrate surface. Although deceptively simple in principle, the skilled practitioner must be well versed in vacuum physics, material science, mechanical and electrical engineering, as well as in elements of thermodynamics, kinetic theory of gases, surface mobility, and condensation phenomena. Evaporants cover an extraordinary range of varying chemical reactivity and vapor pressures. This variety leads to a large diversity of source components including resistance-heated filaments, electron beams; crucibles heated by conduction, radiation, or RF-induction; arcs, exploding wires, and lasers. Additional complications include source-container interactions,

requirements for high vacuum, precise substrate motion (to ensure uniformity) and the need for process monitoring and control.

1.3.2   Chemical Vapor Deposition

Chemical vapor deposition (CVD)[7-18], is a materials synthesis process whereby constituents of the vapor phase react chemically near or on a substrate surface to form a solid product. Such other chemical depositions, a fluid precursor undergoes a chemical change at a solid surface, leaving a solid layer. Since the fluid surrounds the solid object, deposition happens on every surface, with little regard to direction; thin films from chemical deposition techniques tend to be *conformal,* rather than *directional*.
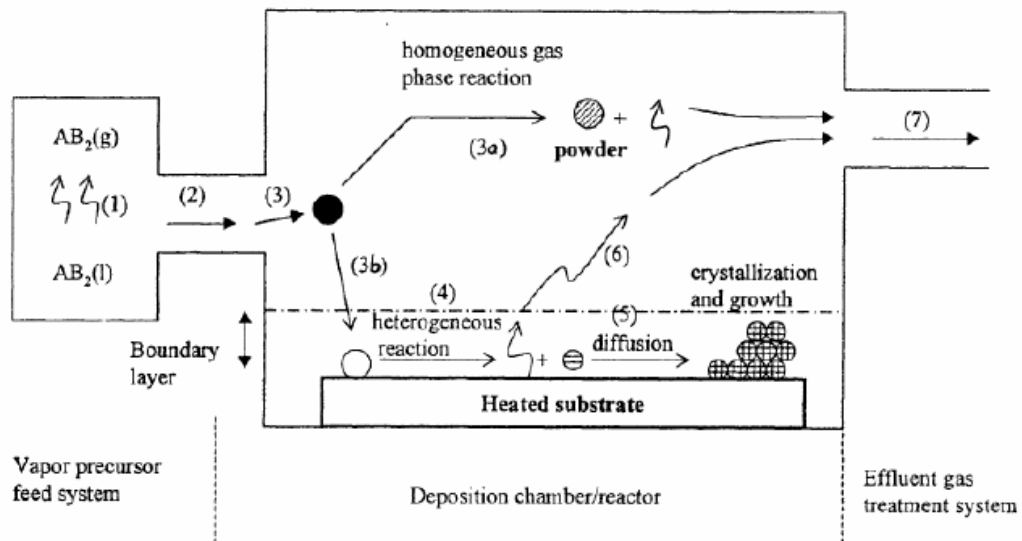
Fig. 1.3 Schematic diagram of CVD process

The deposition technology has become one of the most important means for creating thin films and coatings of a very large variety of materials essential to advanced technology, particularly solid-state electronics where some of the most sophisticated purity and composition requirements must be met. The main feature of CVD is its versatility for synthesizing both simple and complex

compounds with relative ease at generally low temperatures. Both chemical composition and physical structure can be tailored by control of the reaction chemistry and deposition conditions. Fundamental principles of CVD encompass an interdisciplinary range of gas-phase reaction chemistry, thermodynamics, kinetics, transport mechanisms, film growth phenomena, and reactor engineering.

Chemical reaction types basic to CVD include pyrolysis (thermal decomposition), oxidation, reduction, hydrolysis, nitride and carbide formation, synthesis reactions, disproportionation, and chemical transport. A sequence of several reaction types may be involved in more complex situations to create a particular end product. Deposition variables such as temperature, pressure, input concentrations, gas flow rates and reactor geometry and operating principle determine the deposition rate and the properties of the film deposit. Most CVD processes are chosen to be heterogeneous reactions: they take place at the substrate surface rather than in the gas phase. Undesirable homogeneous reactions in the gas phase nucleate particles that may form powdery deposits and lead to particle contamination instead of clean and uniform coatings. The reaction feasibility (other than reaction rate) of a CVD process under specified conditions can be predicted by thermodynamic calculations, provided reliable thermodynamic data (especially the free energy of formation) are available. Kinetics controls the rate of reactions and depends on temperature and factors such as substrate orientation. Considerations relating to heat, mass, and momentum transport phenomena are especially important in designing CVD reactors of maximum efficiency. Since important physical properties of a given film material are critically influenced by the structure (such as crystallinity), control of the factors governing the nucleation and structure of a growing film is necessary.

Thin-film materials that can be prepared by CVD cover a tremendous range of elements and compounds. Inorganic, organometallic, and organic reactants are used as starting materials. Gases are preferred because they can be readily metered and distributed to the reactor. Liquid and solid reactants must be

vaporized without decomposition at suitable temperatures and transported with a carrier gas through heated tubes to the reaction chamber, which complicates processing, especially in the case of reduced-pressure systems. Materials deposited at low temperatures (e.g., below 600°C for silicon) are generally amorphous. Higher temperatures tend to lead to polycrystalline phases. Very high temperatures (typically 900°C to 1100°C in the case of silicon) are necessary for growing single crystal films. These films are oriented according to the structure of the substrate crystal; this phenomenon, known as *epitaxy*, is of crucial practical importance in solid-state device technology.

CVD has become an important process technology in several industrial fields. As noted, applications in solid-state microelectronics are of prime importance. Thin CVD films of insulators, dielectrics (oxides, silicates, nitrides), elemental and compound semiconductors (silicon, gallium arsenide, etc.), and conductors (tungsten, molybdenum, aluminium, refractory metal silicides) are extensively utilized in the fabrication of solid-state devices. Hard and wear-resistant coatings of materials such as boron, diamond-like carbon, borides, carbides and nitrides have found important applications in tool technology. Corrosion resistant coatings, especially oxides and nitrides, are used for metal protection in metallurgical applications. Numerous other types of materials, including vitreous graphite and refractory metals, have been deposited mainly in bulk form or as thick coatings. Many of these CVD reactions have long been used for coating of substrates at reduced pressure, often at high temperatures.

Reactors. The reactor system (comprising the reaction chamber and all associated equipment) for carrying out CVD processes must provide several basic functions common to all types of systems. It must allow transport of the reactant and diluent gases to the reaction site provide activation energy to the reactants (heat, radiation, plasma), maintain a specific system pressure and temperature, allow the chemical processes for film deposition to proceed optimally, and remove the by-product gases and vapors. These functions must be implemented with adequate control, maximal effectiveness, and complete safety.

The most sophisticated CVD reactors are those used for the deposition of electronic materials. Low-temperature (below 600°C) production reactors for normal- or atmospheric-pressure CVD (APCVD) include rotary vertical-flow reactors and continuous, in-line conveyorized reactors with various gas distribution features. They are used primarily for depositing oxides and binary and ternary silicate glass coatings for solid-state devices. Reactors for mid-temperature (600°C to 900°C) and high-temperature (900°C to 1300°C) operation are either hot-wall or cold-wall types constructed of fused quartz. Hot-wall reactors, usually tubular in shape, are used for exothermic processes where the high wall temperature avoids deposition on the reactor walls. They have been used for synthesizing complex layer structures of compound semiconductors for microelectronic devices. Cold-wall reactors, usually bell-jar shaped, are used for endothermic processes, such as deposition of silicon from the halides or the hydrides. Heating is accomplished by RF induction or by high-intensity radiation lamps. Substrate susceptors of silicon carbide-coated graphite slabs are used for RF-heated systems.

Reactors operating at low pressure (typically 0.1–10 torr) for low pressure CVD (LPCVD) in the low-, mid-, or high-temperature ranges are resistance-eated hot-wall reactors of tubular, bell-jar, or close-spaced design. In the horizontal tubular design, the substrate slices (silicon device wafers) stand up in a carrier sled and gas flow is horizontal. The reduced operating pressure increases the mean free path of the reactant molecules, which allows a closely spaced wafer stacking. The very high packing density achieved (typically 100 to 200 wafers per tube) allows a greatly increased throughput, hence substantially lower product cost. In the vertical bell-jar design, the gas is distributed over the stand-up wafers, hence there is much less gas depletion and generation of few particles, but the wafer load is smaller (50 to 100 wafers per chamber). Finally, the close spaced design developed most recently processes each wafer in its own separate, closed space chamber with the gas flowing across the wafer surface to achieve maximal uniformity. In LPCVD, no carrier gases are required, particle contamination is reduced and film uniformity and conformality are better

than in conventional APCVD reactor systems. It is for these reasons that low-pressure

CVD is widely used in the highly cost-competitive semiconductor industry for depositing films of insulators, amorphous and polycrystalline silicon, refractory metals, and silicides. Epitaxial growth of silicon at reduced pressure minimizes autodoping (contamination of the substrate by its dopant), a major problem in atmospheric-pressure epitaxy.

Vapor-Phase Epitaxy. Vapor-phase epitaxy (VPE)[9,10,14–18] and metal-organic chemical vapor deposition (MOCVD)[9,10,14–18] are used for growing epitaxial films of compound semiconductors in the fabrication of optoelectronic devices. Composite layers of accurately controlled thickness and dopant profile are required to produce structures of optimal design for device fabrication.

Photo-Enhanced Chemical Vapor Deposition (PHCVD). PHCVD[19–21] is based on activation of the reactants in the gas or vapour phase by electromagnetic radiation, usually short-wave ultraviolet radiation. Selective absorption of photonic energy by the reactant molecules or atoms initiates the process by forming reactive free-radical species that then interact to form a desired film product. Mercury vapor is usually added to the reactant gas mixture as a photosensitizer that can be activated with the radiation from a high-intensity quartz mercury resonance lamp (253.7 nm wavelength). The excited mercury atoms transfer their energy kinetically by collision with the reactants to generate free radicals. The advantages of this versatile and very promising CVD process is the low temperature (typically 150°C) needed to form films such as SiO_2 and Si_3N_4, and the greatly minimized radiation damage (compared to PECVD). The limitations at present are the unavailability of effective production equipment and the need (in most cases) for photoactivation with mercury to achieve acceptable rates of film deposition.

Laser-Induced Chemical Vapor Deposition (LCVD). LCVD[22–24] utilizes a laser beam for highly localized heating of the substrate that then induces film deposition by CVD surface reactions. Another mode of utilizing laser (or electron radiation) is to activate gaseous reactant atoms or molecules by their absorption

of the specific wavelength of the photonic energy supplied. The resulting chemical gas phase reactions are very specific, leading to highly pure film deposits. On the other hand, the activation matching of the spectral properties with the reactant species limits the choice of reactions and hence the film deposits that can be obtained. LCVD is still in its early development stages but promises many interesting and useful applications in the future.

Ion Implantation. Recently, ion implantation[25−27] has been used to form silicon-on-insulator structures by implanting large doses of atomic or molecular oxygen ions in single-crystal silicon substrates to produce a buried oxide layer with sharp interfaces after annealing.[63] Simultaneous high-dose implantation of low energy oxygen and nitrogen ions into silicon yields very thin films of silicon oxynitride, whereas low-energy implantation of nitrogen or ammonia into silicon yields a low-density silicon nitride layer.[28]

1.3.3 Other deposition processes

Some methods fall outside these two categories, relying on a mixture of chemical and physical means.

1.3.3.1 Glow-Discharge Technologies

: The electrode and gas-phase phenomena in various kinds of glow discharges (especially RF discharges) represent a rich source of processes used to deposit and etch thin films. Creative exploitation of these phenomena has resulted in the development of many useful processes for film deposition

Sputtering

The most basic and well-known of these processes is sputtering[29−37], the ejection of surface atoms from an electrode surface by momentum transfer from bombarding ions to surface atoms. From this definition, sputtering is clearly an etching process, and is, in fact, used as such for surface cleaning and for pattern delineation. Since sputtering produces a vapor of electrode material, it is also

(and more frequently) used as a method of film deposition similar to evaporative deposition.

Sputter deposition has become a generic name for a variety of processes.

Diode Sputtering. Diode sputtering uses a plate of the material to be deposited as the cathode (or RF-powered) electrode (target) in a glow discharge. Material can thus be transported from the target to a substrate to form a film. Films of pure metals or alloys can be deposited when using noble gas discharges (typically Ar) with metal targets.

Reactive Sputtering. Compounds can be synthesized by reactive sputtering, that is, sputtering elemental or alloy targets in reactive gases; alternatively, they can be deposited directly from compound targets. In reactive sputtering, a small amount of some non-noble gas such as oxygen or nitrogen is mixed with the plasma-forming gas. After the material is sputtered from the target, it reacts with this gas, so that the deposited film is a different material, i.e. an oxide or nitride of the target material.

Bias Sputtering. Bias sputtering or ion-plating is a variant of diode sputtering in which the substrates are ion bombarded during deposition and prior to film deposition to clean them. Ion bombardment during film deposition can produce one or more desirable effects, such as resputtering of loosely-bonded film material, low-energy ion implantation, desorption of gases, conformal coverage of contoured surface, or modification of a large number of film properties. The source material need not originate from a sputtering target, but can be an evaporation source, a reactive gas with condensable constituents, or a mixture of reactive gases with condensable constituents and other gases that react with the condensed constituents to form compounds.

It should be noted that all glow discharge processes involve sputtering in one form or another, since it is impossible to sustain a glow discharge without an electrode at which these processes occur. In "electrodeless" discharges, RF power is capacitively coupled through the insulating wall of a tubular reactor. In this case, the inside wall of the tube is the main electrode of the discharge.

However, sputtering can also lead to undesirable artifacts in this and other glow-discharge processes.

Magnetron Sputtering. Another variant in sputtering sources uses magnetic fields transverse to the electric fields at sputtering-target surfaces. This class of processes is known as *magnetron sputtering*[32–34]. Sputtering with a transverse magnetic field produces several important modifications of the basic processes. Target-generated secondary electrons do not bombard substrates because they are trapped in cycloidal trajectories near the target, and thus do not contribute to increased substrate temperature and radiation damage. This allows the use of substrates that are temperature-sensitive (for example, plastic materials) and surface sensitive (for example, metal-oxides-semiconductor devices) with minimal adverse effects. In addition, this class of sputtering sources produces higher deposition rates than conventional sources and lends itself to economic, large-area industrial application. There are cylindrical, conical, and planar magnetron sources, all with particular advantages and disadvantages for specific applications. As with other forms of sputtering, magnetron sources can be used in a reactive sputtering mode. Alternatively, one can forego the low-temperature and low radiation-damage features and utilize magnetron sources as high-rate sources by operating them in a bias-sputtering mode.

Ion-Beam Sputtering. Ion beams, produced in and extracted from glow discharges in a differentially pumped system, are important to scientific investigations of sputtering, and are proving to be useful as practical film-deposition systems for special materials on relatively small substrate areas. There are several advantages of ion-beam sputtering deposition[35]. The target and substrate are situated in a high-vacuum environment rather than in a high-pressure glow discharge. Glow discharge artifacts are thereby avoided, and higher-purity films usually result. Reactive sputtering and bias sputtering with a separate ion gun can be used.

Plasma Processes The fact that some chemical reactions are accelerated at a given temperature in the presence of energetic reactive-ion bombardment is the basis of processes for surface treatments such as plasma oxidation, plasma

nitriding, and plasma carburizing[38−40]. A metal to be oxidized, nitrided or carburized is made the cathode of a glow discharge and is simultaneously heated by radiant or RF induction means. The discharge gas is either O_2, N_2 plus H_2, or CH_4. Very thick (0.1–2 mm) protective coatings on a variety of metals can be produced in this way to render surfaces hard and/or corrosion resistant.

Deposition of Inorganic/Organic Films. Plasma deposition of inorganic films[39,41−49] and plasma polymerization of organic reactants to produce films of organic polymers[50] involve the introduction of a volatile reactant into a glow discharge which is usually generated by an RF force. The reactant gases or vapors are decomposed by the glow discharge mainly at surfaces (substrate, electrodes, walls), leaving the desired reaction product as a thin solid film. Plasma deposition is a combination of a glow-discharge process and low-pressure chemical vapor deposition, and can be classified in either category. Since the plasma assists or enhances the chemical vapor deposition reaction, the process is usually denoted as PACVD or PECVD. The possibilities for producing films of various materials and for tailoring their properties by judicious manipulation of reactant gases or vapors and glow-discharge parameters are very extensive.

Plasma deposition processes are used widely to produce films at lower substrate temperatures and in more energy-efficient fashion than can be produced by other techniques. For example, they are widely used to form secondary-passivation films of plasma silicon nitride on semiconductor devices, and to deposit hydrogenated, amorphous silicon layers for thin-film solar cells.

1.3.3.2 Wet chemical techniques: sol-gel

Sol-gel chemistry is a remarkably versatile approach for fabricating materials. The sol-gel process is a wet-chemical technique for the fabrication of materials (typically a metal oxide) starting either from a chemical solution (sol short for solution) or colloidal particles (sol for nanoscale particle) to produce an integrated network (gel).

Although first discovered in the late 1800s and extensively studied since the early 1930s, a renewed interest[51-52] surfaced in the early 1970s when monolithic inorganic gels were formed at low temperatures and converted to glasses without a high temperature melting process[53].
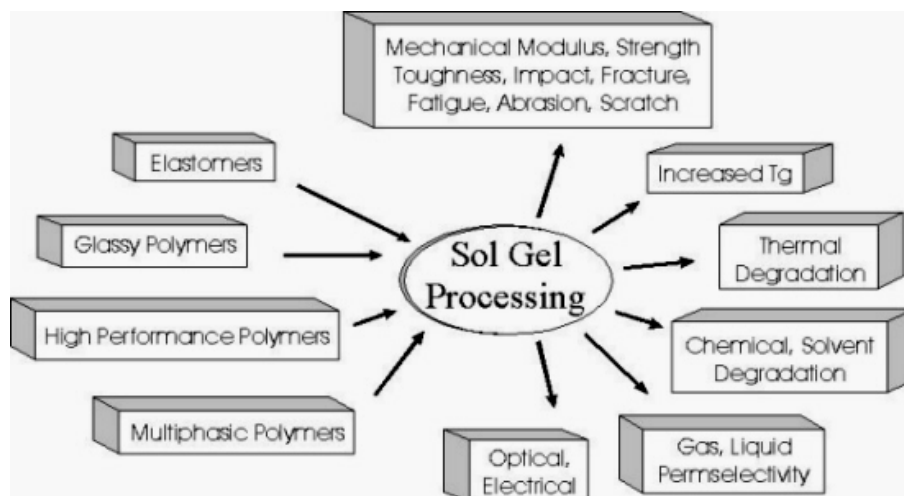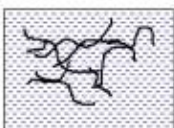

Fig.1.4 Sol-Gel applications

The sol-gel process involves the transition of a system from a liquid "sol" (mostly colloidal) into a solid "gel" phase. The specificity of the sol-gel techniques is that the starting state of the material is a liquid, **sol**ution state, which will during the transformation mutate in a **gel**. Typically, the solution is composed of particles with a size between 1 up to 100 nm, dispersed homogeneously in an aqueous or in a solvent middle.

	Sol	Gel formation	Gel
acid solution			
basic solution			

Sol: Dispersion of metal organical Polymers
(Size 1 - 100 nm)

Fig. 1.5 Gel glass process sequence

During the sol-gel transformation, the nanoparticles will create a three-dimensional network in the solution, which is the precursor of the gel. This technique allows scientists to change the composition and structure of materials on the nanometer (billionth-of-a-meter) scale. In addition, this process can be modified to produce sol-gel materials in different forms, such as powders, films, fibers, and freestanding pieces of material called monoliths. For example, a gel can be dried in a sol-gel process to make aerogels, a special class of ultralow-density materials. This chemistry produces a variety of inorganic networks from silicon or metal alkoxide monomer precursors.
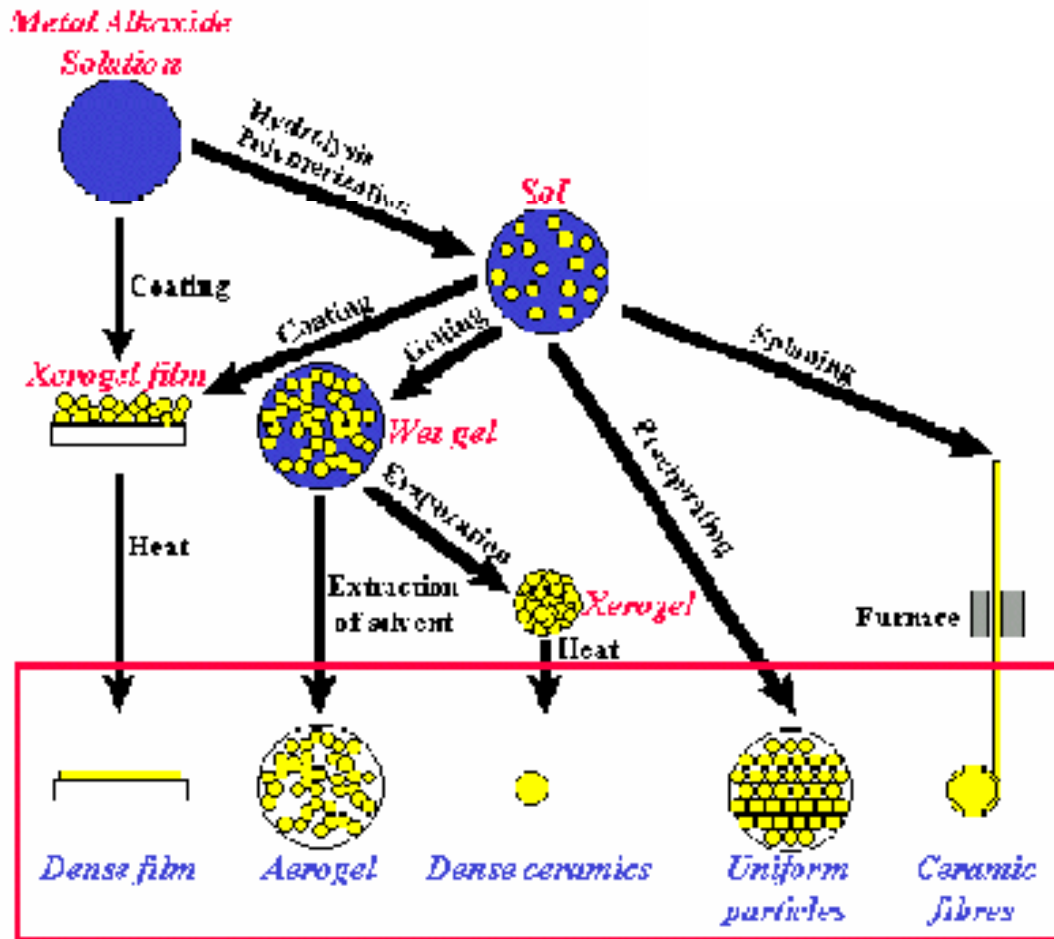
Fig 1.6 Sol-Gel technologies

In the sol-gel process, simple molecular precursors are converted into nanometer-sized particles to form a colloidal suspension, or sol. The colloidal nanoparticles are then linked with one another in a 3D, liquid-filled solid network. The *sol* is made of solid particles of a diameter of few hundred of nm suspended in a liquid phase. Then the particles condense in a new phase (*gel*) in which a solid macromolecule is immersed in a liquid phase (solvent).

This transformation to a gel can be initiated in several ways, but the most convenient approach is to change the pH of the reaction solution. Even the method used to remove liquid from a solid will affect the sol-gel's properties. For example, to preserve a gel's original 3D structure and produce low-density

aerogels, chemists use a technique called supercritical drying. If, instead, the gel is dried slowly in a fluid-evaporation process, the gel's structural network collapses, which creates a high-density material known as a xerogel.
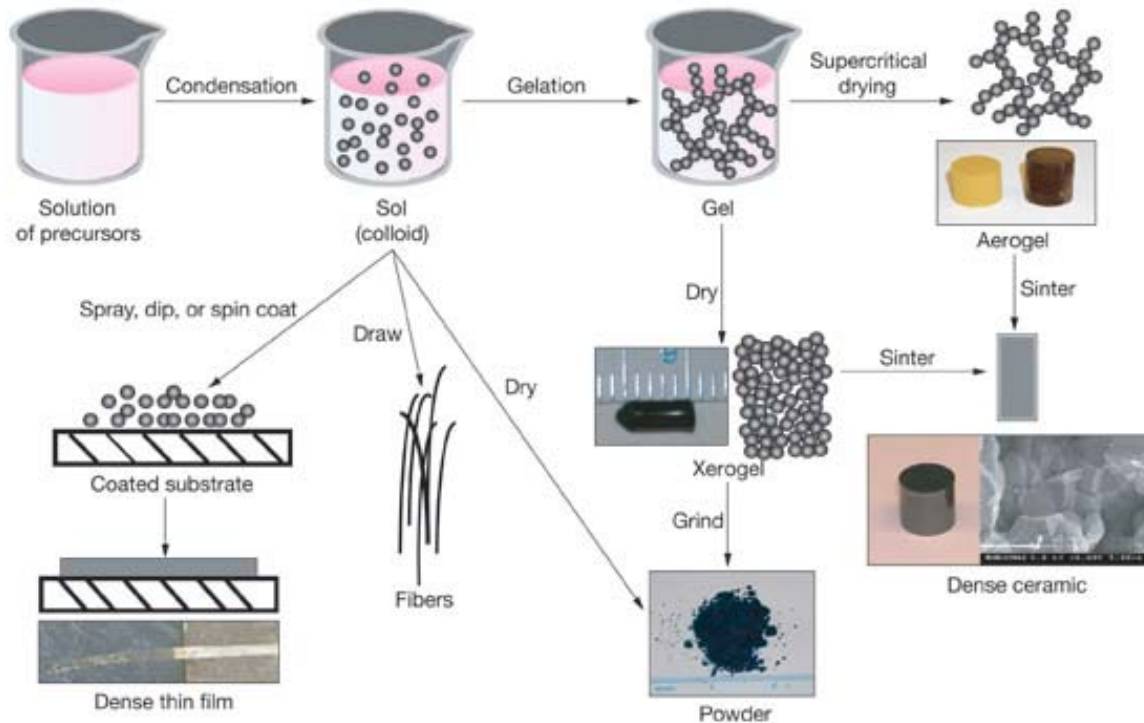
Fig.1.7

In sol-gel chemistry, molecular precursors are converted to nanometer-sized particles, to form a colloidal suspension, or sol. Adding epoxide to the sol produces a gel network. The gel can be processed by various drying methods (shown by the arrows) to develop materials with distinct properties.

The fundamental property of the sol-gel process is that it is possible to generate ceramic material at a temperature close to room temperature. Therefore such a procedure opened the possibility of incorporating soft dopants, such as fluorescent dye molecules and organic cromophores.
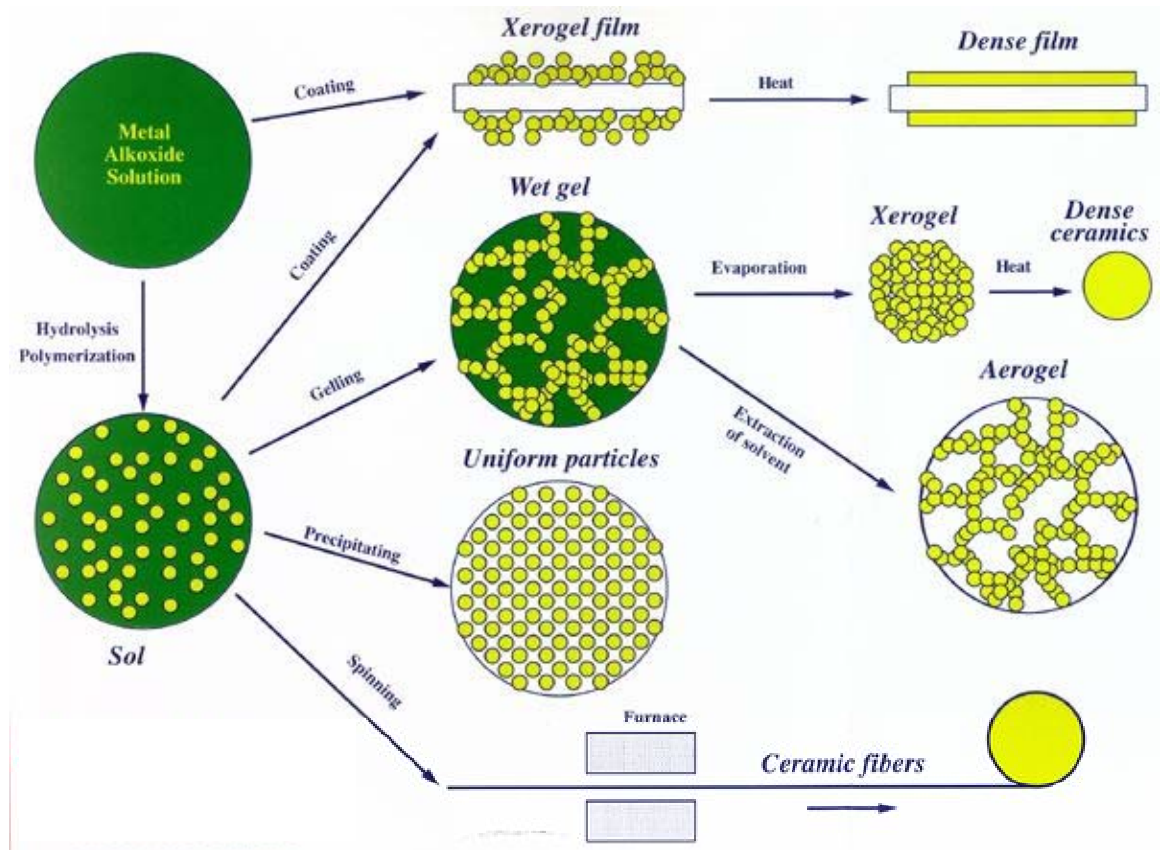
Fig.1.8 Sol-gel technologies and their products

Thin films can be produced on a piece of substrate by spin-coating or dip-coating. The initial liquid state of the solution is leads to the gel state after a short drying. A heat-treatment on free air is following. For temperature bellow 400°C, organic components will be decomposed in CO_2 and in water. The formed film is then amorphous and nanoporous. The crystallographic arrangement will take place at about 500°C. From an amorphous film, it is possible to obtain a crystallographically arranged film, composed of nanocrystals. The chemical composition of the solution, the deposition parameters, those from the heat-treatment (temperature, time, cooling down conditions) will influence the properties of the film.
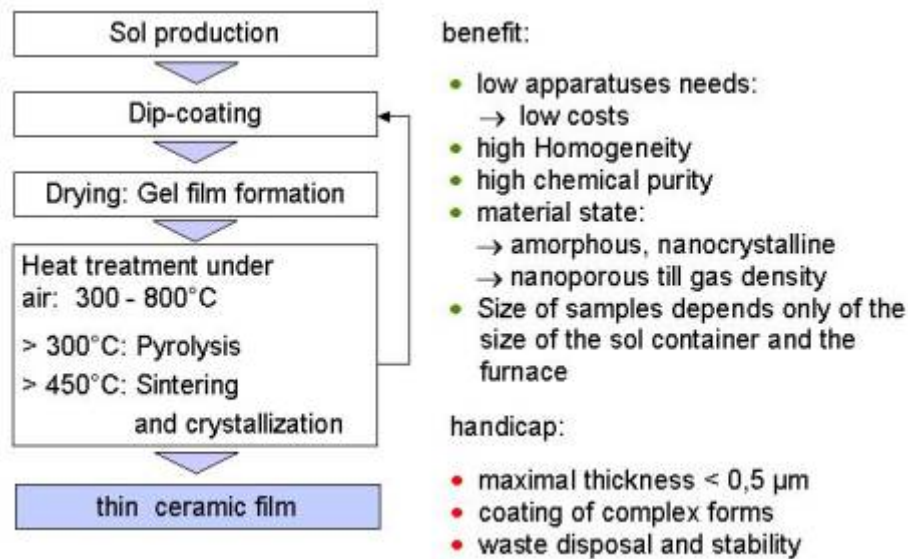
Fig. 1.9   Example of steps for thin ceramic film formation (dip-coating)

Spin coating is perfectly adapted for substrates which present rotation symmetry, as moulding tools for the production of optical components. The solution is versed in a continuous flux on the rotating sample. The solution is then homogeneously dispersed on all the surface of the sample. Spin coating technique allows the production of homogeneous film in term of thickness.
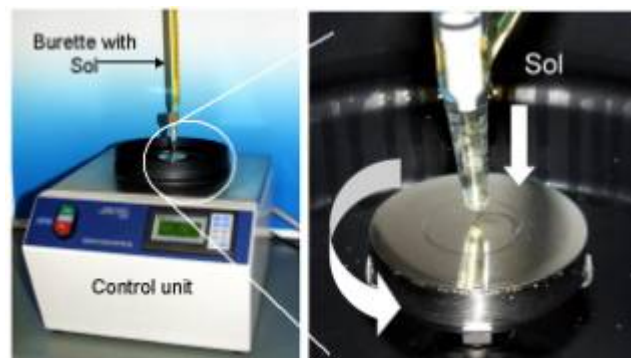

Fig. 1.10   Spin coating

Dip coating is the ideal technique for translation symmetric substrates. The substrate is placed in the solution and is withdrawn with a controlled constant velocity, that the film covers uniformly the immerged surface. This film is left drying for some minutes to allow the sol-gel transition to take place.

Corrosion protection against chlorine attack on Beryllium X-ray windows (L= 200 mm)
Charge: about 60 pieces
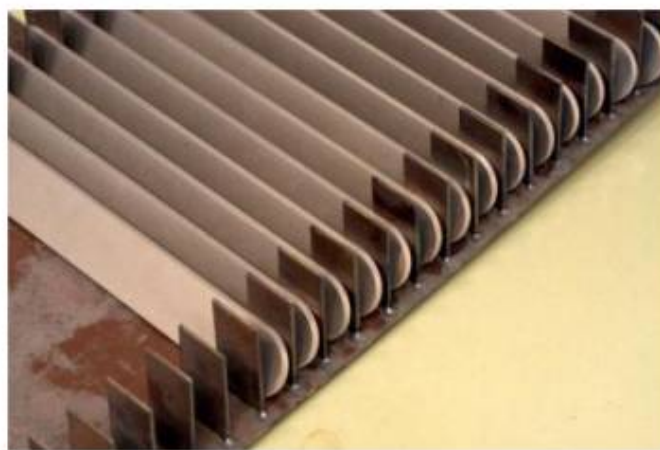
Dip-coating process   Charge for 600°C 2 h

Fig. 1.11   Dip coating process

Many specific applications include optics, protective and porous films, optical coatings, window insulators, dielectric and electronic coatings, high temperature superconductors, reinforcement fibers, fillers, and catalysts[54].

There are some limitations in the using of sol-gel coatings. For example, oxydoceramics films processed by sol-gel which are cracks- and defects free are never thicker than some hundreds of nm. The figure below shows the variation of the weight per area, which allows, through the theoretical density, to calculate the theoretical film thickness. Experimental results showed that the maximal thickness for a crack free film is about 500 nm.
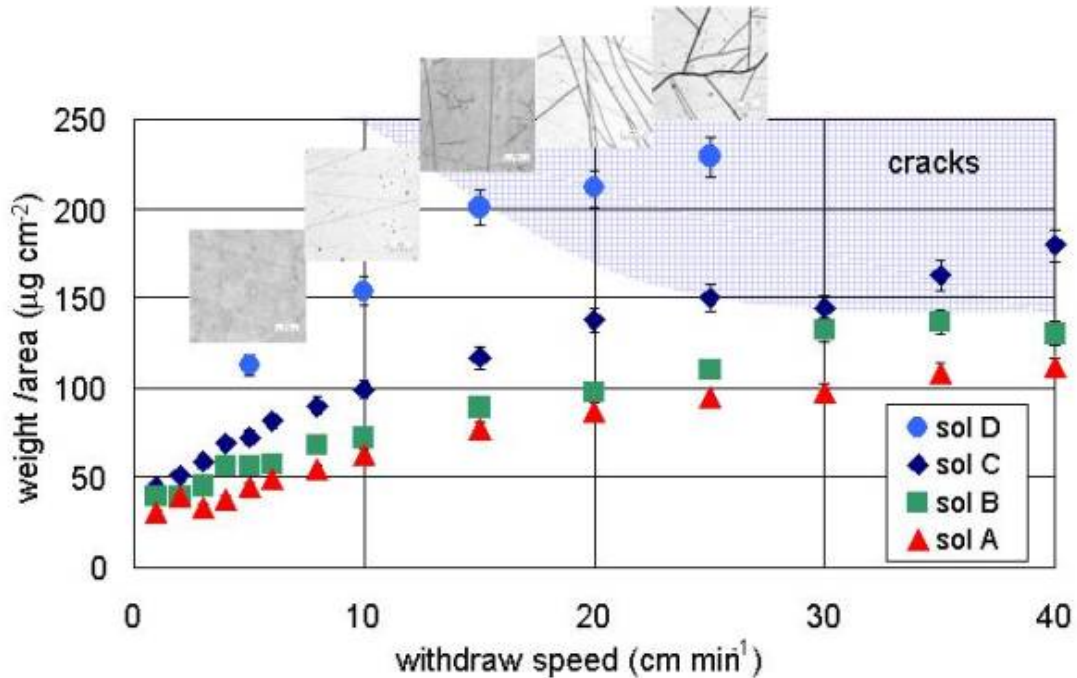
Fig. 1.12

The main reason for the apparition of cracks in the film is the presence of high traction residual stresses. These stresses appear during the expulsion of the solvent, which corresponds to a contraction of the film on a form of a gel. The networking of the polymers chains lead to a reduction of the ductility within the gel which leads to a reduction of the relaxation of traction stresses. If the stresses go higher than a critical value, cracks will appear. Under this border, no cracks will be visible, which proves that the accumulated elastic energy is high enough to stop the formation of cracks.

Thicker oxydoceramic film can be obtained by the accumulation of several layers. For each layer, it's necessary to drive a full process, which leads to a very repetitive and inconvenient process for films thicker than 2 µm. Anyway, the accumulation of defects for each layer leads to a maximal available system including more than 5 layers impossible.

1.4 Thermal spraying

The origins of thermal spraying date back at the beginning of the 20th century. Generally the birth of this technology is associated with the invention of the molten metal spraying by Schoop (Schoop e Guenther, 1917). The development of this process is grown up and today with "Thermal spraying" are identified a broad class of deposition techniques unified by the characteristics of transmitting energy, both kinetics and thermal, to the particles to deposit: all thermal spraying processes rely on the same principle of heating a feed stock, (powder or wire) and accelerating it to a high velocity and then allowing the particles to strike the substrate. The particles will then deform and freeze onto the substrate. The coating is formed when millions of particles are deposited on top of each other.

Originally born for microparticles deposition, this method is a quite low cost process that, relying on several physical and chemical phenomena, presents a high degree of complexity[55]. In addition, agglomeration and bad flooding make this technique generally not suitable for high quality nanostructured material productions.
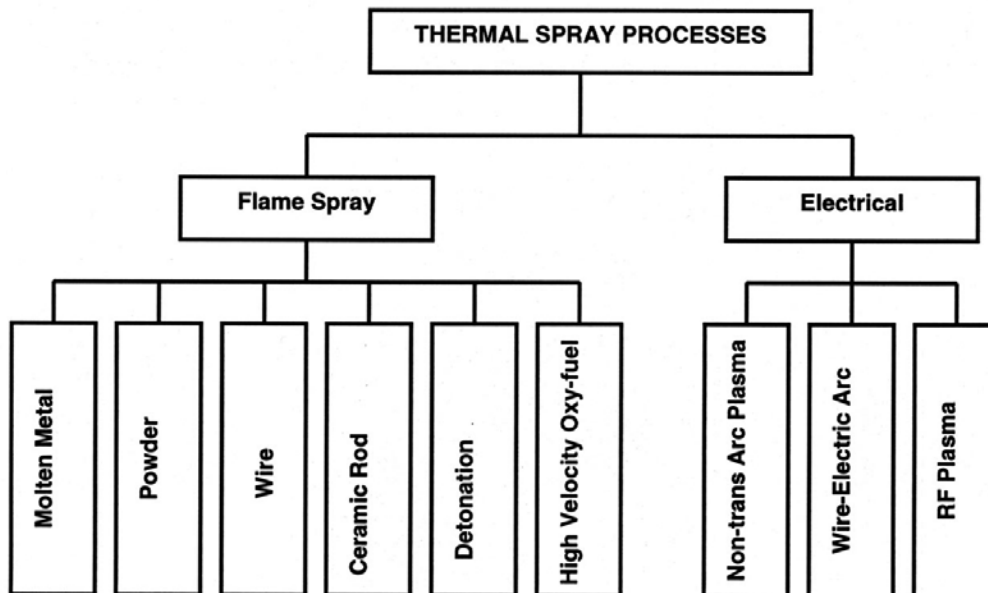

Fig.1.13 Thermal spraying processes

Some common processes are:

- FS (Flame Spraying)
- APS (Atmospheric Plasma Spraying).
- AS (Arc Spraying).
- D-Gun Spraying (Detonation Gun Spraying).
- HVOF (High Velocity Oxy-Fuel Spraying).
- VPS (Vacuum Plasma Spraying).
- CAPS (Controlled Atmosphere Plasma Spraying).

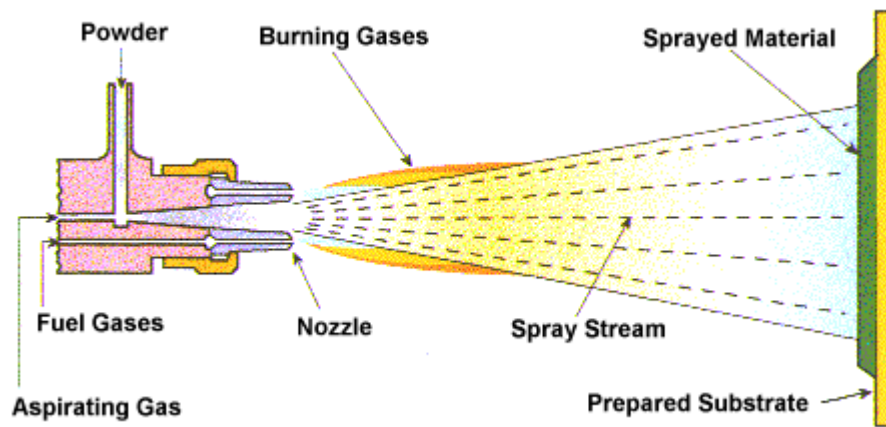Next figures explain some of the listed process.

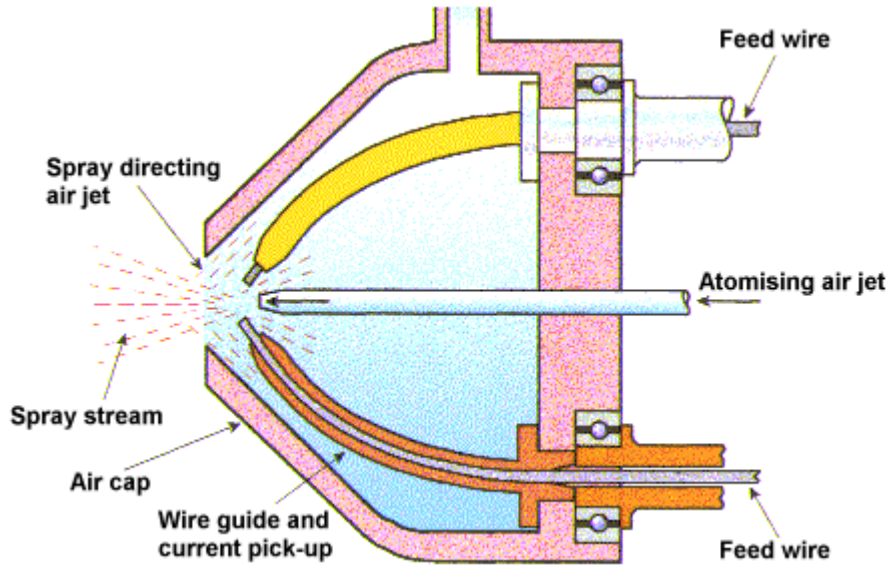**Fig. 1.14**   Powder Flame Spraying Process

Fig. 1.15   Arc Spraying Process
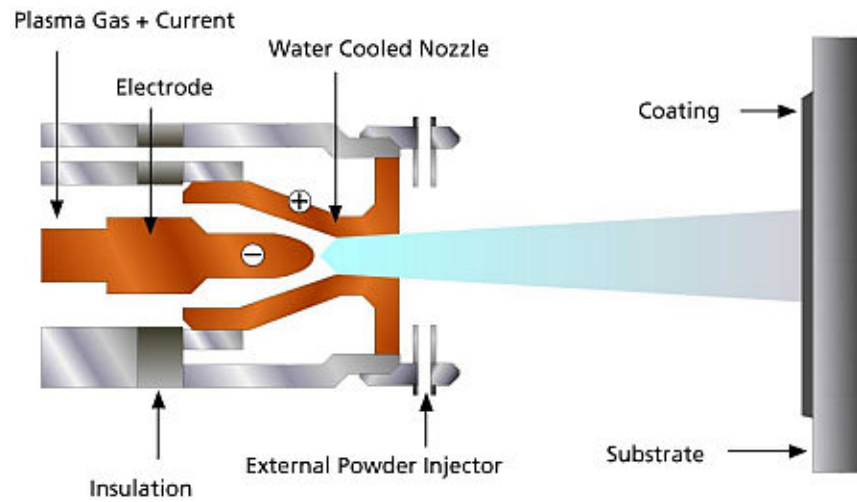
Fig. 1.16   Plasma Spraying Process
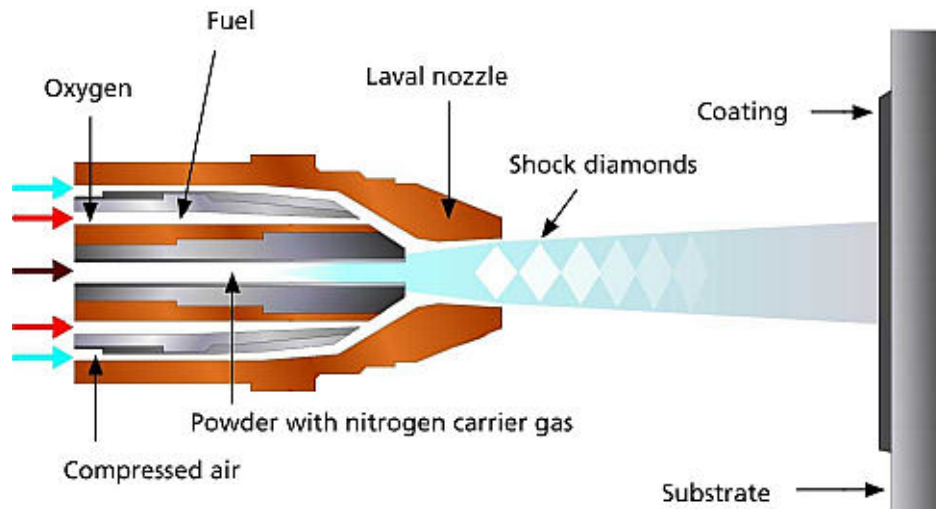
Fig. 1.17   High Velocity Oxy Fuel (HVOF) Spraying Process

A difference between these processes is connected the way the energy is transmitted to the particles. For example, in the Flame spraying process the melted particles are not very accelerated, while in the HVOF process the fraction of the kinetic energy transmitted to the particles is very high. Obviously the performances of the resulting coating are dramatically different: HVOF is one of the techniques that allow a low porous and very hard coating.

<table>
</table>

[A]	[B]
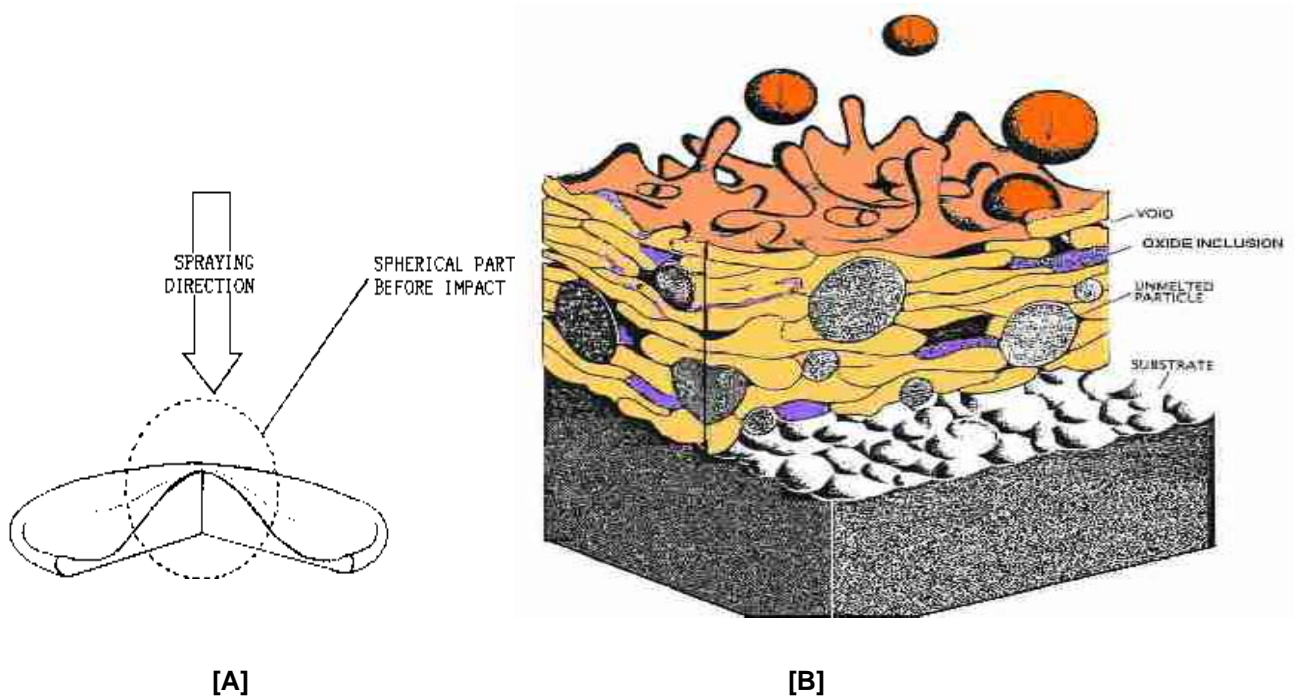
Fig. 1.18 A - Splatter formation: particle before and after impact onto the substrate
B - Formation of the coating layer

The melted particles are sprayed onto the desiderate substrate and their shape is changed because of the deformation caused by the impact (figure 1.18-A). The final shapes are so called splatters. The coating grows up by overlapping of several splatters, as described in figure 1.18-B.

Fig.1.20   Flame spraying gun

Fig.1.21   Sulzer Metco Diamond Jet HVOF;

Fig. 1.22   a) Diamond Jet (Sulzer Metco); b) JP-5000 (Praxair-Tafa)

REFERENCES

[1] R.P. Feynmann, *There's plenty of room at the bottom*, Eng. Sci (Febrary 1960)

[2] P.W. Anderson, *More is different*, Science (1972)

[3] Krishna Seshan, *Handbook of Thin-Film Deposition Processes and Techniques*

[4] Glang, R., Ch. I, pp. 1-3 to 1-130 in Ref. 1

[5] Glang, R., Holmwood, R. A. and Kurtz, J. A., Ch. 2, pp. 2-1 to 2-142 in Ref. 1
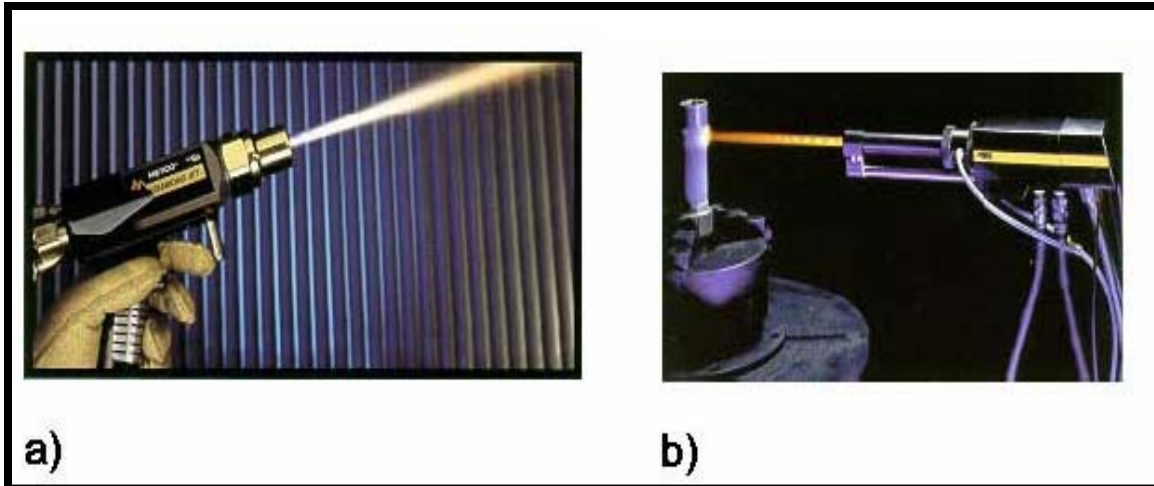
[6] Bunshah, R. F., Ch. 4, pp. 83–169 in Ref. 3

[7] Campbell, D. S., Ch. 5, pp. 5-1 to 5-25 in Ref. 1

[8] Adams, A.C., in *VLSI Technology*, (S. M. Sze, ed.), pp. 93–129, McGraw- Hill, New York (1983)

[9] Neugebauer, C. A., Ch. 8, pp. 8-3 to 8-44 in Ref. 1

[10] Kern, W., and Ban, V. S., Ch. III-2, pp. 258–331 in Ref. 2

[11] Kern, W., and Schnable, G. L., *IEEE Transact. on Electron Devices*, ED-26:647–657 (1979)

[12] 49. Hersee, S. D., and Duchemin, J. P., in: Ann. Rev. Mater. Sci., (R. Huggins,ed.), 12:65–80, Annual Reviews, Inc., New York (1982)

[13] 50. Blocher, J. M., Jr., Ch. 8, pp. 335–364 in Ref. 3

[14] Ghandhi, S. K., Ch. 8, pp. 419–474 and Ch. 5, pp. 213–297 in Ref. 4

[15] See also numerous excellent papers in Proc. *Ninth Internat. Conf. on Chemical Vapor Deposition 1984*, (M. Robinson, C. H. J. van den Brekel, G. W. Cullen, and J. M. Blocher, Jr., eds.), Vol. 84-6, The Electrochem. Soc. Inc., Pennington, NJ (1984)

[16] Burggraaf, P., *Semiconductor International*, 9(5):68–74 (May 1986)

[17] Burggraaf, P., *Semiconductor International*, 9(11):46–51 (Nov. 1986)

[18] Mawst, L. J., Costrini, G., Emanuel, M. A., Givens, M. E., Zmudzinski, C. A. and Coleman, J. J., *Semiconductor International,* 9(11):61–63 (Nov. 1986)

[19] Peters, J. W., Gebhart, F. L., and Hall, T. C., *Solid State Technol.*, 23(9):121–126 (Sept. 1980)

[20] Mishima, Y., Hirose, M., Osaka, Y., Nagamine, K., Ashida, Y., Kitagawa, N., and Isogaya, K., *Jpn. J. Appl. Phys.*, 22(1):L46–L48 (Jan. 1983)

[21] Numasawa, Y., Yamazaki. K., and Hamano, K., *Jpn. J. Appl. Phys.*, 22(12):L792–L794 (Dec. 1983)

[22] Osgood, R. M., and Gilgen, H. H., *Ann. Rev. Mater. Sci.*, (R. Huggins, ed.), 15:549–576, Annual Reviews, Inc., New York (1985)

[23] Solanski, R., Moore, C. A., and Collins, G. J., *Solid State Technol.*, 28(6): 220–227 (June 1985)

[24] Houle, F. A., *Appl. Phys.*, A41:315–330 (1986)

[25] Ghandhi, S. K., Ch. 6, pp. 299–370 in Ref. 4.

[26] Pinizotto, R. F., *J. Vac. Sci. Technol.*, A2(2):597–598 (April-June 1984)

[27] Wilson, S. R., *Proc. Semicond. Silicon 1986*, (H. R. Huff, T. Abe, and B. Kolbesen, eds.), 86-4:621–641, The Electrochem. Soc. Inc., Pennington, NJ (1986)

[28] Chin, T. Y. and Oldham, W. G., *J. Electrochem. Soc.*, 131(9):2110–2115 (Sept. 1984)

[29] Wehner, G. K., and Anderson, G. S., Ch. 3, pp. 3-1 to 3-38 in Ref. 1

[30] Maissel, L., Ch. 4, pp. 4-1 to 4-44 in Ref. 1

[31] Vossen, J. L., and Cuomo, J. J., Ch. II-l, pp. 12–73 in Ref. 2

[32] Thornton, J. A. and Penfold, A.S., Ch. II-2, pp. 76–113 in Ref. 2

[33] Fraser, D. B., Ch. II-3, pp. 115–129 in Ref. 2

[34] Waits, R. K., Ch. II-4, pp. 131–173 in Ref. 2

[35] Harper, J. M. E., Ch. II-5, pp. 175–206 in Ref. 2

[36] Thornton, J. A., Ch. 5, pp. 170–223 in Ref. 3

[37] Mattox, D. M., pp. 244–287 in Ref. 3

[38] Campbell, D. S., Ch. 5, pp. 5-1 to 5-25 in Ref. 1

[39] Ojha, S. M., *Phys. of Thin Films*, (G. Hass, M. H. Francome and J. L. Vossen, eds.), 12:237–296, Academic Press, New York (1982)

[40] Ghandhi, S. K., Ch. 7, pp. 371–417 in Ref. 4

[41] Hollahan, J. R. and Rosler, R. S., Ch. IV-1, pp. 335–360 in Ref. 2

[42] Reinberg, A. R., *Ann. Rev. Mater. Sci.*, (R. Huggins, ed.), 9:341–372, Annual Reviews, Inc., New York (1979)

[43] Thornton, J. A., Ch. 2, pp. 19–62 in Ref. 3

[44] Bonifield, T. D., Ch. 9, pp. 365–384 in Ref. 3

[45] Adams, A.C., in *VLSI Technology*, (S. M. Sze, ed.), pp. 93–129, McGraw-Hill, New York (1983)

[46] Sherman, A., *Thin Solid Films*, 113:135–149 (1984)

[47] Catherine, Y., *Proc. Fifth Symp. on Plasma Processing*, (G. S. Mathad, G. C. Schwartz, and G. Smolinsky, eds.), 85-1:317–344, The Electrochem. Soc. Inc., Pennington, NJ (1985)

[48] Adams, A. C., *Symp. on Reduced Temperature Processing for VLSI*, (R. Reif, and G. R. Srinivasan, eds.), 86-5:111–131, The Electrochem. Soc. Inc., Pennington, NJ (1986)

[49] Nguyen, S. V., *J. Vac. Sci. Technol.*, B4(5):1159–1167 (Sept./Oct. 1986)

[50] Yasuda, H., Ch. IV-2, pp. 361–398 in Ref. 2

[51] Hench, L.L.; West, J.K. Chem. Rev. 1990, 90, 35-40.

[52] Lev, O. et al. Analytical Chemistry. 1995, 67(1), 22A-30A.

[53] C. J. Brinker and G. W. Scherer, *Sol-Gel Science - The Physics and Chemistry of Sol-Gel Processing*, New York, Academic Press, 1990.

[54] K.D. Keefer, in: *Silicon Based Polymer Science: A Comprehensive Resource*; eds. J.M. Zeigler and F.W.G. Fearon, ACS Advances in Chemistry Ser. No. 224, (American Chemical Society: Washington, DC, 1990) pp. 227-24

[55] L. Pawlowski, "The Science and Engineering of Thermal Spray Coatings", (Jon Wiley & Sons, New York, 1995)

Chapter 2

Microemulsions and Colloidal Suspensions

While microemulsions are clear, stable, isotropic liquid mixtures of oil, water and surfactant, frequently in combination with a cosurfactant, a colloidal system consists of two separate phases: a dispersed phase (or internal phase) and a continuous phase (or dispersion medium). A colloidal system may be solid, liquid, or gaseous. The dispersed-phase particles have a diameter of between approximately 5 and 200 nanometers.

The results presented in this study are related to flame spraying of colloidal suspension of the nanoparticle to deposit. The home-made flame spray equipment was developed and patented by CSGI, Center for Colloid and Surface Science of Chemical Department of University of Florence to be used with microemulsion feed: nanostructured materials can be prepared by combining microemulsions and flame spraying methods. Nanoclusters of diameter between 10 and 100 nm have been synthesized in microemulsions. These microemulsions have been used to feed a flame spraying system and form a nanostructured film coating.

Since the aim of this work is focused to explore and extend the application of the deposition method, colloidal suspensions were used instead of microemulsions because of their simplicity. So just few words are spent to give

details about microemulsion and more attention is dedicated to colloidal suspension to explain the characteristics of the ones used to obtain the nanostructured materials discussed in next chapters.

2.1 Microemulsions

Microemulsions are composed of two mutually immiscible liquid phases, one spontaneously dispersed in the other with the assistance of one or more surfactants and cosurfactants. The systems may be water continuous (o/w) or oil continuous (w/o), the result being determined by the variables such as the surfactant systems employed, temperature, electrolyte levels, the chemical nature of the oil phase, and the relative ratios of the components. For a given oil phase, it is usually possible to optimize the oil: water ratio by varying the structure of the surfactant and cosurfactant, if needed.

The status of the systems commonly referred to as ''microemulsions'' among surface and colloid chemists is still somewhat uncertain. Various experimental approaches have been used in an attempt to ascertain the details of their structural and thermodynamic characteristics. As a result, new theories of the formation and stability of these interesting but quite complex systems are appearing. Although a great deal has been learned about microemulsions, there is much more to be learned about the requirements for their preparation and the relationships among the chemical structure of the oil phase, the composition of the aqueous phase, and the structures of the surfactant and the cosurfactant, where needed.

The distinction between microemulsions and conventional emulsions or macroemulsions is fairly clear. Although macroemulsions may be kinetically stable for long periods of time, in the end they will suffer the same fate: phase separation to attain a minimum in interfacial free energy. The actions of surfactants, polymers, and other stabilizing aids may shift the rate of droplet coalescence to extremely long time through decreased kinetic rate constants, but the thermodynamic driving force to minimize the interfacial area between

immiscible phases remains unchanged. On the other hand, the microemulsions appear to be thermodynamically stable compositions with essentially infinite lifetimes, assuming no change in such factors as composition, temperature, and pressure.

In addition to the thermodynamic distinction usually drawn between macro and microemulsions, the two classes of colloids differ in several other more tangible characteristics, including the size of droplets formed and the mechanical requirements for their preparation. As far as droplet size is concerned, the conventional macroemulsions are generally found to have diameter dimension of 1-10 μm, meaning that such systems are usually quite turbid or opaque. Microemulsions, however, normally have droplet diameters of 100 nm or less; many are only slightly larger than simple micellar systems. Because those particles are much smaller than the wavelength of visible light, they are normally transparent or slightly bluish.

A micelle is an aggregate of surfactant molecules dispersed in a liquid colloid. A typical micelle in aqueous solution forms an aggregate with the hydrophilic "head" regions in contact with surrounding solvent, sequestering the hydrophobic tail regions in the micelle centre.
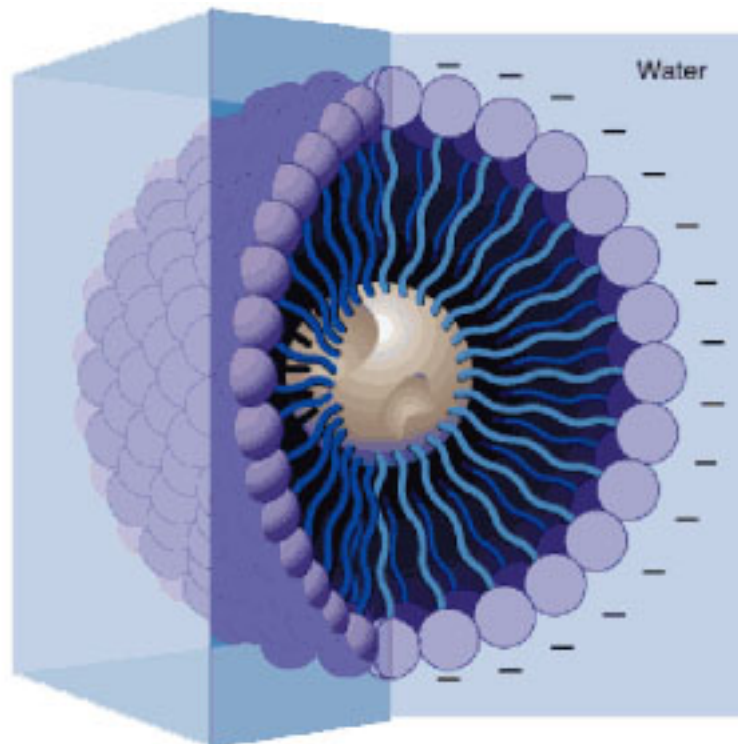
Fig.2.1 Micelle

This type of micelle is known as a normal phase micelle (oil-in-water micelle).

Reverse micelles have the headgroups at the centre with the tails extending out (water-in-oil micelle). In a non-polar solvent, it is the exposure of the hydrophilic head groups to the surrounding solvent that is energetically unfavourable, giving rise to a water-in-oil system. In this case the hydrophilic groups are sequestered in the micelle core and the hydrophobic groups extend away from the centre. These inverse micelles are proportionally less likely to form on increasing headgroup charge, since hydrophilic sequestration would create highly unfavourable electrostatic interactions.
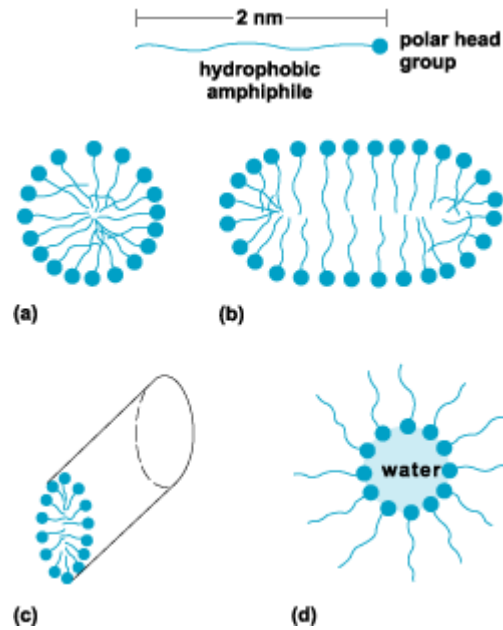
Fig. 2.2 Several forms of micelle: (a) spherical, (b) disk, (c) rod, and (d) reversed.
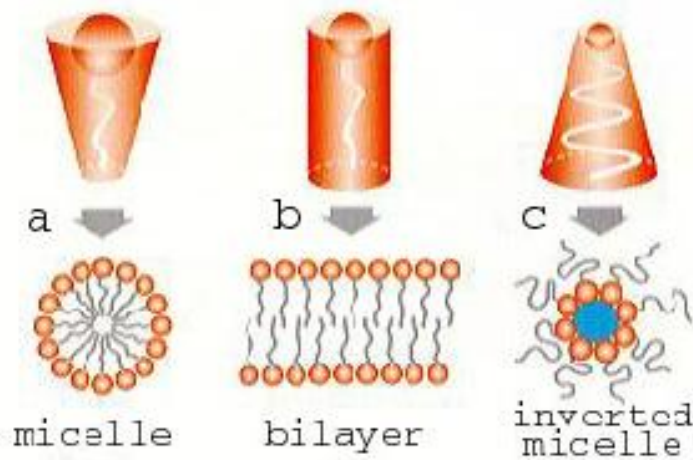

Fig. 2.3 Aggregation behaviour of emulsifier molecules
(a) Head group larger than the tail: micelle formation in water   (b) Cylinder-shaped molecule: formation of parallel bilayers   (c) Head group smaller than the tail: formation of inverted micelles, enclosing water.

Micelles are approximately spherical in shape. Other phases, including shapes such as ellipsoids, cylinders, and bilayers are also possible. The shape and size of a micelle is a function of the molecular geometry of its surfactant molecules and solution conditions such as surfactant concentration, temperature, pH and ionic strength.

While emulsion are macrodispersed systems of opaque and instable drops, microemulsions are thermodynamically stable thanks to the presence of a right surfactant and, eventually, of a co-surfactant[1]. Their stability is related to the value of the interfacial tension between water and oil: its value is low enough to be compensating by the dispersion entropy[2].

Surfactant molecules, arranging at the water-oil interface, allow the formation of a stable microdispersion. Moreover a microemulsion, thanks to the little dimension of its constitutive clusters (about one thousand time smaller than a macroemulsion) is optically transparent and presents low viscosity characteristics.

The most important properties of microemulsions are the macroscopic homogeneity, the low interfacial tension, the high surface area and the capability to solubilize both water and oil soluble compounds.

The energy requirements for the formation of macroemulsions can be quite substantial. The formation of small droplets requires that the system overcome both the adverse positive interfacial free energy between the two immiscible phases working toward drop coalescence and bulk properties of the dispersed phase such as viscosity. Microemulsions, on the other hand, form spontaneously or with very gentle agitation when the proper composition is reached. When one compares microemulsions and micelles, the demarcation line can become quite blurred and, in some cases, does not exist. In the present work no distinction between the two terms is underlined, such usually accepted from most part of the authors.
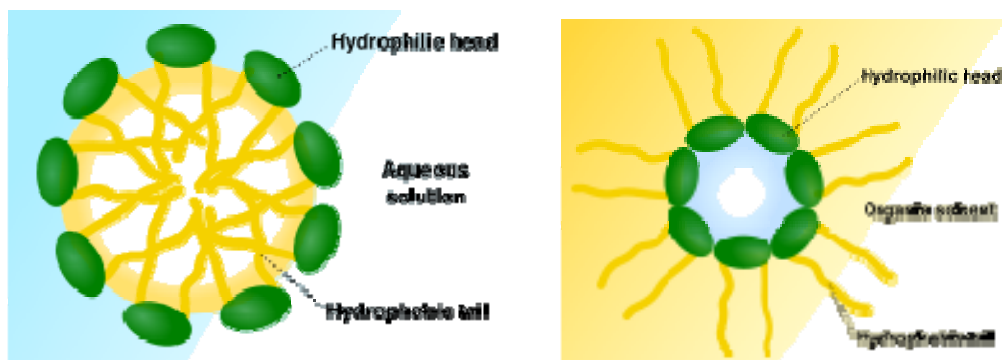
Fig. 2.4 Micelle and reverse micelle
Scheme of a **micelle** formed by phospholipids in an aqueous solution.
Scheme of a **reverse micelle** formed by phospholipids in an organic solvent.

The activity developed at CSGI is involved with microemulsion of water in oil (W/O), composed by nano-drops of water dispersed in oil. The micelles of the W/O microemulsion are called reversed micelles. Metal nanoclusters of well-defined size are obtained by reduction of a metal salt inside the water compartment of water in oil (w/o) microemulsions, formed by water in hexane and stabilized by an appropriate surfactant. Metal nanoclusters are separated from the mother solution by spraying the microemulsion solution into an air/acetylene flame. In this way, nanostructured coating or powder, almost preserving the original structure of the nanoparticles synthesized in the microemulsion system, can be obtained in quantities sufficient for industrial applications.[3]

2.1.1   Microemulsion applications in the production of nanostructured materials

Microemulsions can be usefully applied in the production of nanostructured materials[4,5,6,7,8] because of their use such as microreactors to manage the growth of the produced particles.

This technique present many advantages compared with other techniques used to obtain the same results: no critical temperature or pressure conditions are required, it can be applied theoretically to all the chemical reactions producing nanoparticles in homogeneous solution, and no special equipments are required.

However also some difficulties have to be considered: first of all the problems to control the chemical reaction behaviours. For example some reactions have a really slower rate in microemulsion, while others don't occur.

The most important microemulsion properties to be used to control the chemical reactions, is the capability to exchange the content of the dispersed drops. About W/O microemulsions, thanks to different experimental techniques, it was underlined a exchange mechanism with intermediate steps proceeding thanks the formation of transient dimer species, as explained in figure 2.5.
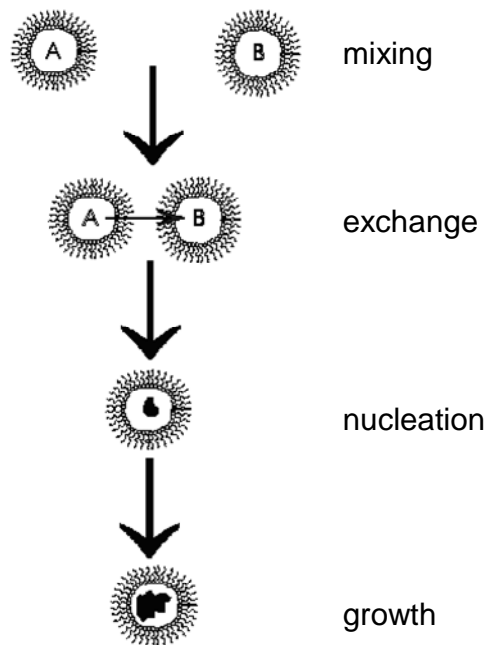

Fig. 2.5 Particle formation mechanism

The lifetime of the dimer specie produced from the collision between two different micelles is long enough to arrange randomly the species solubilized in the water core, the water and surfactant molecules that compose the reversed micelles. Kinetic studies[9] show how some of the most common surfactants imply a lifetime of the dimmer in the order of about a microsecond: it is an enough long time to allow molecules to diffuse inside the dimmer.

Moreover a longer lifetime realizes phase separation because other micelles could be united with the transient dimmer. Successive dimmer evolution concerns its separation and the consequent formation of two species alike the starting ones. The step that controls the rate of the whole process seems to be the addiction of two micelles. About just one impact among one thousand brings to the formation of a dimer, with the consequent substances exchange. Addition process is characterized by high value of activation enthalpy and strongly positive entropy: the performance of these two kinetic parameters is explainable with the increase of the coulomb repulsion, as a consequence of the interface area compression, and with the release of some surfactant molecules from surfactant layer at the interface while the dimer is forming.

The exchange process is extremely important for reversed micelles systems because it helps to control some properties of the resulting particles, such as dimensions and polydispersivity.

It is clear how reversed micelles are water micro-compartments that can be used for in situ synthesis of nanoparticles. So, just mixing two different microemulsions, one with the metal salt and the other with the reduction agent, metallic particles can be obtained. About reactions with a slower rate than exchange process in water, water phase can be considered such as continuous; about faster reactions, the limiting step is the exchange process between micelles so it control the rate of the reaction.

The use of microemulsions allows the direct control of the nanoparticle formation kinetic and of their dimensions.

To synthesise monodispersed particles with small size, the two processes of nucleation and growth have to happen in different time scale. To satisfy this

condition it is necessary a fast production of a great number of nuclei and sequentially a slow growth of the particles.

To have monodispersed samples, some stabilization effect have to occur when nuclei arrive at a critical dimension N, to ensure no more growth.

Reactant compartmentalization inside the water drops of a W/O microemulsion allow to obtain quite monodispersed metal particles with a size of few nanometers.

Several parameters affect the final dimension of the clusters: concentration, the kind of the reducing agent and, most of all, the water and surfactant content in the microemulsion. Those usually are defined by the parameter W_0

$$W_0 = \frac{[H_2O]}{[tensioattivo]}$$

(2.1)

Once the particles realize the desired dimension, they are stabilized by the surfactant: by adsorbing on the nanoparticle surface, it prevents their further growth allowing the formation of a stable suspension.

2.2 Colloidal Suspensions

The results exposed in the next chapters are related to two different suspension used during flame spraying deposition process.

Those are generally composed by the nanoparticles to deposit, a solvent such as cyclohexane and a surfactant to stabilize the suspension and to ensure the absence of aggregation phenomena.

2.2.1 TiO$_2$ nanoparticle suspensions

Colloidal suspensions were prepared starting from TiO$_2$ (anatase and rutile mixture) nanopowder (99.9% on a metals basis, Aldrich), having a particle

diameter size less than 100 nm as determined by BET. Cyclohexane (95%, Sigma-Aldrich) was chosen as organic dispersing medium and oleic acid (68%, Carlo Erba) as dispersing agent. The dispersion was sonicated for 1 hour (Branson Digital Sonifier 450) at room temperature. Figure 2.6 represents the SEM images of these nanoparticles.
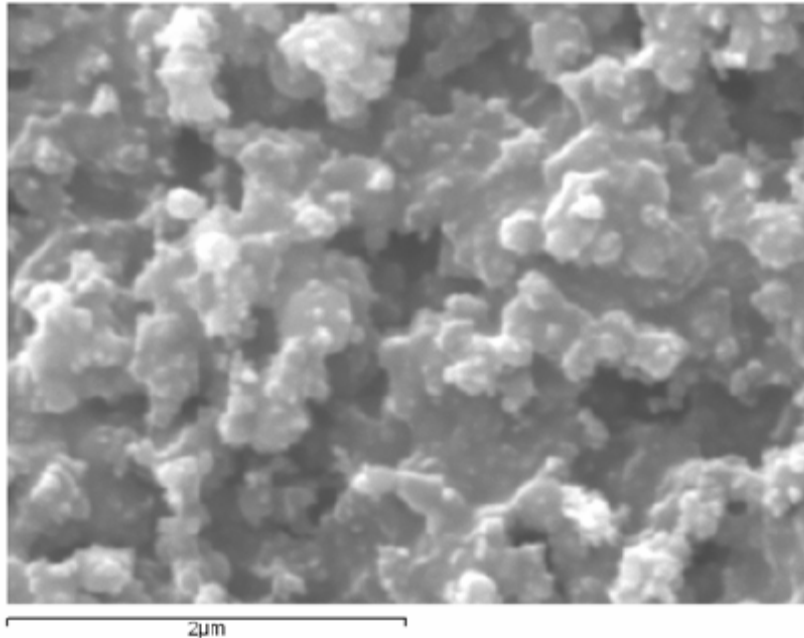

Fig.2.6 SEM images of the TiO2 nanoparticles: diameter of less than 100nm (about 50nm)

To evaluate the importance of the particle size, also powder with a diameter of about 350 nm were applied, synthesized in CSGI laboratories.

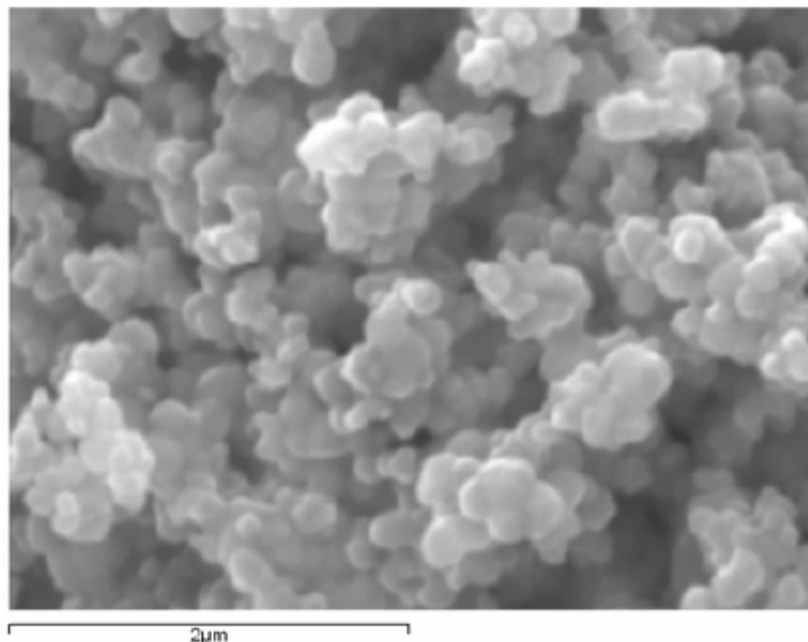The figure 2.7 represents the SEM mages of this second powder.

Fig.2.7 SEM images of the TiO2 nanoparticles: diameter of about 350nm

The resulting nanostructured materials present a very low level of deposited particles, as demonstrated by AFM analysis. Also photocatalytic activity tests[10] underlined no observable photocatalytic behaviour by TiO_2.

2.2.2   Ag nanoparticle suspension

Colloidal suspensions were prepared starting from Ag nanopowder, synthesized in the CSGI laboratories[11]. It is out of interest of the present work to explain the details of the method used: however the as-synthesized silver nanocrystals were stabilized with a monolayer hydrocarbon chain through covalent bidentate bridging of carboxylate in dodecanoic acid. Also, oleate- and dodecanethiolate-protected silver nanoparticles could be synthesized easily using this method and no further addition of dispersing agent is necessary.

Their size is less than about 5 nm, as observable by TEM images of the resulting suspension (Fig.2.7), with some bigger cluster of about 10 nm.

Cyclohexane (95%, Sigma-Aldrich) was chosen as organic dispersing medium. Because the nanoparticles are synthesized with a layer of lauric acid onto their external surface, as explained briefly above, no other dispersing agent

is added. The dispersion was sonicated for 30 minutes (Branson Digital Sonifier 450) at room temperature.

The resulting suspension presents a regular lattice as shown in the TEM images below (figure 2.8).

The figure 2.9 illustrates the diffraction pattern of the Ag nanoparticles: it corresponds to the face-centered cubic crystal structure.
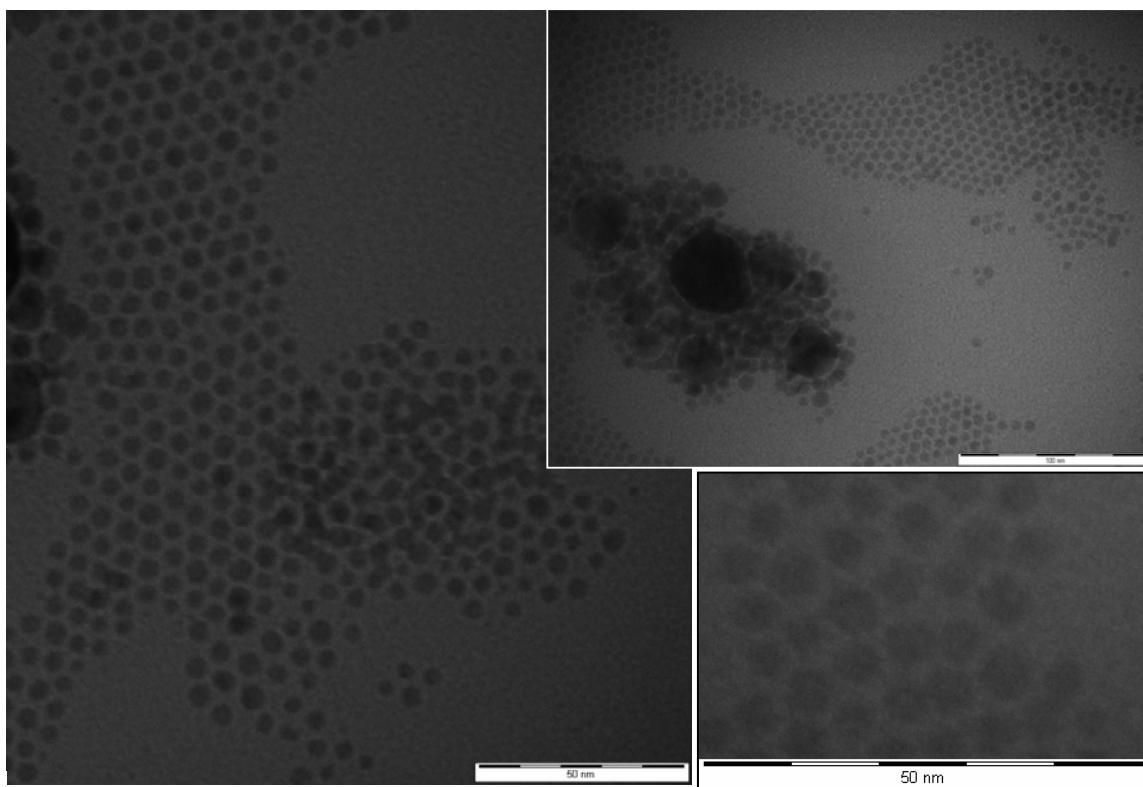

Fig.2.8 TEM images of the colloidal suspension from Ag nanoparticles synthesized at CSGI laboratories.
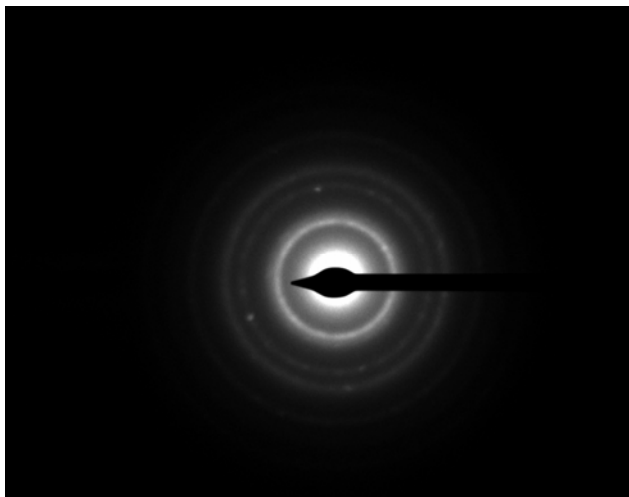
Fig.2.9 Diffraction pattern of the Ag nanoparticles

REFERENCES

[1] B. H. Robinson, *Nature* **320**:309 (1986)

[2] G. Gilberg, in *Emulsions and Emulsion Technology* (K. J. Lissant, ed.), Marcel Dekker, New York, 1984, pp. 1-43

[3] P. Baglioni, U. Bardi, M. Bonini, Eur. Pat. 1,134,302 A1, 2000

[4] M. P. Pileni, I. Lisiecki, L. Motte, C. Petit, J. Cizeron, N. Moumen, and P. Lixon, *Prog. Colloid Polym. Sci.* **93**:1

[5] J. P. Wilcoxon, U.S. Patent 5, 147, 184 to *United States Department of Energy* (1992)

[6] J. B. Nagy and A. Claerbout, in *Surfactant in Solution* **11** (K. L. Mittal and D. O. Shah, eds.), Plenum, New York, 1991, pp. 362-382.

[7] V. Pillai, P. Kumar, and D. O. Shah, *J. Mag. Mag. Mater.* **116**:L299 (1992).

[8] J.N. Israelachvilli, D. J. Mitchell, and B. W. Niham, *J. Chem. Soc. Faraday Trans. I* **72**: 1525 (1976).

[9] K. Thomas, *J. Am. Chem. Soc.* **103**, (1981), 3543.

[10] See chapter 5.

[11] K.J. Lee et al. *Journal of Colloid and Interface Science* 304 (2006) 92–97

Chapter 3

Flame spraying of Colloidal Suspension

Nowadays many techniques are developing to allow nanoparticles deposition onto different substrates.

Sol-gel technique[1] is widely used for nanoparticles deposition because it allows to easily controlling the characteristic of the deposited particle. It is a two-step process (dip coating and calcinations) usually presenting technological complications and very expensive industrial equipments. Moreover, the presence of impurities in the deposited powder could influence the characteristics of the resulting materials.

Thermal spraying processes represent a valid alternative for particles deposition[2,3]. Originally born for microparticles deposition, this method is a quite low cost process that, relying on several physical and chemical phenomena, presents a high degree of complexity. In addition, agglomeration and bad flooding make this technique generally not suitable for high quality nanostructured material productions. The use of liquid suspensions instead of powders can overcome these problems.

In the present study, nanoparticle coated glass substrates are produced by flame spraying of colloidal suspensions or microemulsions[4], patented by CSGI, Center for Colloids and Surface Science: it is a new way to prepare nanosized materials as well as thin films of nanoparticles.

The equipment used is a home built flame spraying set up, modified in order to be used with a liquid feed.

The obtained nanostructured coating almost preserves the original structure and the purity of the starting nano-powder. This deposition method allows a strict control of the final composition and nano-morphology and could be of great utility in many fields involving the use of photocatalytic and self-cleaning glasses for special application. The use of a stable suspension instead of a powder avoids both flooding difficulties and nanoparticles agglomeration in the coating film. The addition of a surfactant ensures both the stability and the homogeneity of the suspension5. The flame spraying system was optimized to completely burn the solvent and the surfactant before the deposition hence insuring a high purity level of the deposited film

3.1 Deposition process description

The home-built flame spraying setup used during these experiments has been designed to spray the microemulsions as an aerosol directly into the flame.

Starting from an ordinary flame spraying[6] with powder injection, some changes were applied to adapt the equipment for the use of liquids, instead of powders.

The colloidal suspension (or the microemulsion)[7] was used as feedstock material in the home-made flame spraying equipment described in Figure 3.1. A suspension/air mixture was forced to pass throughout a spray nozzle in order to generate the aerosol that directly fed the GPL/Oxygen flame. The suspension flow-rate was continuously monitored by means of a flow-meter positioned on the feeding line.
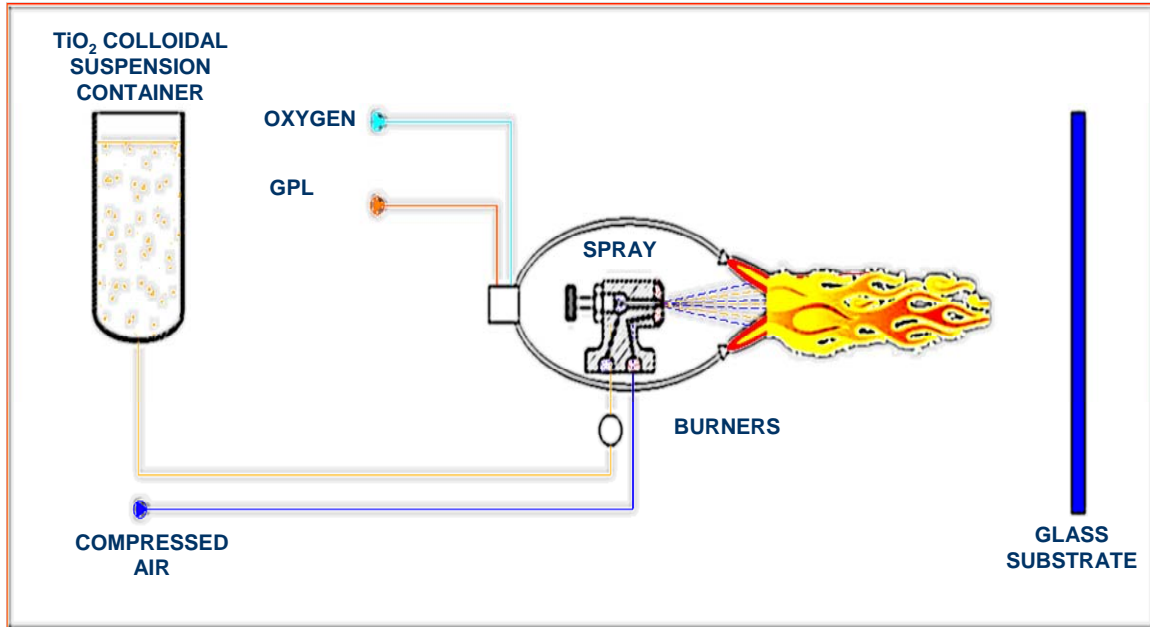
Fig. 3.1 Scheme of the flame spraying equipment

3.2   Equipment description

The Flame-spraying equipment actually in use is represented in Figure 3.3. It is possible to identify different parts: the first one (A) is the core of the flame spraying device with the atomizing nozzle and the burning set and the suspension feeder.

It also possible to observe the sample holder (B) to ensure the mobility of the piece to spray, the thermocouples (C) and the flow-meter (D) to check the temperature at the surface of the substrate and the flow rate of the liquid feed containing the nanoparticles to deposit.

Fig. 3.2 Flame spraying set up

Fig. 3.3 Picture of the flame spraying equipment.

(A) Flame; (B) Sample holder; (C) Thermocouples; (D) Flow-meter

Fig. 3.4 Detail of the Flame spraying equipment with the burning set and atomizing nozzle.

Fig. 3.5 Detail of the Flame spraying equipment with the burning set and atomizing nozzle.

Lateral view.

In figures 3.4 and 3.5, it is observable the detail of the flame spraying device representing the atomizing nozzle and the six torches from where the flame is developed.

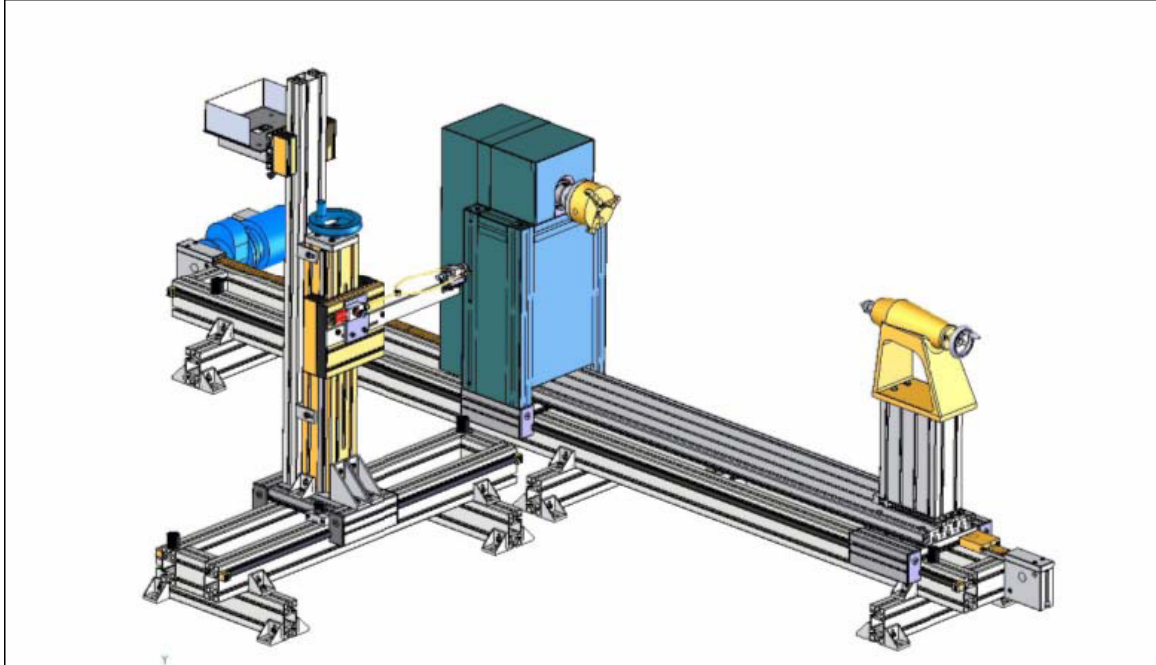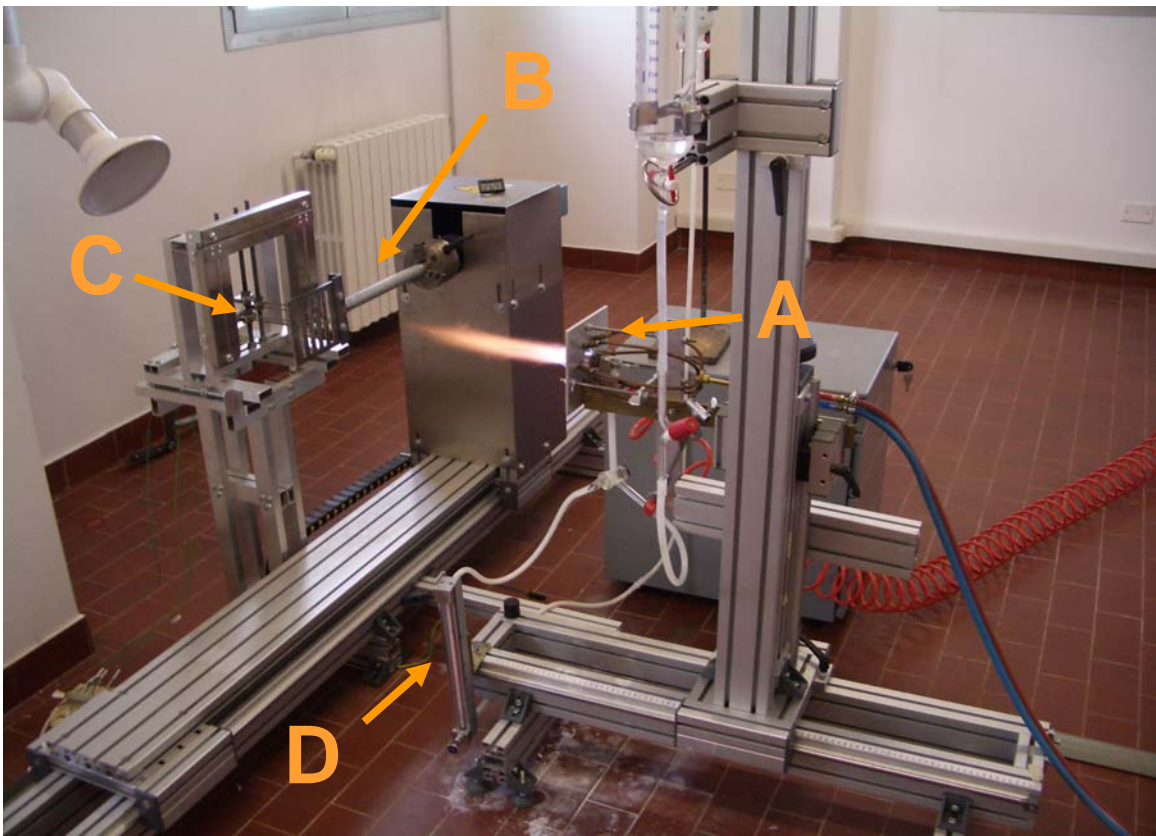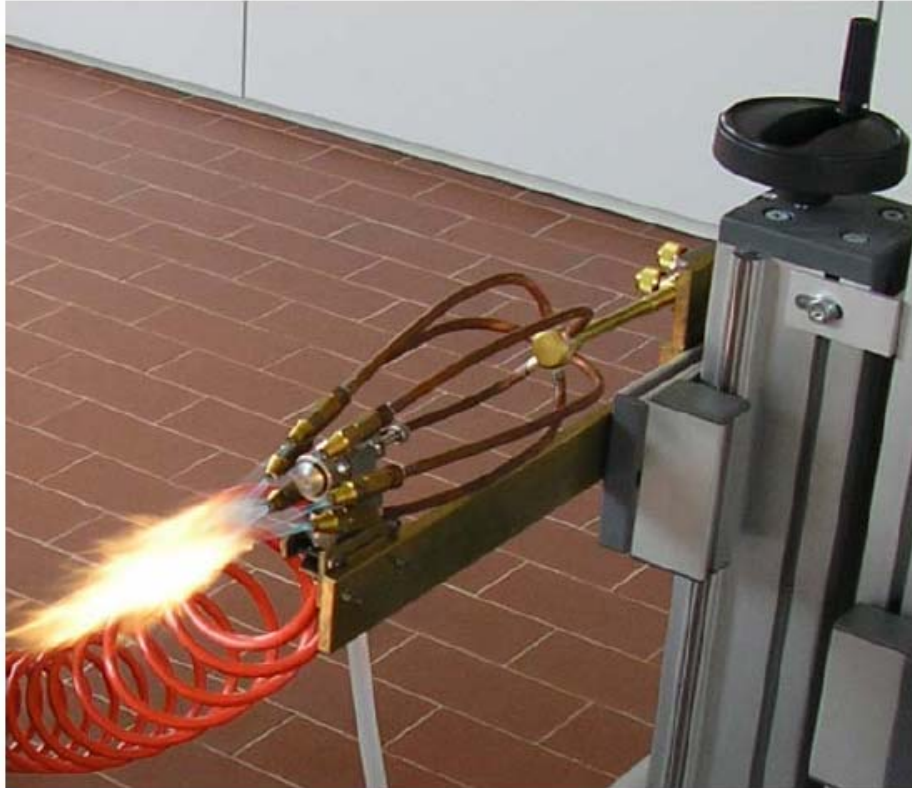The burning set is composed by six ordinary oxy-propane welding torches assembled to allow operation using propane or acetylene as a fuel gas. GPL was chosen as the fuel gas. The torches of the set are planned to ensure an optimal direction of the flames with a small angle of incidence compared to the horizontal axis of the atomizing nozzle, so that the aerosol flow is not disturbed.

The atomizing nozzle (Spraying System Co, mod. ¼ JACN-SS + SU1A-SS) is placed in the centre of the burning set to ensure the homogeneous burning of the suspension because of the symmetry.

In the same pictures it is visible the vertical support that keep all the flame sprayings set and the solvent feeder to reach the desiderated temperature of the substrate before starting deposition.

This support allows also vertical height regulation of the flame spraying set, while the horizontal distance from the sample holder is regulated by a guide bar placed on the floor level that allows the movement of all the vertical support.

The atomizing nozzle is fixed on a support to ensure that the aerosol was fed into the flame from a nearly parallel direction to the flame direction. The droplet size and the velocity of the stream (suspension and combustion gases) were optimized to make sure the residence time of the microemulsion droplets into the flame was sufficient in order to complete the combustion process.

The nozzle has two inlets on the bottom side, one for compressed air and the other for the suspension.

Air		Liquid Capacity (l/h)								Spray dimension with 20 cm siphon height			
		Gravity fed			Siphon heigh								
Air Press (bar)	Air Capacity (Nl/min)	45 cm	30 cm	15 cm	10 cm	20 cm	30 cm	60 cm	90 cm	Air (bar)	Spray Angle A (º)	B (cm)	D (m)
0.7	11.3	1.5	1.3	1.1	0.87	0.68	0.53	-	-	0.7	18º	28	1.8
1.5	17.0	1.8	1.7	1.5	1.3	1.2	1.1	0.62	-	1.5	18º	28	1.9
3.0	28	2.1	1.9	1.7	1.5	1.4	1.3	1.1	0.76	3.0	18º	30	2.3
4.0	36	2.2	2.0	1.8	1.6	1.5	1.4	1.2	0.87	4.0	18º	36	2.6

Specifications

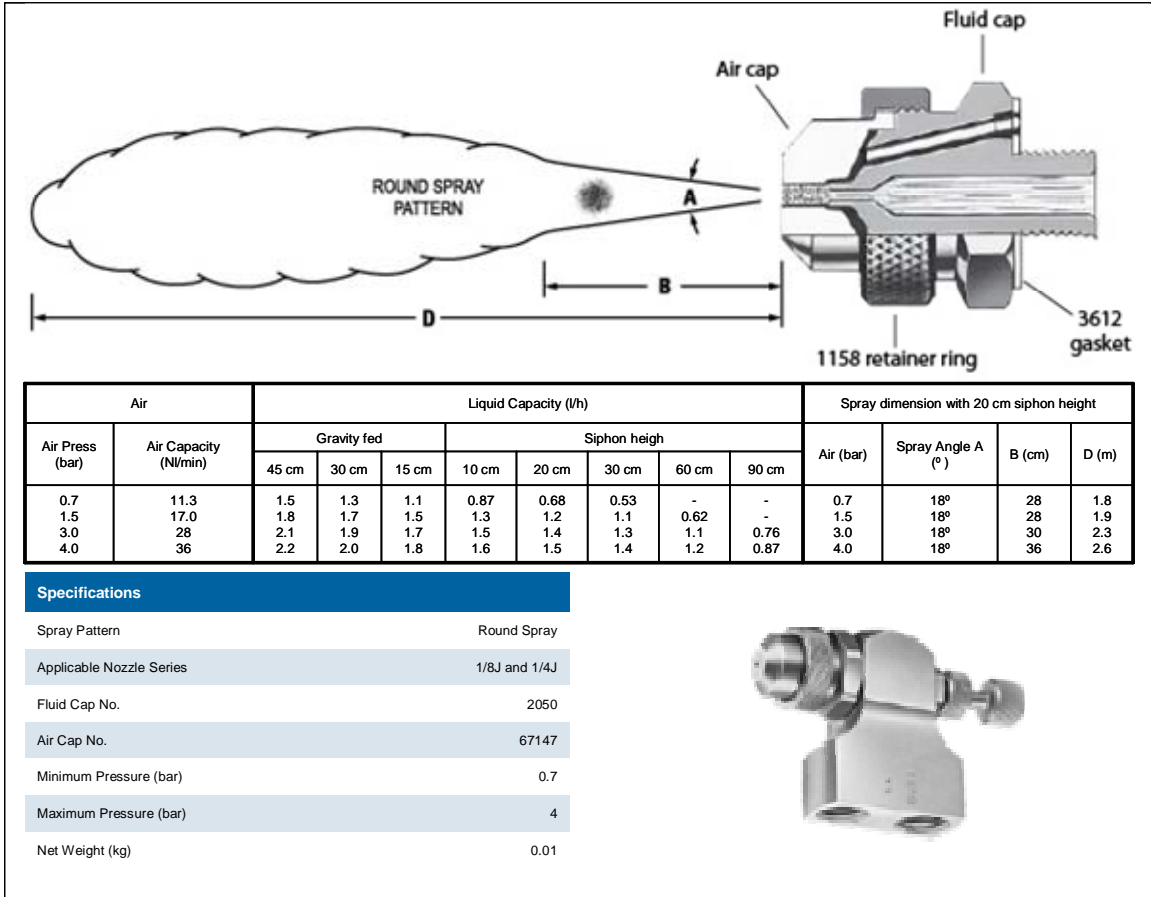|	
Spray Pattern	Round Spray
Applicable Nozzle Series	1/8J and 1/4J
Fluid Cap No.	2050
Air Cap No.	67147
Minimum Pressure (bar)	0.7
Maximum Pressure (bar)	4
Net Weight (kg)	0.01

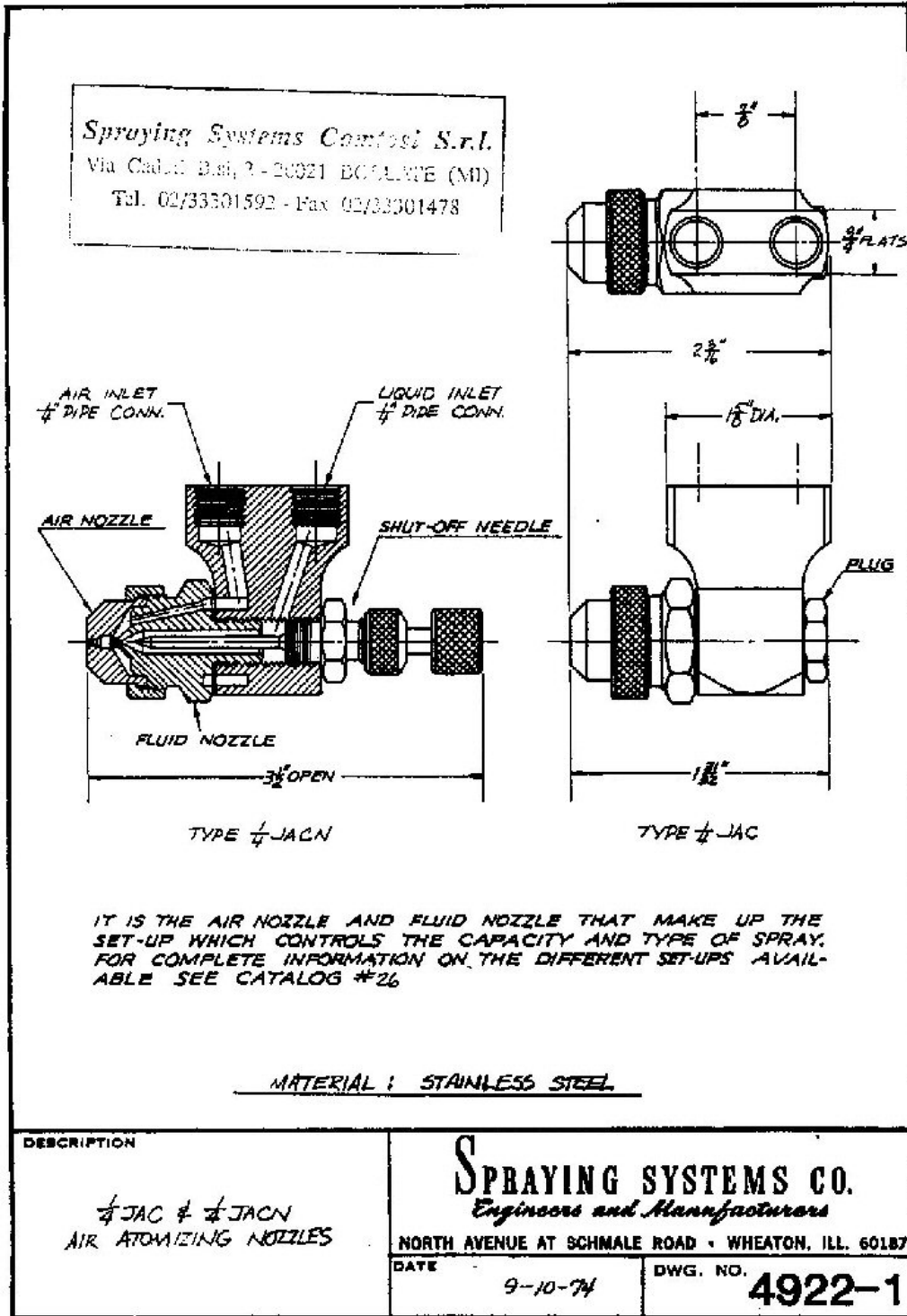**Fig. 3.6** Atomizing nozzle and technical data sheet (Spraying System Co)

Fig. 3.7 Atomizing nozzle and technical data sheet (Spraying System Co)

Two different suspension feeding schemes are possible, as explained in the figure 3.8. In the first one, suspension handling from the container to the nozzle is ensured by gravity, while the siphon system is based on the depression caused by compressed air in the nozzle. Compressed air allows to atomizing the liquid feed with a resulting flow with small drop (aerosol) that is directly inlet in the flame.
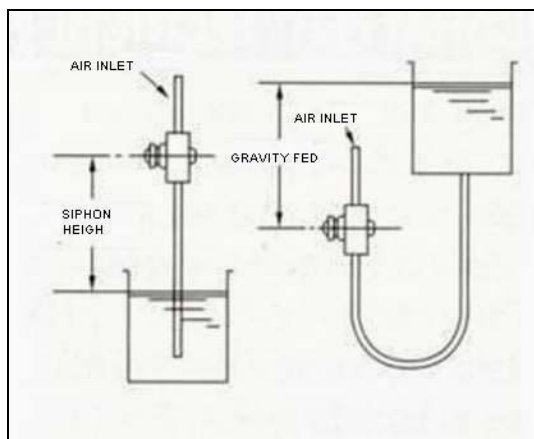
Fig. 3.8 Suspension feeding schemes

The suspension feeder is allocated in the top of a support to ensure a wide range of possible flowrates. The suspension, before arriving at the nozzle, passes through a to small flow instant reading flowmeter (figure 3.9) with integral needle valve to check and control its flowrate.

A three way valve (figure 3.9) is used to switch the feeder line between the suspension one and solvent one.

A thermocouple connected to PC (Labview software) is used for monitoring the temperature of the flame on the substrate during the deposition process.

The thermocouple position/ positioning is illustrated in the picture of figure 3.10

Fig. 3.9 Detail of flowmeter and three way valve.

Fig. 3.10 Thermocouple positioning during a deposition onto glass substrate

3.3   Deposition process setting

The whole equipment is planned to realize a wide range of working conditions, changing the deposition process parameters. Different conditions were selected concerning the substrate material, the type of the nanoparticles to deposit and the desired results. The flexibility of the equipment is helpful to extend the applications field of this deposition technique. Development of the process thanks to changes in the experimental equipment allowed to analyze different substrate-coating combinations and to discover how many unexpected possibilities can be realized.

3.3.1   Material choice for coating

The results exposed in the present work are related to the deposition of nanoparticles of:

- Ag
- TiO_2

The selection of these materials is connected with their peculiar properties, such antibacterial activity for Ag and Photocatalytic behaviour of TiO_2 as better explained in chapter 5, where their functional properties are deeply discussed. This choice is based on the intention to take in evidence the peculiarity of the flame spraying of colloidal suspension process, especially the possibility to obtain extremely thin films with a high purity level for special application.

3.3.2   Material choice for substrate

During the experimentations, the possibility to deposit onto unusually substrates for a flame spraying deposition process progressively takes more importance. Starting from glass for antifogging and self-cleaning applications, it was observed how the conditions of the process allow testing also different substrate such as plastics or fabric. Moreover it seems to be very interesting the development of the equipment explore new conditions and parameters of the process.

At the present time thin films were sprayed onto the materials reported in table 3.1.

Table 3.1 Materials of interest as substrate for nanoparticle deposition

Material	thickness	Glass transition temperature Tg
Glass	1 mm	
PET	0.5 mm	75 °C
PMMA	5 mm	*115 °C
Epoxy	5 mm	112 °C
Cotton	--	--

∗Vicat softening temperature

3.3.3 Deposition Process Conditions and operating parameters

Flame spraying process is characterized by a set of values of the parameters that are necessary to manage the process. Each set identify a condition of process.

Table 3.2 Operating parameter to manage the process.

Parameter	Measured by
Suspension Flowrate	Flowmeter (l/h)
Suspension Concentration	---
Oxygen Pressure	Manometer (bar)
GPL pressure	Manometer (bar)
Air Pressure	Manometer (bar)
Distance between the burning set and the sample holder	(cm)
Deposition Time	Clock (min)

Temperatures on the substrate during the deposition process were registered by thermocouples connected to PC (Labview software). It is a very important aspect of the process, but it is not considerable as parameters to manage the process. It depends on others parameters primarily distance and air pressure (see table 3.3).

Most of these parameters can influence the process both directly and because of their combination with others. For example, the pressure of the compressed air, together with the suspension flowrate, is strongly connected with the size of the droplets and the aerosol shape. At the same time the air pressure value influences, together with GPL and Oxygen pressures, the turbulence and the length of the flame. To better evaluate the parameter weight in the process

performances and in the resulting sprayed materials, Design of Experiment (DoE) technique was applied. The measurable inputs are compared with other measurable outputs, using dedicated software (Minitab® and Excel®) to value statistically the influence of each parameter (input) and to reach a better understanding of the whole process. About the output variables the preference was directed to find quantifiable variables connected with the goal of the set of experiment of interest.

For the production of antifogging and self-cleaning glasses, the output variables were chosen among measurable functional properties: contact angles and photocatalytic activity. Thus several samples obtained by flame spraying of TiO$_2$ suspension, having different values of deposition variables, were tested. No significant variations in photocatalytic efficiencies and photo-induced hydrophilicity were found, thus confirming the good stability and reproducibility of the process.

The research underlined two different process conditions to take into consideration; each of them is characterized by some measurable parameters that allow managing the process and optimizing the results.

Two different sets of deposition conditions are exposed:

- High substrate temperature (applied to glass substrates)
- Low substrate temperature (applied to plastic and fabric substrates, but also to glass substrate)

The preference between the first and the second set is related to:

- The limiting temperature of the substrate
- The nature of the nanoparticle to deposit
- The application of interest for the resulting nanostructured material

The glass transition temperature of the substrate material is the main limiting aspect (table 3.1). Some materials, such steel or also glass, with high glass transition temperature are not strongly restricted, while this limitation is important when the deposition process is applied to plastic substrates.

The others requisites are connected each other because the choice of the nanoparticles is related to the application of interest. For example, thin films of

metal nanoparticles, could be obtained at high temperature with improved mechanical properties but their deposition, if used as catalyst, presents some limitations in additions because of their loose of surface area when too melted (see chapter 4 paragraph 4.1).

The examined sprayed samples have been obtained mainly in the low temperature condition because the resulting thin films show better characteristics for the applications of interest in the present study.

The table below takes in evidence the key parameters that allow changing the condition temperature. The substrate temperature reported is the average of the temperatures registered during the deposition time.

Table 3.3 Parameters representing high and low temperature deposition conditions.

Parameter	High substrate temperature	Low substrate temperature
Air Pressure (bar)	0.8	0.3
Distance (cm)	20-25	50 - 53
Average substrate temperature (ºC)	450-500	80 - 100

3.4 Deposition of ceramic nanoparticles: TiO$_2$

This set of experiments was directed to valuate the validity of the deposition process for self-cleaning and antifogging glass application. This step of the work was aimed to optimize the process parameters for realizing the desiderated result.

To estimate the quality of the sprayed glass were chosen two quantifiable functional properties strongly related with the goal of this set of experiment and with the considered application. Thus contact angles and photocatalytic activity

measurement were performed and the results are exposed in chapter 5, but those are out of interest in this part of the discussion. Since few differences in the functional properties were enhanced, the set of process parameter that better optimized the process were established taking into account also the costs of the process as an important factor for possible industrial applications.

Table 3.4 - Process variables adopted for the deposition of TiO2 on glass plates

Parameter	Value
Suspension Flowrate (l/h)	0.35
Suspension Concentration (g/l)	0.5
Mean Particle Size (nm)	50
Oxygen Pressure (bar)	0.3
GPL pressure (bar)	0.25
Air Pressure (bar)	0.8
Substrate temperature (ºC)	450
Distance (cm)	20

Table 3.5 - Process variables adopted for the deposition of TiO2 onto plastic substrate

Parameter	Value
Suspension Flowrate (l/h)	0.35
Suspension Concentration (g/l)	0,5
Oxygen Pressure (bar)	0.3
GPL pressure (bar)	0,25
Air Pressure (bar)	0.3
Substrate temperature (ºC)	80
Distance (cm)	53

3.5 Deposition of metal nanoparticles: Ag

Thin films of Ag nanoparticles onto glass substrate were obtained at high temperature with improved mechanical properties. However, when Ag is used as catalyst, the deposition process presents some limitations in additions because of the decrease in surface area. The surface profile results to be more homogeneous (see chapter 4, paragraph 4.1) because, during the deposition process, the particles became too melted too keep their spherical shape.

Table 3.6 - Process variables adopted for the deposition of Ag onto plastic and fabric (cotton) substrates

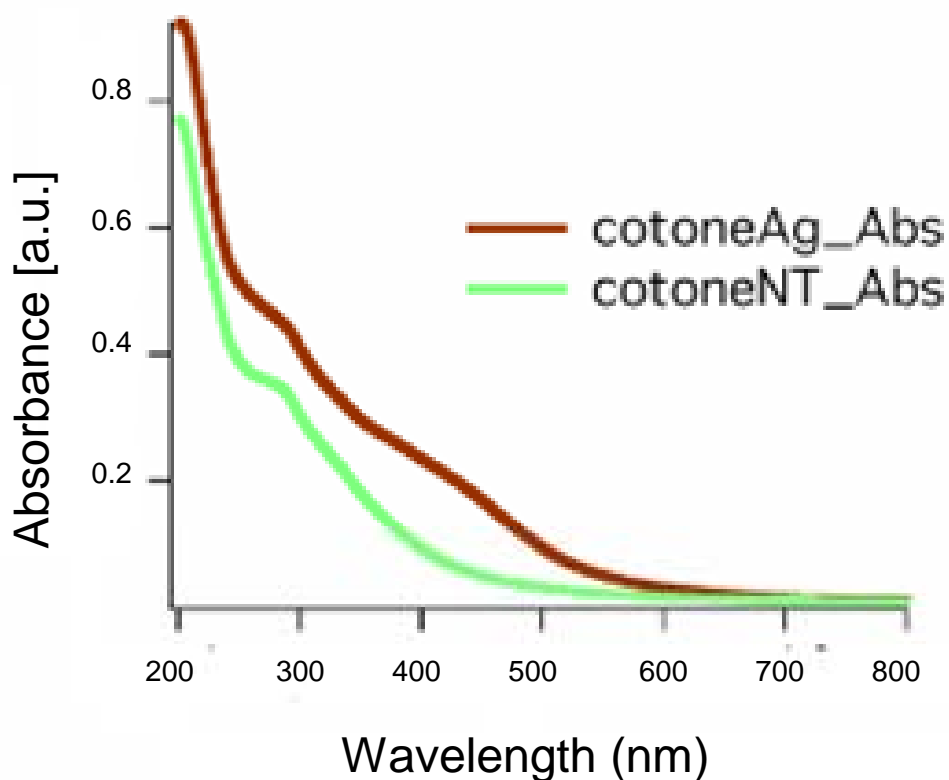| Parameter	Value
Suspension Flowrate (l/h)	0.35
Suspension Concentration (g/l)	0,5
Oxygen Pressure (bar)	0,2
GPL pressure (bar)	0,25
Air Pressure (bar)	0.3
Substrate temperature (ºC)	80
Distance (cm)	50

Fig. 3.11 UV spectra of the Ag sprayed cotton (red line) compared with the same cotton before deposition (green line)

3.6 Deposition onto plastic substrates

Development of the process was carried on with the choice of substrates different from the glass. The work was continued with deposition onto plastic materials. The process conditions were chosen to obtain the lower temperature possible on the substrates. Obviously the choice of the conditions is applied to a narrower range than the glass substrate case, depending on the lower glass transition temperature.

Deposition of selected nanoparticles was tested also onto plastic substrate, particularly PET, Epoxy resin and PMMA. Table 3.7 summarize the values of the parameter set used.

Table 3.7 - Process variables adopted for the deposition of TiO2 onto plastic substrate

Parameter	Value
Suspension Flowrate (l/h)	0.35
Suspension Concentration (g/l)	0.5
Mean Particle Size (nm)	50
Oxygen Pressure (bar)	0.3
GPL pressure (bar)	0.25
Air Pressure (bar)	0.3
Substrate temperature (ºC)	70-80
Distance (cm)	50-55

Deposition onto PET substrates presents stronger difficulties because of its thickness and its low glass transition temperature. Thus the deposition was carried out by sliding movement of the sample holder during the process. The PET samples were kept intermittently to the higher temperature region and their macroscopic characteristics were preserved. It imply a loss of nanoparticles, but it is acceptable because of the very low quantity of TiO_2 required.

Table 3.8 Plastics of interest as substrate for nanoparticle deposition

Material	thickness	Glass transition temperature Tg
PET	0.5 mm	75 °C
PMMA	5 mm	*115 °C
Epoxy	5 mm	112 °C

∗Vicat softening temperature

REFERENCES

[1] C. J. Brinker, G. W. Scherer , *The Physics and Chemistry of Sol-Gel Processing*, (Academic Press, Boston, 1990)

[2] L. Pawlowski, *The Science and Engineering of Thermal Spray Coatings*, (Jon Wiley & Sons, New York, 1995)

[3] A. Killinger, M. Kuhn, R. Gadow *Surface Coating Technol.* 2006**;** 201, 1922-1929

[4] P. Baglioni, U. Bardi, M. Bonini, M. *Eur. Pat. 1,134,302 A1*, 2000

[5] M. Bonini, U. Bardi, D. Berti, C. Neto, and P. Baglioni *J. Phys. Chem.* B 2002, 106, 6178

[6] See paragraph chapter1

[7] See next paragraph 2.2

Chapter 4

Morphology and mechanical properties of the sprayed thin films

The results presented in this study are related to flame spraying of colloidal suspension of the nanoparticles to deposit. The home-made flame spray equipment was developed and patented by CSGI, Center for Colloids and Surface Science.

The morphology of the TiO_2 samples has been characterized by Atomic Force Microscope (AFM): the resulting images clarify the homogeneity and regularity of the deposits. Atomic Force Microscopy, AFM, was used to characterize the shape and size distribution of the flame-sprayed nanoparticles onto the glass substrate. Samples were scanned in contact mode and at room temperature (XE-100E SPM System from PSIA) using a silicon chip with force constant of 0.6 N/m and resonance frequency of 75 kHz. Images were taken with on-line filtering and subsequently processed by flattening to remove the background slope (XEI version 1.6 software).

Ag sprayed samples were characterized morphologically by Focused Ion Beam technique, FIB, (DualBeam Helios Nanolab 600 from FEI). AFM analysis were unsatisfactory because the size of the Ag nanoparticles (5-10 nm, see chapter 2) was in the same range of the roughness of the glass substrate, so the nanoparticles were not clearly visible.

Adhesion and hardness have been investigated by Nanoindentation and nanoscratch techniques[1-7], which helped to identify all the mechanical properties of the thin films. Reduced Young's Modulus and absolute hardness

were calculated from nanoindentation loading and unloading curve (MTS Nanoindenter G200 XP Head); 12 indentation tests (MTS XP-Nanoindenter) were performed for each sample adopting the following test parameters: Berkovich indenter, 300 nm maximum penetration depth, 0,05 s-1 constant strain rate, 10 s hold at peak load for creep, 20 s hold at 90% for thermal drift correction. Oliver & Pharr method was adopted for hardness and elastic modulus evaluation.

The measured values underline how the coating characteristics ensure a lifetime long enough to guarantee the complete functionality they were planned for. The thin films presented in this study are for specials applications (see chapter 5): protection against corrosion or wear phenomena are out of the purpose of our work.

Measurements were applied to both TiO_2 and Ag coating, but just the glass substrates were considered because of their controlled roughness that is a useful standard. Plastics were not satisfying substrates for AFM analysis because of the irregularities that influence the final results, but they are also a too soft substrate for nanoindentations and nanoscratch test.

4.1 Morphology

Surface morphology was analysed in order to investigate the shape and size distribution of the flame sprayed nanoparticles.

Figure 4.1 shows the surface structure of the TiO_2 nanostructured film as obtained by AFM. It is very important to notice that the film present an extremely homogeneous distribution of quite monodisperse entities. The narrow size range of the nanoclusters, as observed in Figure 4.1(a) and 4.1 (b), shows that agglomeration phenomena did not take place before, during and after spraying. From figure 4.1(c) it is evident that the coating is formed by quasi-spherical clusters with average dimensions of about 200-400 nm. Moreover, it is evident that the flame spraying process induces a flattening of the original nanoparticle on the deposition substrate, in this case glass, which slightly deforms its original shape.
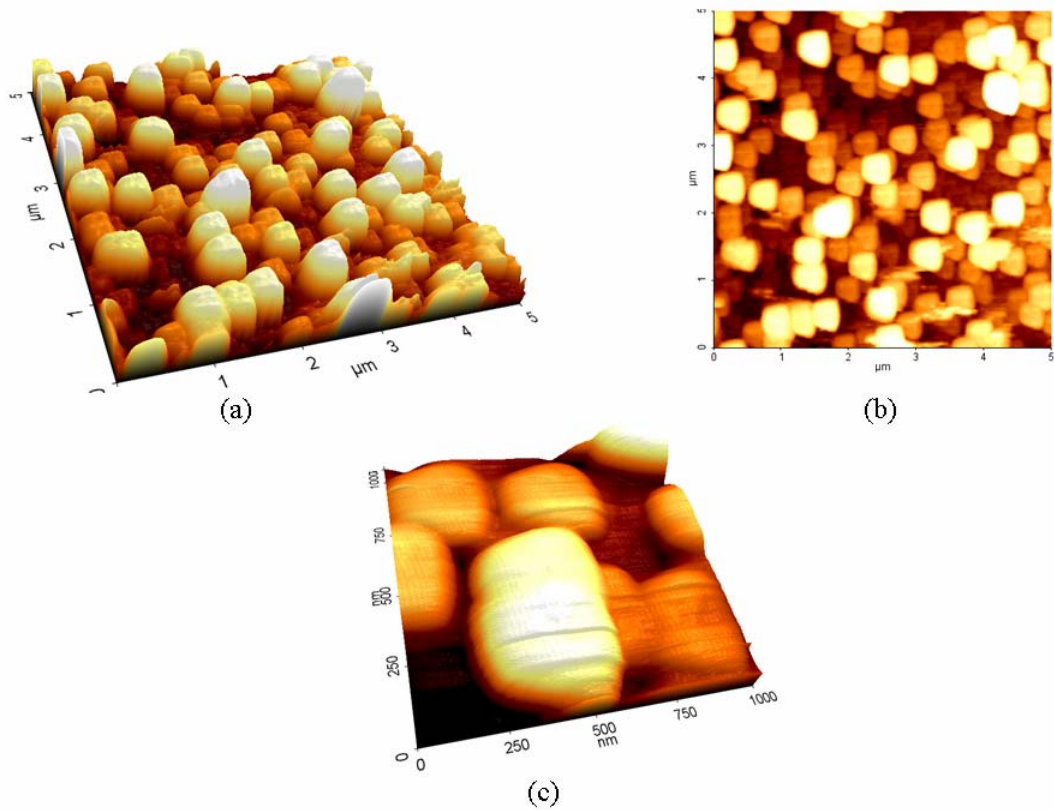
Fig. 4.1 AFM images of TiO2 film deposited onto glass obtained by flame spraying of suspension (a) 3D representation; (b) topography; (c) 3D representation at higher magnification.

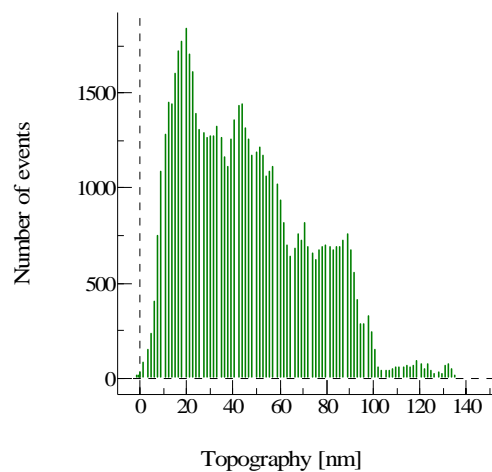|	
RMS roughness	26,6048
Minimum Value	0
Maximum Value	150,073
Peak to peak	150,073
Roughness Average	22,0212
Average height	47,4479
Surface skewness	0,6091
Surface kurtosis	2,7146
Plan offset	0
Ironed surface (m2)	26,6378

Fig. 4.2 Roughness analysis (nm) of the TiO2 sprayed glass

The figure 4.3 shows an AFM images of a TiO_2 deposited glass sample sprayed with high temperature conditions (see chapter 3). No evident changes in the morphology are observable, also if the roughness analysis value are slightly different. It is quite obvious considering that the deposited particles are ceramic oxides with a high melting point (1870 ºC). The consequences are different when the deposited particles are metals such as Ag (melting point 962 ºC). Figure 4.5 represents AFM images of an Ag sprayed sample in high temperature conditions: it is visible how on the bottom of the deposit some particles are partially dissolved.
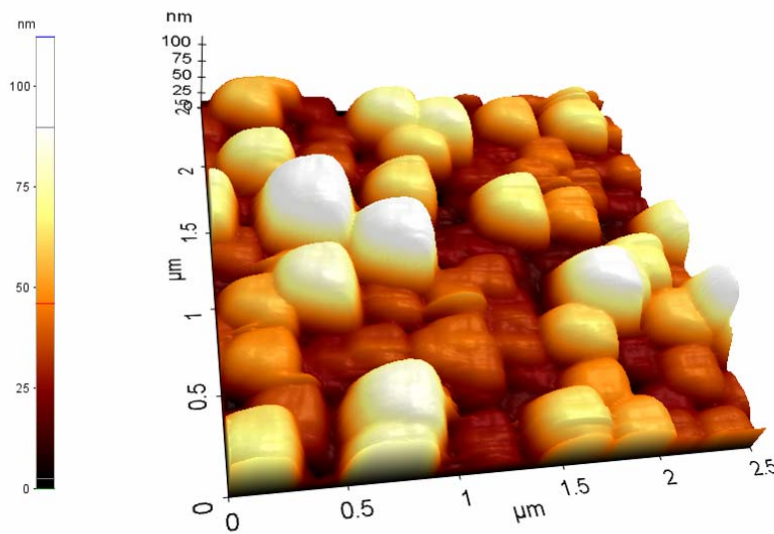

Fig. 4.3 AFM image of TiO2 sprayed glass in high temperature conditions

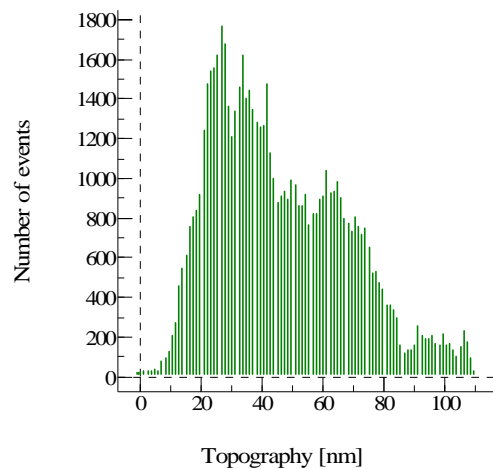|	
RMS roughness	22,1075
Minimum Value	0
Maximum Value	115,103
Peak to peak	115,103
Roughness Average	18,3972
Average height	47,6828
Surface skewness	0,5978
Surface kurtosis	2,7015
Plan offset	0
Ironed surface (m2)	6,6089

Fig. 4.4 Roughness Analysis (nm) TiO2 sprayed glass in high temperature conditions

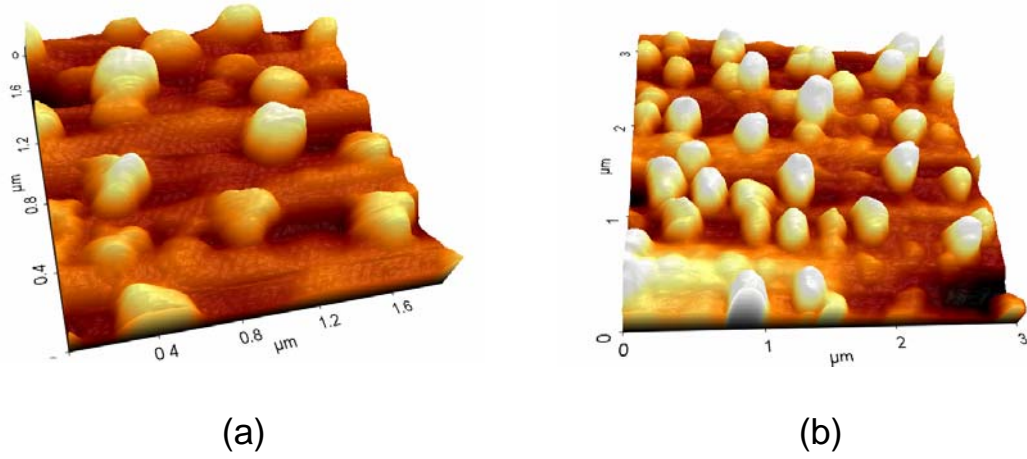(a)   (b)

Fig. 4.5 AFM image of Ag coated glass, sprayed in high temperature conditions
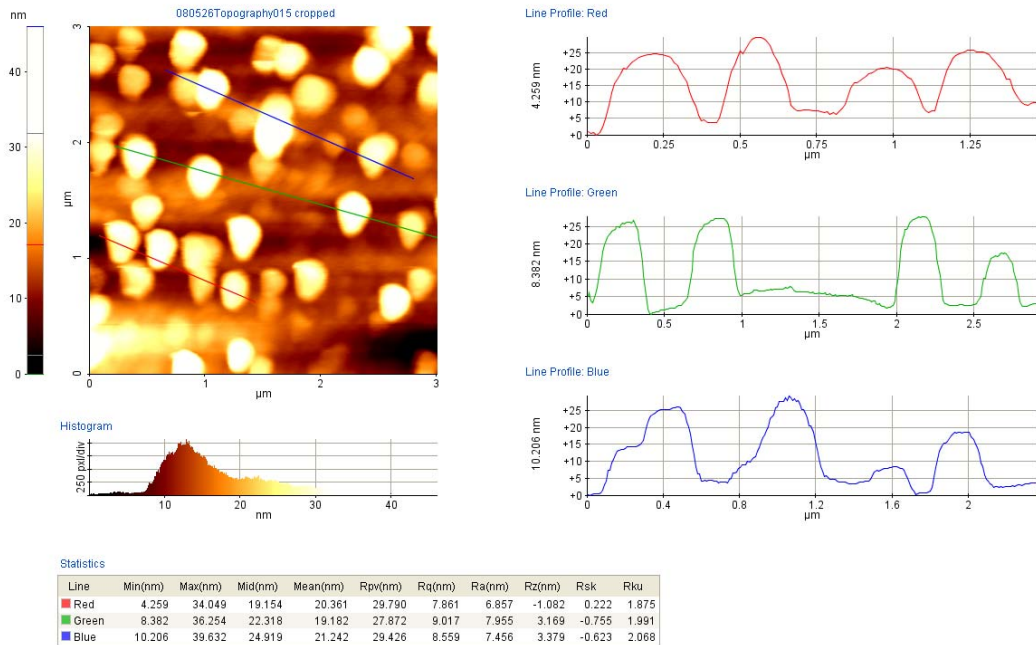

Fig.4.6   Line profile analysis of the Ag sprayed glass (high temperature condition)
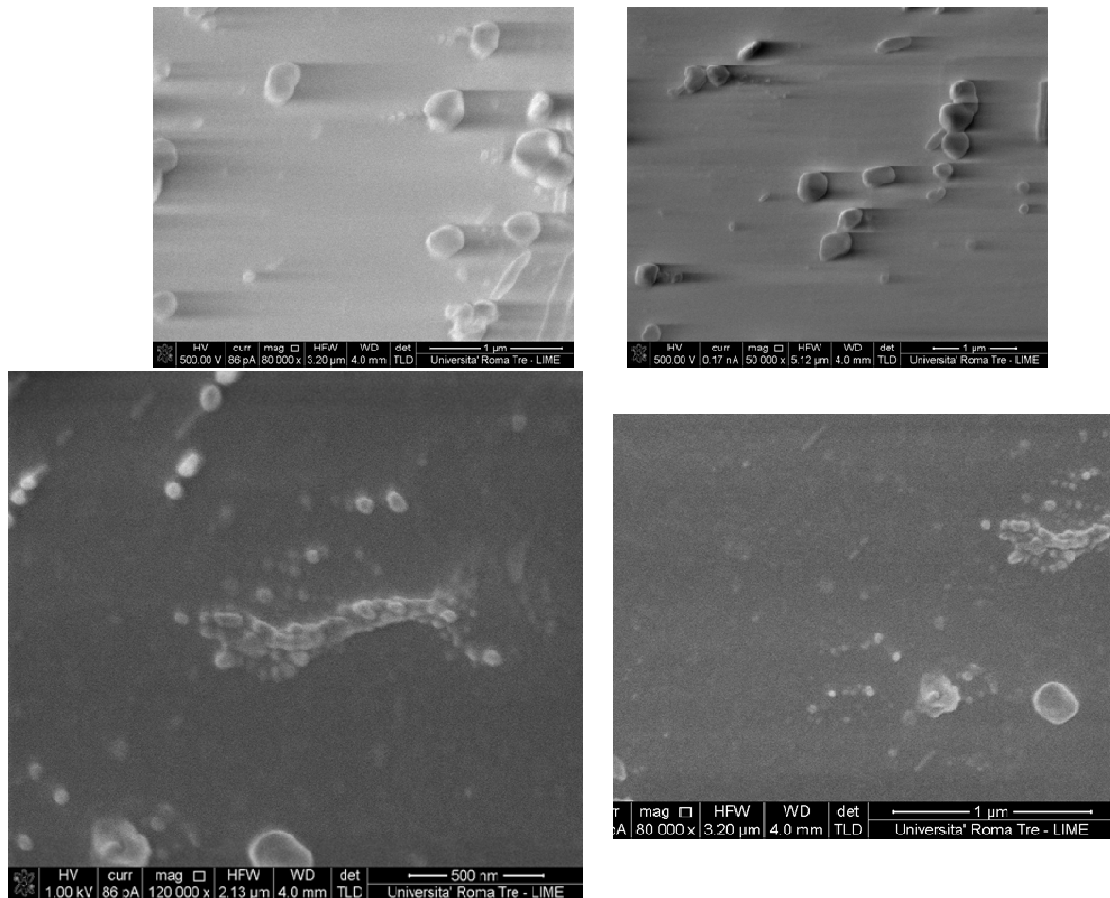
Fig.4.7 Morphology: FIB images of the sprayed Ag glass sample

Figure 4.7 shows the morphology of Ag sprayed samples deposited with low temperature conditions. From the FIB images in figure 4.7, it is observable how more particles are identifiable in the picture with higher magnification than in the others pictures, with lower magnification. It is understandable because of the very small size of the sprayed Ag nanoparticles. (about 5nm as visible from TEM images, chapter 2). It means that the nanoparticles generally keep their initial dimension with few cluster of bigger size.

4.2 Mechanical properties of the sprayed thin films

Next results are related to samples with different thickness (time of deposition of 10 or 30 minutes).

Scratch test results are related to the same samples characterized morphologically by AFM (figure 4.1 and figure 4.5) samples obtained by deposition onto glass substrate and time of deposition of 10 minutes.
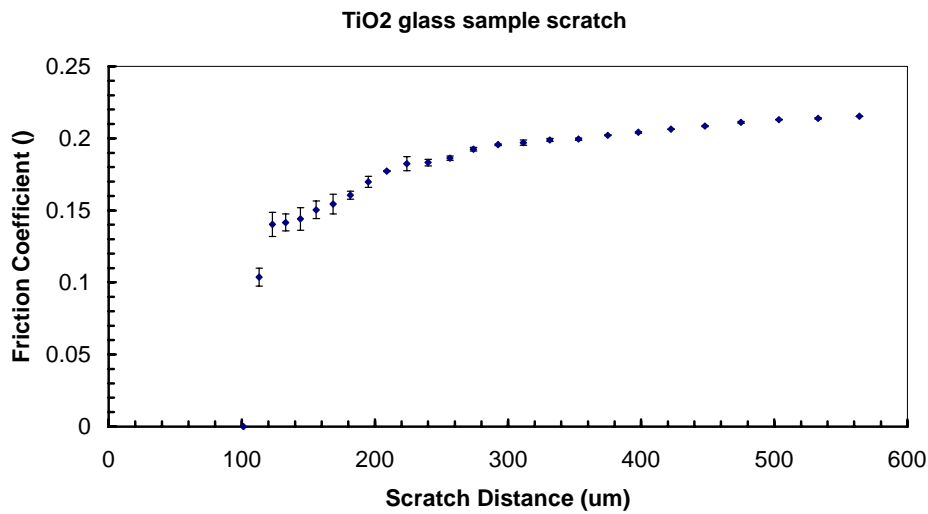
Fig. 4.7 Results of nanoscratch test with sprayed TiO_2 glass sample
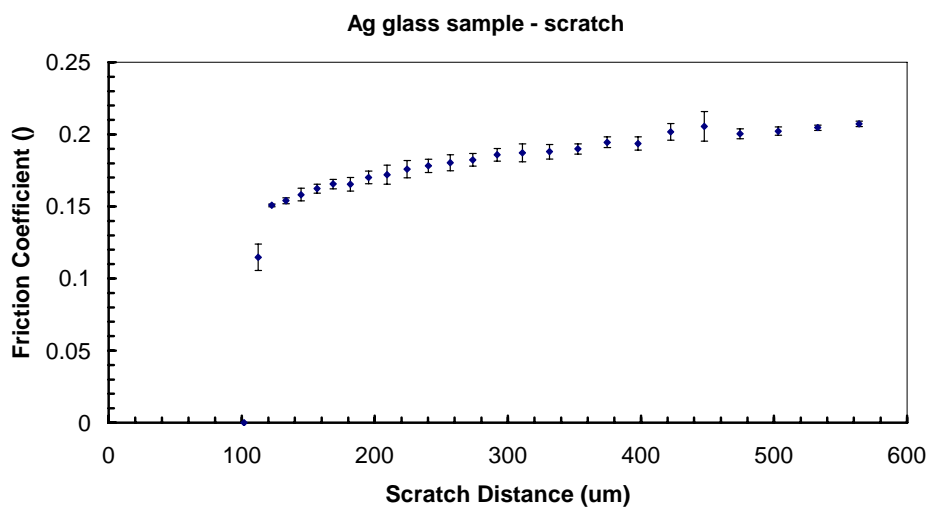
Fig. 4.8 Results of nanoscratch test with sprayed Ag glass sample

The graph in figure 4.10 shows the comparison between two different measure of the same TiO2 sprayed glass and an uncoated glass to underline the different between the two samples. The same parallel is represented in the figure 4.11 for Ag deposited glass.

Fig. 4.9 Fraction of scratch track in TiO2 thin film

Fig. 4.10 Friction coefficient vs. Scratch distance graph

Comparison between uncoated glass and TiO_2 deposited glass
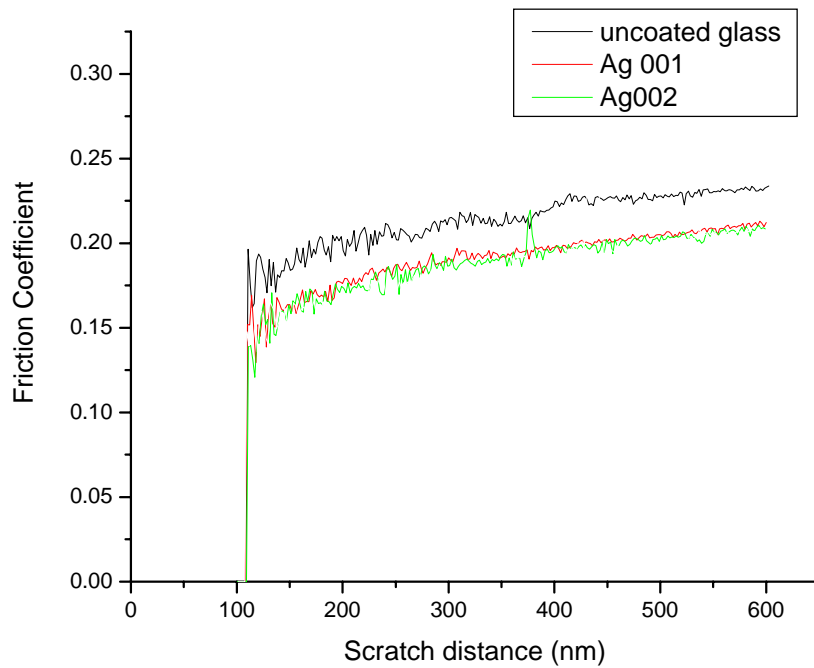
Fig. 4.11 Friction coefficient vs. Load Applied graph

Comparison between uncoated glass and Ag deposited glass

Table 4.1 Scratch test results

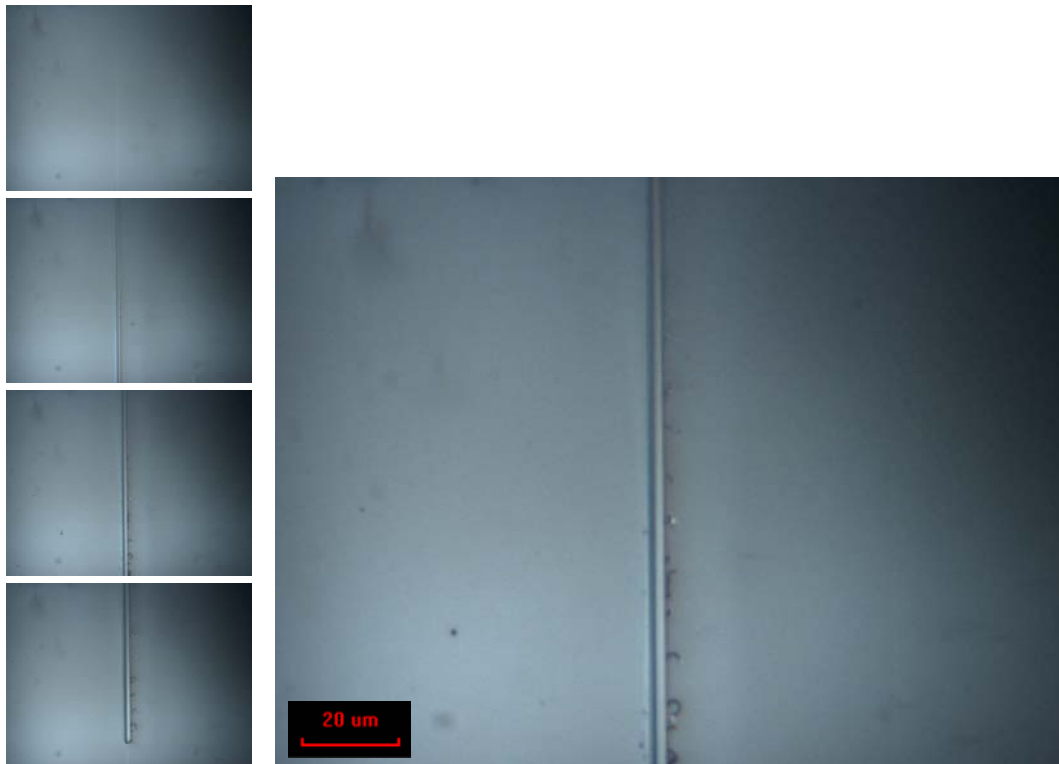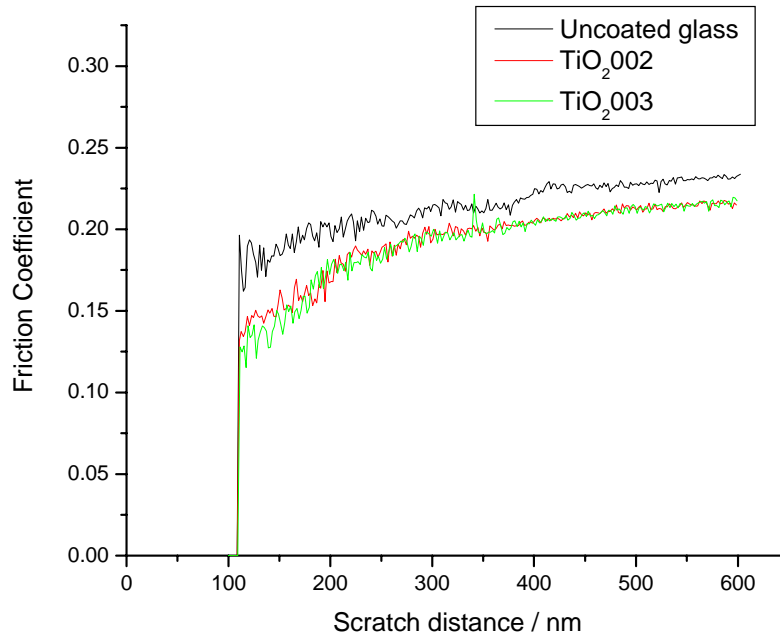| Test	Critical Load	Penetration Depth At Critical Load	Scratch Width	Total Height Of the Groove	Residual Scratch Depth	Pile Up Height
	mN	nm	um	nm	nm	nm
TiO2	8.344	215.501	30.45	178.967	110.036	68.931
Ag	0.021	19.768	55.1	540.973	463.769	77.204

About Nanoindentation test, deposition time of 10 minutes produced a film inadequate to ensure the indentation of the coating: some of the measurements related to the 10 minutes deposited samples show how the thickness of the coating was too thin to guarantee to indenter the deposited particles instead of the glass substrate. It is obviously a consequence of the extremely thin film thickness. Measurements were repeated and reported in next figures with thicker samples obtained with deposition time of 30 minutes.
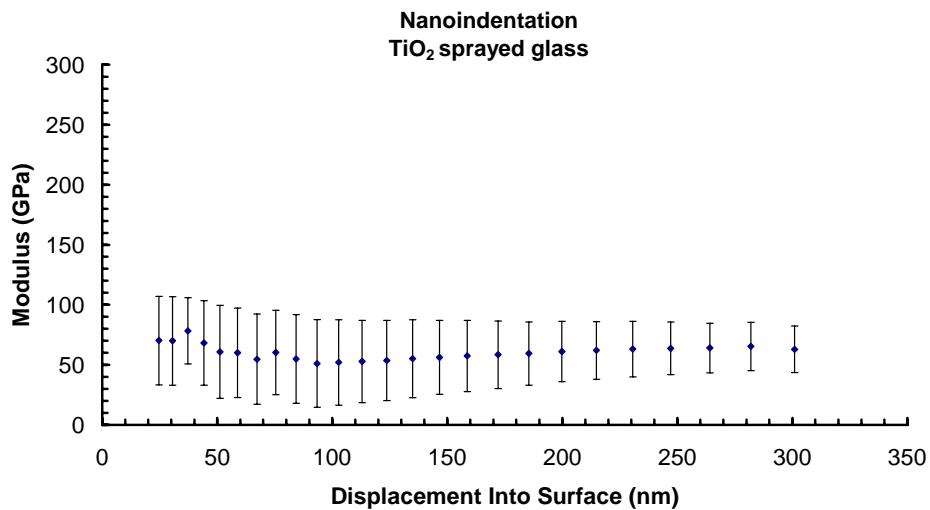
Fig. 4.12 Young's Modulus of the TiO_2 sprayed glass

**Nanoindentation
TiO2 sprayed glass sample**
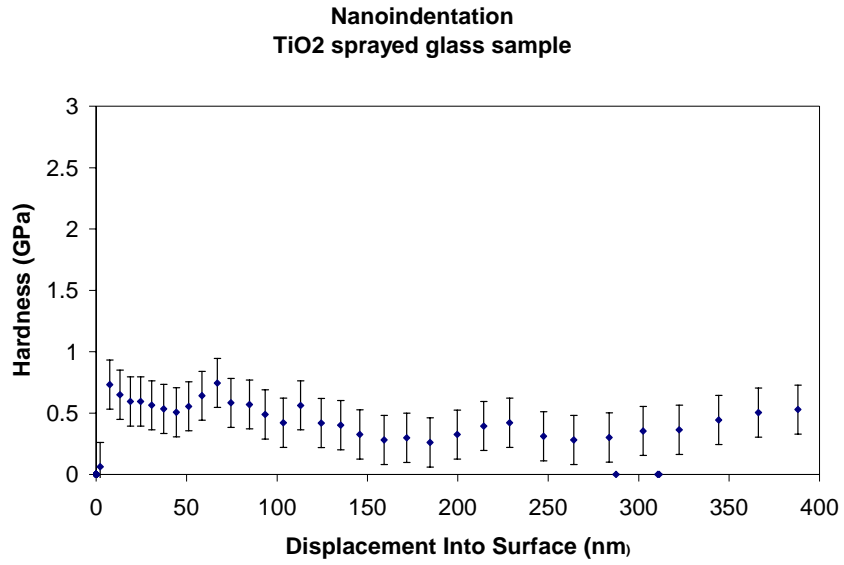
Fig. 4.13 Hardness of the TiO$_2$ sprayed glass

**Nanoindentation
Ag sprayed glass**
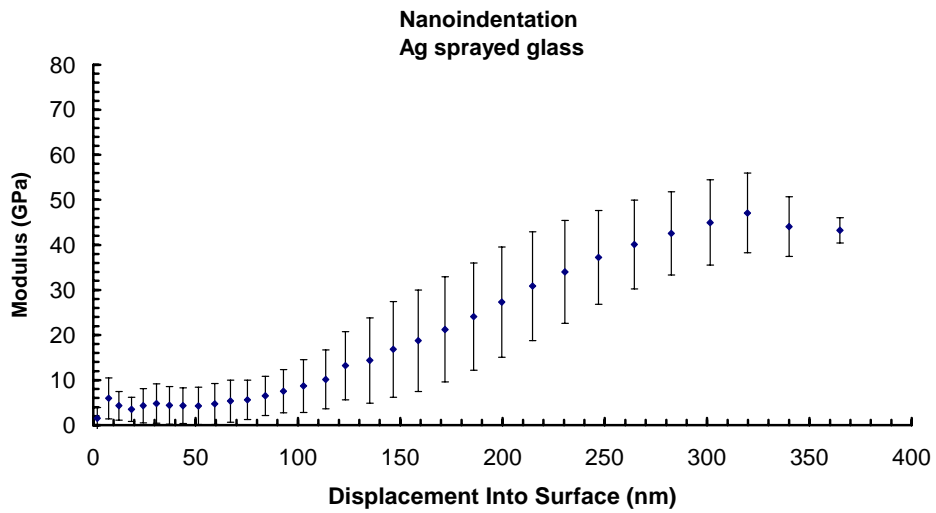
Fig. 4.14 Young's Modulus of the Ag sprayed glass
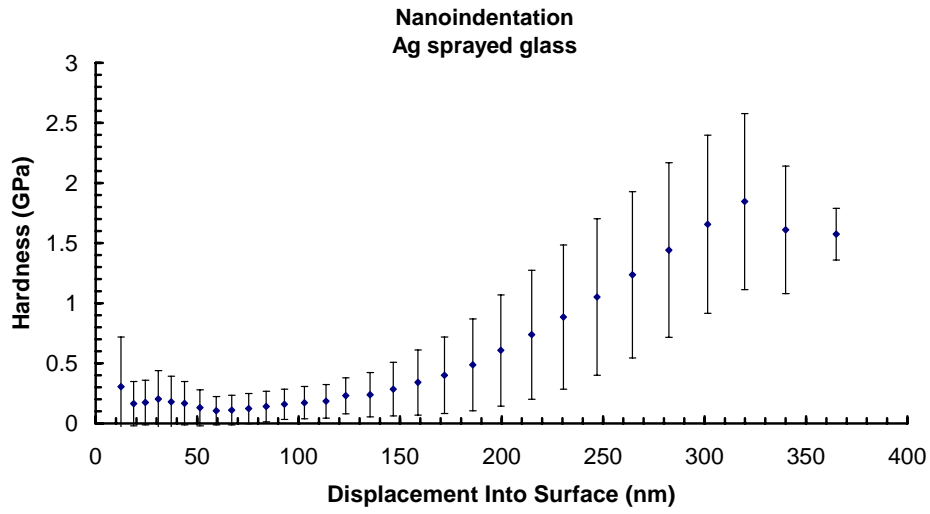
Fig. 4.15 Hardness of the Ag sprayed glass

The above data about the mechanical properties are not comparable with other data from literature, because of the particular characteristics of the studied thin films.

Table 4.1 Nanoindentation test results

Test	*E* Average	H Average
	GPa	GPa
TiO$_2$	51.437	4.636
Ag	4.574	0.12
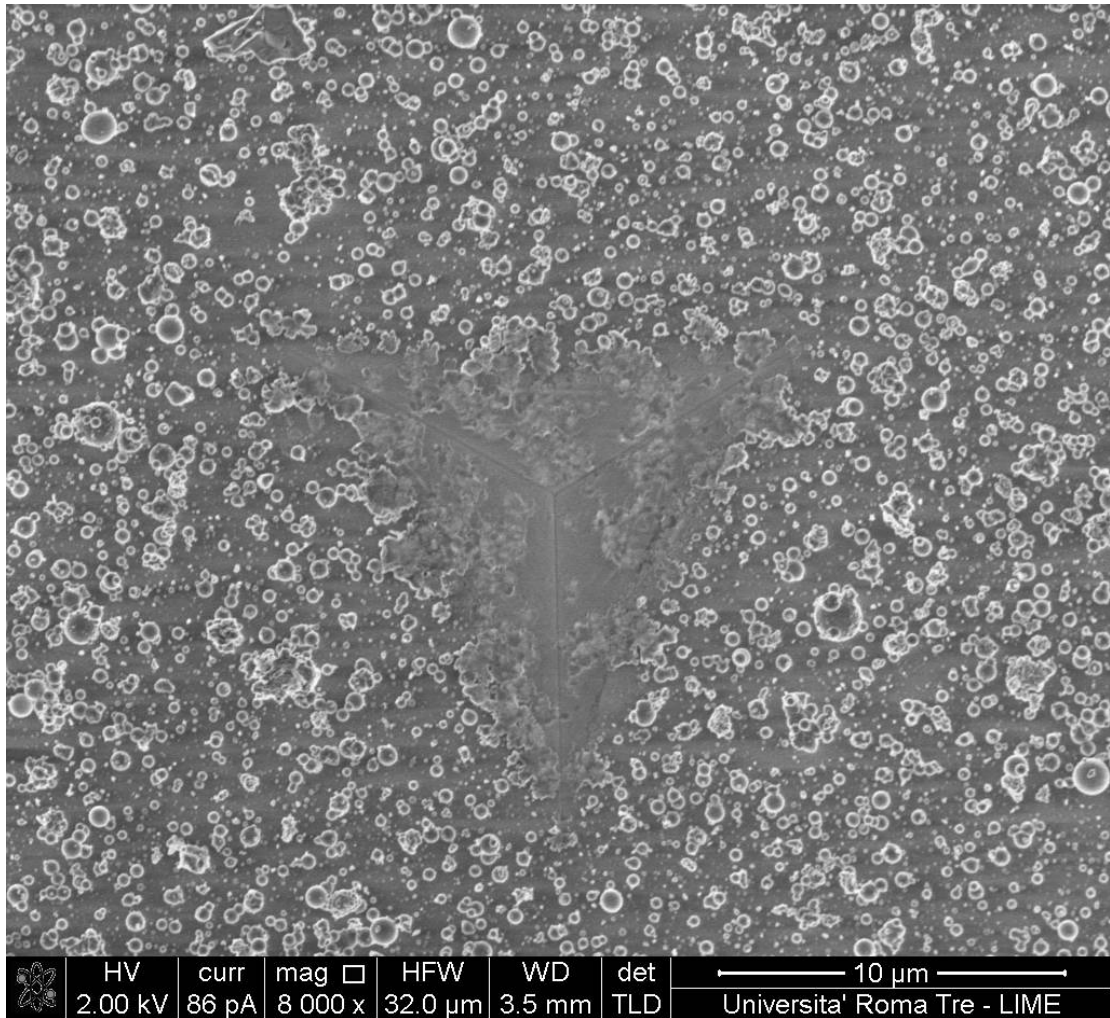
Fig. 4.16 FIB image of a nanoindentation trace on a TiO$_2$ sprayed glass sample

The resulting deposited materials present peculiar properties associated to surface phenomena such as catalytic activities or antibacterial properties, while protection against wear or corrosion is not of interest. Because of the importance of the exposed surface, the research aided to enhance its value, improving the performances of resulting sprayed materials.

Figure 4.16 shows the FIB image of the trace produced by the nanoindentation tip in a TiO$_2$ sprayed samples. It is visible the structure of the deposited thin film, underlining its high porosity. It is understandable because the nanoindentation results are represented with a so high standard deviation. While it is required for its planned applications, it is also a problem for determining the mechanical properties.

The structure of the sprayed coating is not useful for this kind of measurement because of the dislocation burst caused by the nanoindenter tip during the test[8]. At the some time it is a confirmation of the high porosity and of the high value of exposed surface of the sprayed coatings, which are desired characteristics of the structure of the films for the application of interest discussed in chapter 5.

REFERENCES

[1] Stoneham, Ramos, Sutton - *How do they stick together? The static and dynamic of interfaces* (1992)

[2] X. Li, B. Bhushan *Materials Characterization* 48 (2002) 11–36

[3] L. Huang, J. Lu, M. Troyon, *Surface & Coatings Technology* 201 (2006) 208–213

[4] A. Gouldstone, N. Chollacoop, M. Dao, J. Li, A. M. Minor, Y. L. Shen *Acta Materialia* 55 (2007) 4015–4039

[5] Y. Gil Junga) and Brian R. Lawn*, J. Mater. Res.*, Vol. 19, No. 10, Oct 2004

[6] W. Zhang, W. Liu, C. Wang, *Wear* 253 (2002) 377–384

[7] T. H. Fang, W. J. Chang, C. Weng, *Materials Science and Engineering* A 430 (2006) 332

[8] Cao et al., Materials Science and Engineering A 427(2006) 232-240

Chapter 5

Functional properties of the sprayed thin films

In this chapter are presented the results related to the peculiar properties of the elements of the deposited nanoparticles, Ag and TiO_2. Ag is interesting because of its antibacterial activity, but also because of its catalytic action such as many other metal elements.

TiO_2 is actually an important subject of several studies because of its photocatalytic activity. Since the first article by Fujishima and Honda[1], many research groups have investigated the photocatalytic splitting of water into hydrogen and oxygen under the influence of light and the other photoinduced properties. TiO2 mediated photocatalytic reactions are gaining nowadays more and more importance and this is reflected in the increasing number of publications that deal with theoretical aspects and practical applications of these reactions.

The present work is focused to validate the properties of the nanostructured thin films by Flame Spraying of colloidal suspension, but mainly TiO2 films have been considered because of their numerous and interesting applications.

5.1 TiO$_2$ photoinduced process

TiO$_2$ is characterized by the presence of photoinduced phenomena. These are illustrated in figure 5.1. All these photoinduced processes originate from the semiconductor band gap. When photons have a higher energy, than this band gap, they can be absorbed and an electron is promoted to the conduction band, leaving a hole in the valence band. This excited electron can either be used directly to create electricity in photovoltaic solar cells or drive a chemical reaction, which is called photocatalysis. A special phenomenon was recently discovered: trapping of holes at the TiO$_2$ surface causes a high wettability and is termed 'photoinduced superhydrophilicity'.

All photoinduced phenomena involve surface bound redox reactions.
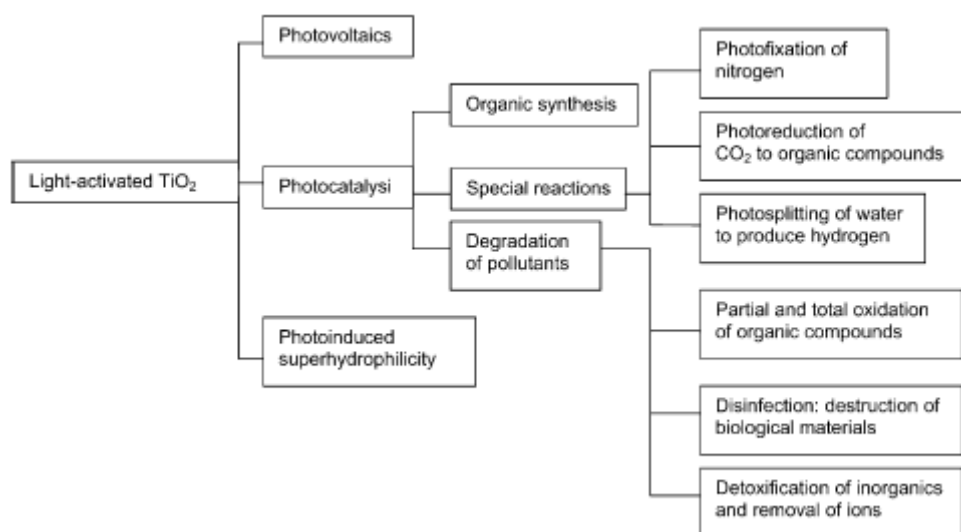
Fig. 5.1 Photoinduced process on TiO$_2$

The self-cleaning effect of TiO$_2$ surface arises from the fact that dirt and grim are washed away on superhydrophilic surfaces. Since water droplets will tend to run off, the surface will also dry very quickly. Complementarily, such materials will not fog, since fogging is characteristic to surfaces with contact angles higher than 20º [2,3].

Additionally, the TiO$_2$ surface can also destroy organic deposits via Photocatalytic degradation, which is an additional self-cleaning action.

For an efficient utilization of near-UV light, either from the sun or artificial sources, the TiO_2 coating should be thick, i.e., typically >1 lm [4], because thinner films have a low absorbance in this region (i.e., 320 > k > 380 nm). They should also exhibit clarity, mechanical robustness, and high photoactivity.

Some self-cleaning and anti-fogging applications are presented in Table 5.1.

Table 5.1 Application of TiO_2 self-cleaning and anti-fogging properties

Function	Material	Application
Cleaning easiness	Materials for road	Tunnel lighting
		Tunnel wall
	Materials for house	Kitchen parts, bathroom and interior furnishing
	Materials for electric and electronic devices	Computer display, electric wires
	Daily necessities and consumer products	Tableware, kitchenware
Self-cleaning by rainfall	Materials for road	Traffic sign, lighting, soundproof wall, guardrail, decorative laminate panel
	Materials for buildings	Exterior tiles, siding boards, curtain wall, painted steel plate, aluminium panel, building stone, crystallized glass, glass film, window, sash, screen door, gate door, sun parlour, veranda parts
	Materials for electric and electronic devices	Upper glass of a solar cell, insulator
	Materials for vehicles	Painting and coating of vehicles, outside of windows, headlight
Anti-fogging properties	Materials for road	Road mirror
	Materials for buildings	Bathroom mirror
	Materials for stores	Refrigerated showcase
	Materials for vehicles	Inside window, glass film, helmet visor
	Material for optical instrument	Optical lens
	Daily necessities and consumer products	Spray of anti-fogging coat, anti-fogging film
Accelerated drying Preventing dewdrops forming	Materials for buildings	Toilet, window, bathroom
	Materials for electric and electronic devices	Heat exchanger of air conditioner, high voltage cable
	Materials for vehicles	Sideview mirror, rearview mirror, windshield of le, sidemirror film

The most active field of TiO_2 photocatalysis is the photodegeneration of organic compounds. TiO_2 has become a photocatalyst in environmental decontamination for a large variety of organics, viruses, bacteria, fungi, algae, and cancer cells, which can be totally degraded and mineralized to CO_2, H_2O, and harmless inorganic anions. This performance is attributed to highly

oxidizing holes and hydroxyl radicals (HO⁻) that are known as indiscriminate oxidizing agents[5,6]. The oxidizing potential of this radical is 2.80 V, being exceeded only by fluorine.

All photoinduced phenomena are activated by an input of super-band gap energy to the semiconductor TiO_2. Absorption of a photon with enough energy leads to a charge separation due to an electron promotion to the conduction band and a generation of a hole (h_+) in the valence band. The subsequent mode of action of the photogenerated electron–hole pair (e^-–h^+), determines which of the phenomena is the dominant process, because even if they are intrinsically different processes, they can and in fact take place concomitantly on the same TiO_2 surface. If the electrons are used in an outer circuit to perform work, we speak about a photovoltaic solar cell.

Photocatalysis is a well-known process and is mostly employed to degrade or transform (into less harmful substances) organic and inorganic compounds and even microorganisms.

The recently discovered wettability, termed by Fujishima[2] as 'superhydrophilicity', presents a large range of applications in cleaning and anti-fogging surfaces. The detailed material properties required for enhanced efficiency are different from each other. For enhanced photocatalysis, deep electron traps and high surface acidity are needed to lengthen the lifetime of photoexcited electrons and holes and to ensure better adsorption of organic substances on the surface. Meanwhile, low surface acidity and, most of all, a large quantity of Ti^{3+} is essential for hydrophilic surface conversion.

5.1.1 Photocatalysis

Overall, photocatalyzed reactions may be summarized as follows:

$$(Ox_1)_{ads} + (Red_2)_{ads} \xrightarrow[h\nu > E_g]{semiconductor} Red_1 + Ox_2$$

(5.1)
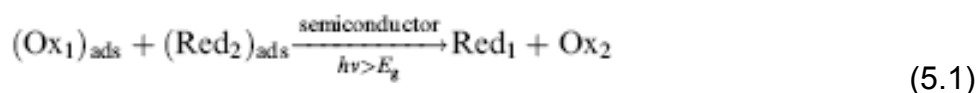
Depending on whether the sign of the change in Gibbs free energy (ΔG^0) of reaction (5.1) is negative or positive, the semiconductor-sensitized reaction

may be an example of photocatalysis or photosynthesis, respectively[7]. For a semiconductor photocatalyst to be efficient, the different interfacial electron processes involving e^- and h^+ must compete effectively with the major deactivation processes involving e^--h^+ recombination, which may occur in the bulk or at the surface (figure 5.2).
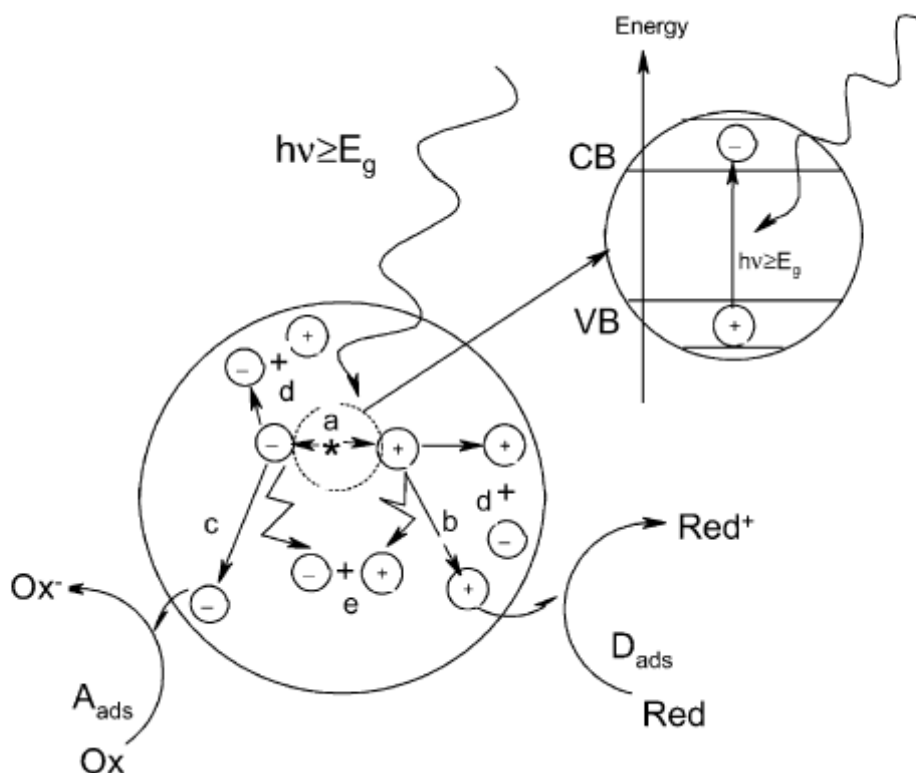
Fig. 5.2. Main processes occurring on a semiconductor particle:
(a) electron–hole generation;(b) oxidation of donor (D); (c) reduction of acceptor (A);
(d) and (e) electron–hole recombination at surface and in bulk, respectively.
Picture taken from Mills A, Le Hunte S. J Photochem Photobiol A: Chem 1997;108:1.

Ideally, a semiconductor photocatalyst should be chemically and biologically inert, photocatalytically stable, easy to produce and to use, efficiently activated by sunlight, able to efficiently catalyze reactions, cheap, and without risks for the environment or humans. Titanium dioxide (with sizes ranging from clusters to colloids to powders and large single crystals) is close to being an ideal photocatalyst, displaying almost all the above properties. The single exception is that it does not absorb visible light.

Both crystal structures, anatase and rutile, are commonly used as photocatalyst, with anatase showing a greater photocatalytic activity[8,9] for most reactions.

It has been suggested that this increased photoreactivity is due to anatase's slightly higher Fermi level, lower capacity to adsorb oxygen and higher degree of hydroxylation (i.e., number of hydroxy groups on the surface)[9,10,11,12].
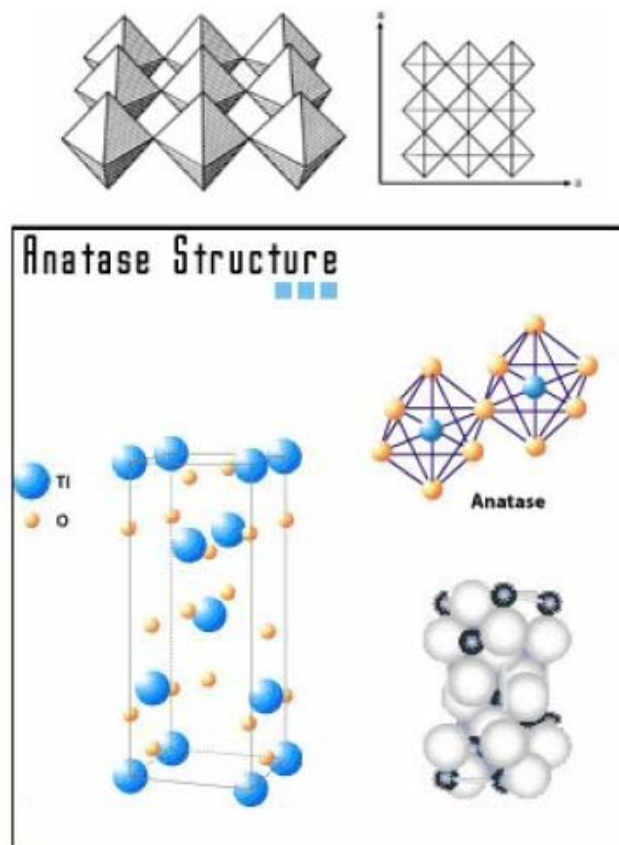
Fig. 5.3 Anatase crystalline structure
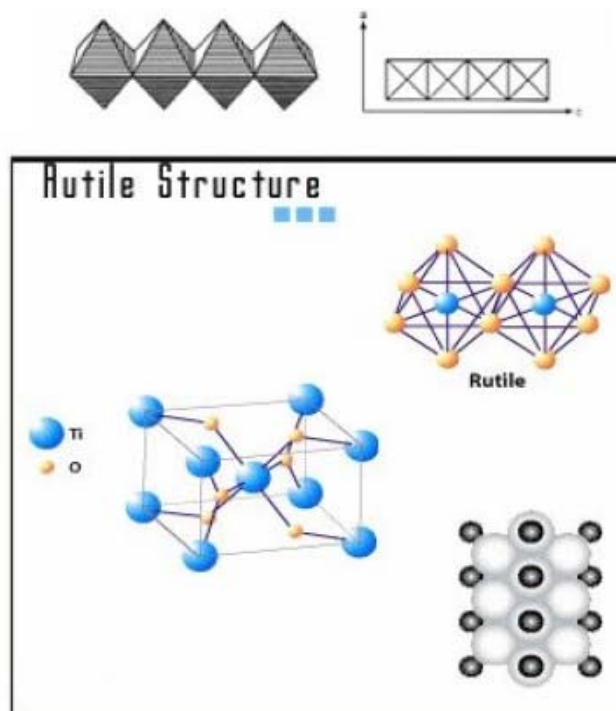
Fig. 5.4 Rutile crystalline structure

Reactions in which both crystalline phases have the same photoreactivity[13] or rutile a higher one[14,15] are also reported. Furthermore, there are also studies which claim that a mixture of anatase (70–75%) and rutile (30–25%) is more active than pure anatase[16,17,18].

The detailed mechanism of the photocatalytic process on the TiO_2 surface is still not completely clear, particularly that concerning the initial steps involved in the reaction of reactive oxygen species and organic molecules.

5.1.2 Photocatalitic activity of the TiO$_2$ thin films obtained by Flame Spraying of Colloidal Suspension

Photocatalytic activity was evaluated by photodegradation of organic compounds, phenol and methylene blue aqueous solutions.

Kinetics parameters were studied with methylene blue degradation, while phenol degradation was studied just qualitatively because of the complex kinetic mechanism in wet oxidation of this compound, that involves several reaction intermediates.

The samples tested were sprayed with a nanoparticle suspension prepared staring from a mixture of both anatase and rutile. In order to confirm that the deposited TiO$_2$ maintained the photocatalytic activity proper of the original nano-powder, this property was evaluated by photo-induced oxidation of methylene blue aqueous solution.

Methylene blue (Sigma-Aldrich) was dissolved in water (Millipore Milli-Q purification system, R>18 MΩ.cm) in order to have about 4.5 $\times$ 10^{-6} M methylene blue solution. 1.5 ml of this solution were transferred into a quartz cell (length, 1 cm) together with the TiO$_2$ coated sample and continuously exposed to an arc lamp system equipped with a 30 W Xe lamp. A cut-off filter (Oriel) ensured that only photons having a wavelength below 390 nm were transmitted to the sample. The time evolution of methylene blue concentration was monitored by a Lambda 5 Perkin-Elmer UV Spectrometer.

Both glass and PET coated samples were tested together with an uncoated glass to verify the degradation efficiency of the TiO$_2$ coated samples. Figure 5.5 shows the concentration level as function of the exposure time for both the TiO2 sprayed sample, glass and PET, and for the uncoated glass sample.
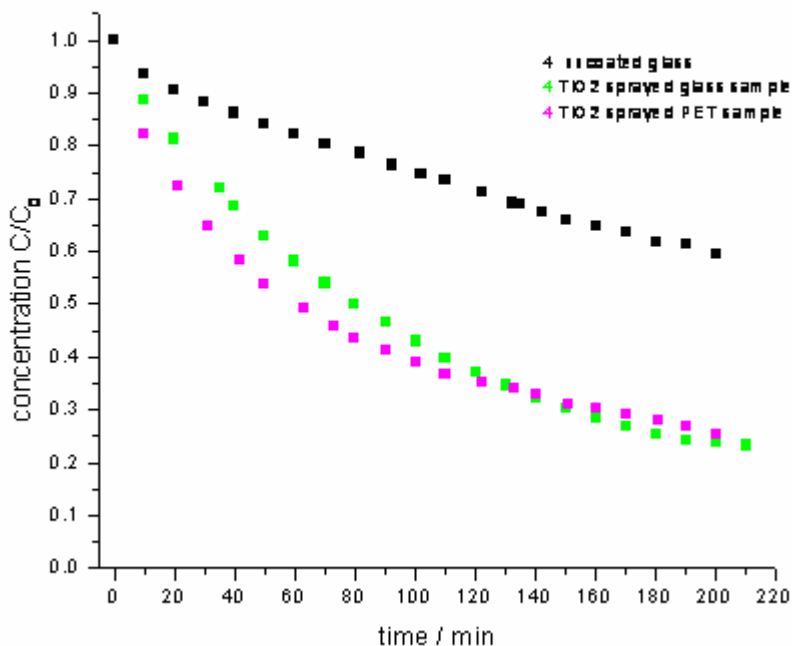
Fig. 5.5 The time evolution of methylene blue concentration, in presence of
(a) TiO2 coated glass (b) TiO2 coated PET (c) uncoated glass.

The methylene blue degradation is clearly accelerated when the TiO_2 coating is present onto the sample.

Moreover it is observable a slightly different behaviour in the concentration trend between the glass sample and the PET sample. It could be determined by the different temperature of deposition, since the two samples present the same deposition time and the same nanoparticle concentration in the suspension. While glass sample was deposited at about 450 °C, deposition onto the PET sample was carried out at about 80°C. Both the temperature are below the rutile-anatase transition temperature (915 °C), and the resident time for the particles in the flame, where the temperature reach a higher value than the request one, should be short enough to be not significant.

The differences in the kinetic trends could be due to two causes. The first one is the slightly different roughness values characterizing the morphology of the two samples as revealed from AFM images (chapter 4). However the kinetic of photocatalysis show how the reaction in presence of PET substrate is faster than the other at the beginning of the degradation: it could be

explained with the different amounts of rutile and anatase in the two samples. Both anatase and rutile are active in the photocatalytic reaction, but a difference in the kinetics could be observed[14,15]. The different performance of the two samples are probably connected with the partial change in the crystalline state that could happen after the nanoparticles arrive at the substrate surface. The time the nanoparticles are exposed to the so-called substrate temperature (450ºC and 70ºC as from data registered) and to the higher temperature region could help the beginning of the anatase – rutile transition also if only few anatase fractions of the original mixture arrive to convert to rutile.

The graph reported in figure 5.6 highlights the kinetic difference just referred. It is built up by subtraction of the time evolution of methylene blue concentration with coated samples from the one with uncoated glass. Thus it explains/represent the change in the concentration due to the photocatalytic activity, since the regular degradation of methylene blue, when exposed to light, is considered in the uncoated sample.
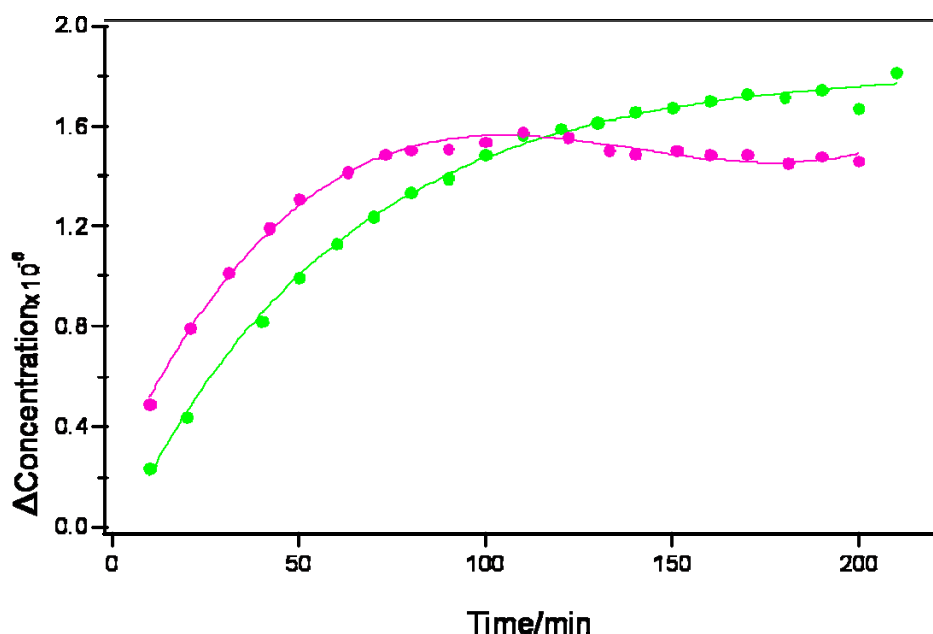
Fig. 5.6   Subtraction between the time evolution of methylene blue concentration with the coated samples and the time evolution with the uncoated one.

Data collected in the graph of figure 5.6 were fitted following a first-order process.

It is in agreement with the kinetics behaviour of photocatalytic oxidation of several dyes over titanium dioxide obey the Langmuir-Hinshelwood kinetics given by equation 5.2:

$$r = -\frac{d[MB]}{dt} = -\frac{kK[MB]}{1+K[MB]}$$

(5.2)

where r is the rate of dye mineralization, k is the rate constant, *[MB]* is the methylene blue concentration, and K is the adsorption coefficient[19].

However, when the concentration of substrate is in the scale of millimoles, an apparent first-order model can be assumed[19]:

$$r = -\frac{d[MB]}{dt} = k'[MB] = kK[MB]$$

(5.3)

Integration result in Equation 5.4 or 5.5:

$$[MB] = [MB]_o\, e^{-k't}$$

(5.4)

$$\ln\left(\frac{[MB]_0}{[MB]}\right) = -kKt = -k't$$

(5.5)

where the apparent rate constant *k'* is in units of time^{-1}. The assumption of a pseudo-first order model was used in several studies to characterize the effect of different experimental conditions on the degradation rate[20,21].

The kinetics values that result from the fitting are listed in the table below.

Table 5.2 kinetics of photodegradation of methylene blue

	TiO$_2$ sprayed glass sample	TiO$_2$ sprayed PET sample
k' (min^{-1})	0.016233± 0.00625	0.038856 ± 0.00212
chi-square fitting	1.95642e-14	3.7092e-14

The values of the apparent rate constant are comparable with data available[21]. It means that flame spraying of colloid dispersion produce no loss of photocatalytic activities in the deposited TiO$_2$ thin films.

Photochemical activity of the selected samples was tested also with the photo-induced oxidation of phenol aqueous solution.

Phenol (>99.5%, Sigma-Aldrich) was dissolved in water (Millipore Milli-Q purification system, R>18 MΩ.cm) in order to have a 3 × 10^{-4} M phenol solution. 1.5 ml of this solution were transferred into a quartz cell (length, 1 cm) together with the TiO$_2$ coated sample and continuously exposed for 8hr to an arc lamp system equipped with a 150 W Xe lamp. A cut-off filter (Oriel) ensured that only photons having a wavelength below 390 nm were transmitted to the sample. The time evolution of phenol concentration was monitored by a Lambda 5 Perkin-Elmer UV Spectrometer.
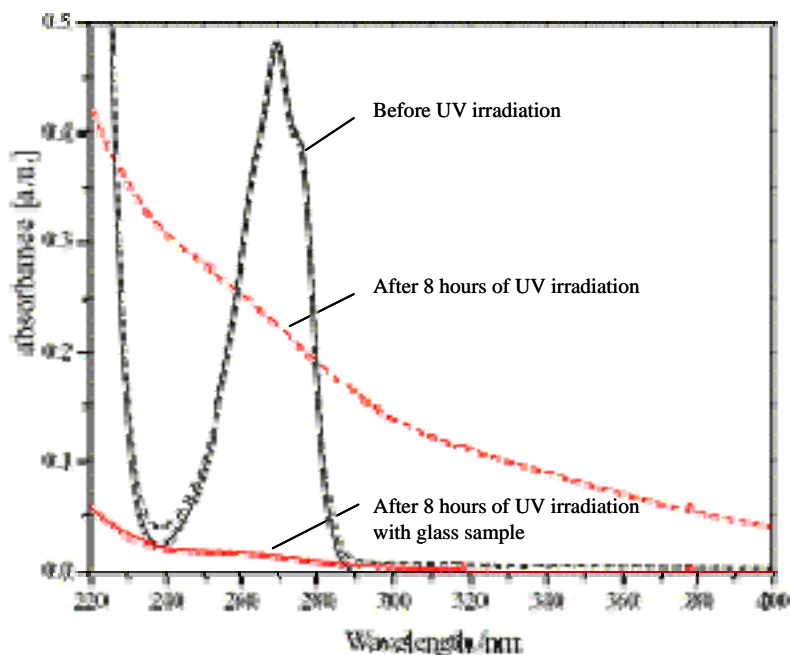
Fig. 5.7   Absorbance of phenol solution measured before and after 8 hours of UV exposure with TiO_2 deposited sample or with uncoated glass.

Figure 5.7 shows the comparison between two series of UV absorption spectra of phenol concentration in the solution with TiO2 deposited sample or with uncoated glass added in solution during UV light irradiation. The spectra resulting after 8 hours of irradiation are clearly different. The phenol degradation is evidently accelerated when the TiO_2 coating is present onto the sample. In particular, the time evolution of UV absorbance evidences that after 8 hours of UV irradiation the decrease in the associated concentration is about 90%, instead of 50% obtained without TiO_2 deposited glass: the TiO_2 deposition causes a strong increase in the degradation efficiency (about 40%).

Photo-induced oxidation of phenol aqueous solution was tested only qualitatively because of the complex mechanism of reaction. Several intermediates were formed during the reaction that, overlapping the UV absorption spectra of the residual phenol solution, makes no possible the time monitoring of the phenol concentration and the consequential kinetic characterization.

5.1.3   Photoinduced hydrophilicity

UV illumination of TiO_2 may induce superhydrophilicity (i.e., photoinduced superhydrophilicity or PSH) across the surface that allows both water and oil to spread[2,22−25]. This photoinduced superhydrophilicity is accompanied by photocatalytic activity, as both phenomena have a common ground; so the surface contaminants will be either photomineralized or washed away by water. A possible application is self-cleaning windows.

Photoinduced superhydrophilicity involves reduction of Ti(IV) cations to Ti(III) by electrons and simultaneous trapping of holes at lattice sites (usually bridging oxygen) or close to the surface of the semiconductor. Such trapped holes weaken the bond between the associated titanium and lattice oxygen, allowing oxygen atoms to be liberated, thus creating oxygen vacancies. The subsequent dissociative adsorption of water at the site renders it more hydroxylated. An increased amount of chemisorbed –OH leads to an increase of Van der Waals forces and hydrogen bonding interactions between H_2O and –OH. Water can easily spread across the surface and hydrophilic properties will be enhanced[26,27] (figure 5.9). Water adsorption does not occur uniformly but produces an amphiphilic surface with alternating hydrophilic and oleophilic regions at the scale of several nanometers (usually <10 nm in size)[22].

The hydrophilic domains align along the bridging oxygen sites. The reduced sites can be reoxidized by air and the weakly bound hydroxyl groups reactively desorb (over some time, typically days in the dark) from the surface that returns to a more hydrophobic form.

The longer the surface is illuminated with UV light, the smaller the contact angle for water becomes (a contact angles close to zero mean that water spreads perfectly across the surface)[23,24]. The hydrophilicizing rate is also increased by repeated UV illumination cycles. This effect is remarkable on (0 0 1) rutile surfaces[28]. The crystal plane dependence can be attributed to differences in oxygen vacancy creation and to the degree of resultant structural distortion between (0 0 1) and (1 1 0) surfaces. This suggests that the hydrophilicizing process of TiO_2 surface is a kind of photocorrosion process[28].

As far as the geometry of the surface is concerned, the hydrophilic properties are known to be enhanced by fine surface roughness [26-30].

To improve the photoinduced superhydrophilic properties of TiO_2 films, doping (Al_{3+}, W_{6+})[31], nitruration ($TiO_{2\_x}N_x$)[32] and combining or mixing the TiO_2 with oxide partners or host oxides such as SiO_2 [33,34] or B_2O_3 [34] is attempted.
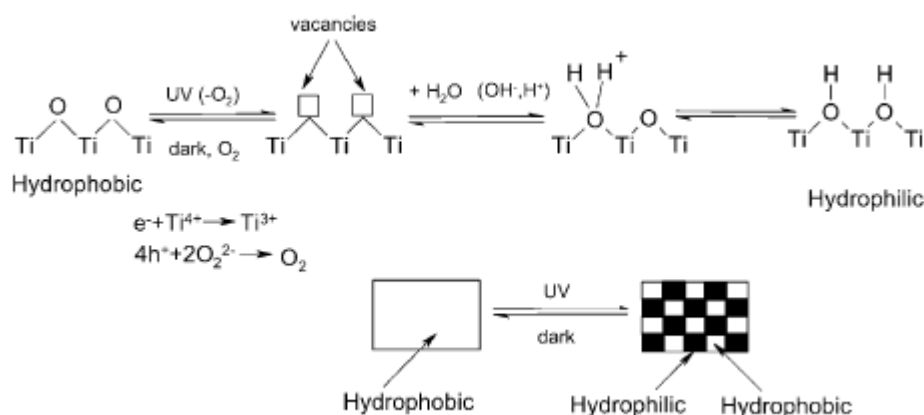
Fig. 5.8 Mechanism of photoinduced superhydrophilicity of TiO_2.

Photoinduced superhydrophilicity was found to be of primary commercial importance due to the anti-fogging and self-cleaning properties of the deposits. The technology is now being increasingly used in commercial applications, particularly in Japan.

5.1.4 Photoinduced hydrophilicity of the TiO_2 thin films obtained by Flame Spraying of Colloidal Suspension

Contact angle measurements were performed on TiO_2 sparyed glass samples and on an unreacted glass reference by using an Advanced Automated Goniometer (Model 300, Rame'-Hart, USA) before and after irradiation of the slide with UV light (λ=365 nm) for 6 hours. The experiment was conducted using water drops of 10μl.

The hydrophilic photo-induced behaviour was observed, as the contact angle decreases from about 40º to 30º after UV irradiation only in the case of

TiO$_2$ treated glasses (see figure 5.9). Negligible changes were measured in the case of not treated glasses before and after UV irradiation.

Fig. 5.9 Image of water contact angles on TiO$_2$ nanoparticles coated glass before and after UV light irradiation.

Fig. 5.10 Image of water contact angles on TiO$_2$ nanoparticles coated PET before and after UV light irradiation.

A similar behaviour was detected also with Tio2 deposits onto PET substrate, with water contact angles reduction from about 75º to 67º before and after UV irradiation while negligible changes in the case of not treated PET.

5.2 Catalytic Properties of the Ag sprayed samples

Catalytic activity of the Ag thin films was tested to evaluate their properties. The same conditions used in the photocatalytic activity test for the TiO$_2$ thin films were applied. Methylene blue (Sigma-Aldrich) was dissolved in water (Millipore Milli-Q purification system, R>18 MΩ.cm) in order to have a about 4.5 × 10^{-6} M methylene blue solution. 1.5 ml of this solution were transferred into a quartz cell (length, 1 cm) together with the Ag coated sample and

continuously exposed to an arc lamp system equipped with a 30 W Xe lamp. The time evolution of methylene blue concentration was monitored by a Lambda 5 Perkin-Elmer UV Spectrometer.

The results of Ag sample are exposed in the graph of figure 5.10 with the ones of uncoated glass and of TiO2 samples discussed above.
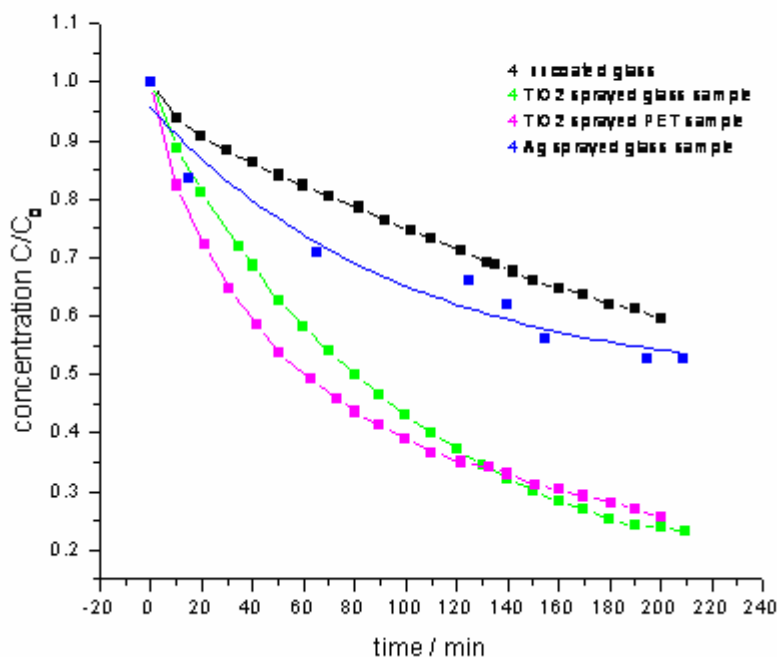
Fig. 5.10   The time evolution of methylene blue concentration, in presence of uncoated glass, TiO2 coated glass, TiO2 coated PET and Ag coated glass

Obviously the rate of reaction of methylene blue wet oxidation in presence of Ag is slower than the ones in presence of TiO_2 because photocatalysis strongly enhanced the degradation phenomenon. However it is observable an increased efficiency of the process, that underline how also the Ag sprayed thin films keep unchanged catalytic properties after Flame spraying deposition.

REFERENCES

[1] Fujishima A, Honda K. Nature 1972;238:37.

[2] Fujishima A, Rao TN, Tryk DA. J Photochem Photobiol C: Photochem Rev 2000;1:1.

[3] Paz Y, Luo Z, Rabenberg L, Heller A. J Mater Chem 1995;10:2848.

[4] Mills A, Hill G, Bhopal S, Parkin IV, O'Neill SA. J Photochem Photobiol A: Chem2003;160:185

[5] Dorfman LM, Adams GE. NSRDS-NB 1973;46:1.

[6] Alberci RM, Jardim WF. Appl Catal B: Environ 1997;14:55.

[7] Bard J. Science 1980;201:139.

[8] Linsbigler AL, Lu GQ, Yates Jr. JT. Chem Rev 1995;95:735.

[9] Tanaka K, Capule MFV, Hisanaga T. Chem Phys Lett 1991;187:73.

[10] Maruska HP, Ghosh AK. Solar Energy 1978;20:443.

[11] Gerischer H, Heller A. J Electrochem Soc 1992;139:113

[12] Bickley RI, Gonzales-Carreno T, Lees JL, Palmisano L, Tilley RJD. J Solid State Chem 1991;92:178.

[13] Deng X, Yue Y, Gao Z. Appl Catal B: Environ 2002;39:135

[14] Watson SS, Beydoun D, Scott JA, Amal R. Chem Eng J 2003;95:213

[15] Mills A, Lee SK, Lepre A. J Photochem Photobiol A: Chem 2003;155:199

[16] Basca RR, Kiwi J. Appl Catal B: Environ 1998;16:19.

[17] Muggli DS, Ding L. Appl Catal B: Environ 2001;32:181.

[18] Ohno T, Sarukawa K, Tokieda K, Matsumura M. J Catal 2001;203:82

[19] Konstantinou I, Albanis T, *TiO2-assisted photocatalytic degradation of azo dyes in aqueous solution: kinetic and mechanistic investigations*. Applied Catalysis B: Environmental 49 (2004)

[20] Lakshmi S. Renganathan R. Fujita S, *Study on TiO2-mediated photocatalytic degradation of methylene blue*. J. Photochem. Photobiol. A. Chem. 88 (1995) 163-167

[21] Zhang T et al., *Photooxidative N-demethylation of methylene blue in aqueous TiO2 dispersions under UV irradiation*. Journal of Photochemistry and Photobiology A: Chemistry 140 (2001) 163–172

[22] Wang R, Hashimoto K, Fujishima A, Chikuni M, Kojima E, Kitamura A, et al. Nature 1997;388:431.

[23] Wang R, Hashimoto K, Fujishima A, Chikuni M, Kojima E, Kitamura A, et al. Adv Mater 1998;10:5918.

[24] Sakai N, Wang R, Fujishima A, Watanabe T, Hashimoto H. Langmuir 1998;14:5918.

[25] Wang R, Sakai N, Fujishima A, Watanabe T, Hashimoto H. J Phys Chem B 1999;103:2188.

[26] Yu JG, Zhao XJ, Zhao QN, Wang G. Mater Chem Phys 2001;68:253

[27] Yu JG, Zhao XJ. J Mater Sci Lett 2001;20:671.

[28] Nakajima A, Koizumi SI, Watanabe T, Hashimoto K. J Photochem Photobiol A: Chem 2001;146:129.

[29] Yu JC, Yu J, Tang HY, Zhang L. J Mater Chem 2002;12:81.

[30] Yu JC, Yu J, Ho W, Zhao J. J Photochem Photobiol A: Chem 2002;148:331.

[31] Lee YC, Hong YP, Lee HY, Kim H, Jung YJ, Ko KH, et al. J Colloid Interface Sci 2000;232:410.

[32] Asachi R, Morikawa T, Ohwaki T, Aoki K, Taga Y. Science 2001;293:269.

[33] Hattori A, Kawahara T, Uemoto T, Suzuki F, Tada H, Ito S. J Colloid Interface Sci 2003;267:127.

[34] Dohshi S, Takeichi M, Anpo M. Catal Today 2003;85:199.

[35] M. Andersson, L. Österlund, S. Ljungström, A. Palmqvist J. Phys. Chem. B 2002, 106, 10674

Conclusions

The aim of this work was to develop the equipment and to extend the applications field of this deposition technique.

Different substrate-coating combinations and the discovery of unexpected possibilities were realized. Since these choices were connected to their possible future industrial applications, the combinations that better emphasizes the peculiarity of the obtainable sprayed material were more deeply analyzed.

Starting from the two core characteristics of the equipment (the possibility of very small film thickness and the high purity of the deposited materials) the work were directed to depositing nanoparticles with particular properties that needs to be very small quantities or in combination with substrates to obtain special product.

The production of antifogging and self-cleaning glasses were investigated with deposition of TiO_2 onto glass substrates. The photocatalytic activity of these materials resulted in agreement with others obtained by more expensive deposition methods. It means that the flame spraying deposition doesn't changes dramatically the structure of the TiO_2.

Nanoparticles were sprayed also onto plastic substrates because this opens new interesting fields of application.

Other choices of substrate and coating materials combinations were directed to Ag onto textile or plastic support because of its antibacterial activity.

The present work gives some ideas to possible industrial applications for future productions. Some of this applications are actually obtained with expensive methods that slow up the opening of nanotechnologies to the market, while flame spraying of nanoparticle suspension is a low cost process and quite easy to manage.

APPENDIX A

Wettability of Surfaces

1 Surface tension and contact angle

Surface tension and contact angle are two different things, although they are closely related. Surface tension is a property of the interface between two phases, whereas the contact angle describes the edge of the twotesi-phase boundary where it ends at a third phase. Two phases must be specified to describe surface tension; three phases are needed to describe contact angle.

2 Contact angle

The contact angle θ is defined as the angle that is formed at the junction of three phases, for example, at the solid-liquid-gas junction as shown in Fig.1.

A contact angle on a solid can be defined, and is physically meaningful, only when a solid is such that a unique tangent plane to the solid surface can be constructed. A fluid-fluid interface approaches the solid surface in such a way that the observable tangent to the fluid-fluid interface meets the solid (tangent) plane in a line, which is referred to as the "**three-phase line**" or "wetting line"[1].
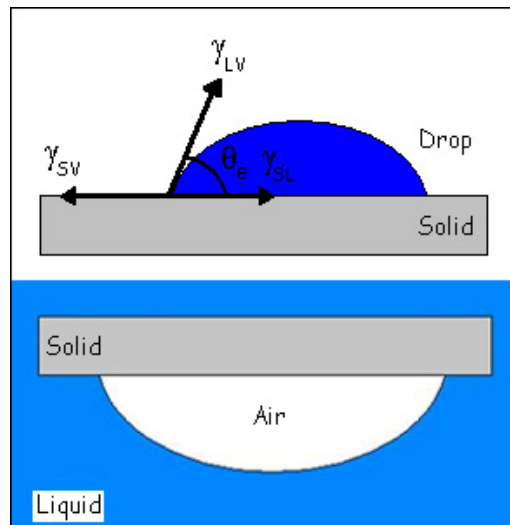
Fig.1

Contact angle analysis characterizes the wettability of a surface by measuring the surface tension of a solvent droplet at its interface with a homogenous surface. In more technical terms, contact angle measures the attraction of molecules within the droplet to each other versus the attraction or repulsion those droplet molecules experience towards the surface molecules.

When a drop of liquid is placed on a solid surface[2], the liquid will either spread across the surface to form a thin, approximately uniform film (Fig.2*a*) or spread to a limited extent but remain as a discrete drop on the surface. The final condition of the applied liquid on the surface is taken as an indication of the wettability of the surface by the liquid or the wetting ability of the liquid on the surface, depending on your point of view. The quantitative measure of the wetting process is taken to be the contact angle.

In the case of a liquid that forms a uniform film ($\theta = 0$), the solid is said to be completely wetted by the liquid, or that the liquid wets the solid.

If a finite contact angle is formed ($\theta > 0$), some investigators describe the system as being partially wetted. Others prefer to make a distinction based on the size of the contact angle. Alternatively, any system with $0° < \vartheta < 180°$ would be partially wetting, and only for $\vartheta = 180°$ would the nonwetting.
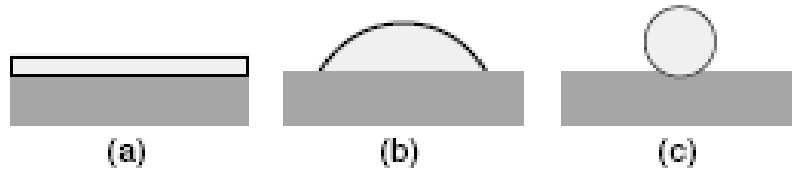
Fig. 2 A liquid placed on a solid surface can take one of three shapes.
It may spread into a uniform duplex film (*a,* θ = 0), it may form a convex lens with a section less than the radius of curvature (*b,* 0<θ<90º), or it may form a section greater than the radius of curvature (*c,* θ>90º).

2.1 Techniques for contact angle measurement

Contact angle is one of the most sensitive and inexpensive surface analysis technique[1,2,3]. There are five common techniques that can be employed to measure the contact angle, (in Fig.3). The experimental choice will depend principally on the geometry and location of the surface or coating to be studied. In all the methods, the contact angle (θ) is the angle of the liquid at the interface relative to the plane of the model surface.
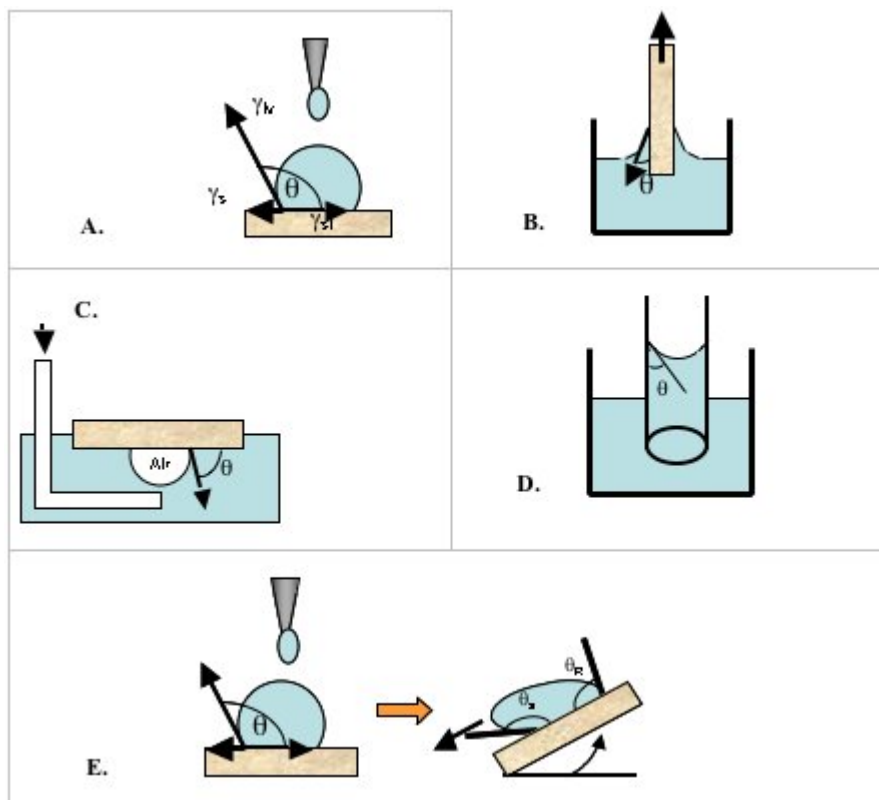
Fig.3 Five ways that the contact angle (θ) can be measured.
(A) Sessile or Static drop. (B) Wilhelmy plate method. (C) Captive air bubble method. (D) Capillary rise method. (E) Tilting substrate method.
Figure adapted from Biomaterials science: An introduction to materials in medicine. Ratner BD, Hoffman AS, Schoen FJ, Lemons JE, editors. San Diego, CA: Academic Press, 1996.

Static or Sessile Drop Method

The most commonly used technique is the static or sessile drop method (Fig. 3A) with the direct measurement of the angle from the drop profile (Fig.4).

Fig.4 Images of water contact angles obtained by static drop method

The experiment normally calls for the successive addition of fluid droplets until a plateau in the contact angle is reached. This plateau is known as the "advancing contact angle". Immediately following the advancing contact angle experiment, it is useful to measure a "receding contact angle" value by monitoring the contact angle as equivalent volume droplets of fluid are successively retracted from the droplet (see text below). It is important to understand that the advancing and retreating angles are usually not equal. There is normally a high level of experimental hysteresis resulting from sample pre-hydration, surface roughness, chemical heterogeneity, evaporation and/or molecular movement. Thus, the receding contact angle allows one to measure the degree of hysteresis inherent in the sample surface.

Wilhemly Plate Method

The Wilhemly plate method (Fig. 3B) is ideal for double-sided samples that need to be tested in temperature-controlled conditions. Certain surfaces may be temperature-sensitive; they are hydrophobic at one temperature and hydrophilic at another. The temperature of a beaker of water is easier to monitor and maintain at a constant temperature than the temperature of fluid droplet. So, the contact angle method has been inaccurate for those samples that need a higher level of control.

Captive Air Bubble Method

An alternative to the Wilhemly plate method is the captive air bubble method (Fig. 3C). In this method, the contact angle is measured between an air bubble of defined volume and the solid surface immersed in a temperature controlled bath.

Capillary Rise Method

The capillary rise method (Fig. 3D) presents the only method of contact angle measurement available for the measurement of tubular materials and coatings. Temperature may be maintained in this method over a short period of time.

Tilted-drop Measurement

The tilted-drop measurement (Fig. 3E) is another angle measurement. In this technique, a droplet is added to the surface and the advancing and retreating contact angle are measured as the surface is tilted up until the droplet reaches a point where it almost moves. This technique is useful to measure both the receding and advancing contact angles at the same time. In general, contact angle measurements serve as a good initial technique to characterize a surface. However, contact angle measurements need to be analyzed with care as a number of factors including operator error, surface roughness, surface heterogeneity, contaminated fluids, and sample geometry can influence the overall result.

2.2 Advancing and receding contact angles and hysteresis

For systems that have nonzero contact angles, even if the most careful experimental techniques are employed on carefully prepared surfaces, contact angle data are frequently confusing. The problem is that the contact angle is different at different points of contact with the support. When discussing contact angle data, one must always be aware of how the angle has been measured in order to interpret its significance properly.

It is conventional to call the larger value the advancing angle ϑ_a and the smaller one the receding angle ϑ_r (Fig.3E, 5). The two may be quite different.

The determination of thermodynamic contact angle requires very clean experimental conditions. In many practical situation, one finds that the liquid edge line is pinned and immobile, not only for $\vartheta = \vartheta_{equilibrium}$ but whenever ϑ lies within a finite interval around $\vartheta_{equilibrium}$,

$$\vartheta_r < \vartheta < \vartheta_a$$

The angle θ_a (advancing angle) is measured when the solid/liquid contact area increase, while θ_r (receding angle) is measured when the contact area shrinks.

Hysteresis is ordinarily defined as the difference between the angle observed after an advance, ϑ_a and that observed after retreat ϑ_r.

$$H \equiv \vartheta_a - \vartheta_r$$

The interval $\vartheta_a - \vartheta_r$ may be 10 or more for surfaces that have not been specially prepared[4].

In dynamic contact angle studies, additional complications arise because the movement of the wetting line is not always a steady, continuous process. It is often observed that the movement is "jerky," with the drop or liquid front holding a position for a time and then jumping to a new configuration.

This phenomenon is often referred to as a "stick–slip process" and is still not fully understood. It has also been observed that in dynamic systems, the values of θ_a and θ_r will vary as a function of the velocity of wetting line movement, with θ_a increasing with velocity and θ_r decreasing[2].

Contact angle hysterisis = θ_A – θ_B
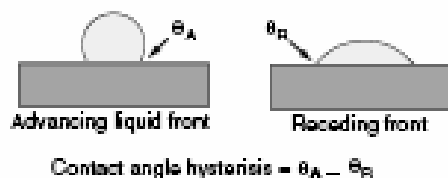
Fig 5. In dynamic liquid systems, a liquid front advancing across a new surface may exhibit a large contact angle (the advancing contact angle, θ_a), while the same liquid receding from an already wetted surface will have a much smaller contact angle (the receding contact angle, θ_r). The difference between θ_a and θ_r is referred as the contact angle hysteresis.

When used with Young's equation (see text below) and other such relationships, the contact angle provides a relatively simple yet sensitive insight into the general chemical nature of a surface through such

thermodynamic quantities as the work of adhesion. Unfortunately, as already mentioned, contact angles often exhibit hysteresis and cannot be defined unambiguously by experiment. It is always important to know as much as possible about the cleanliness, topography, homogeneity, and other characteristics of a solid surface, as well as the purity and composition of the liquid employed, when attempting to interpret contact angle data.

Three major causes of hysteresis have been identified[4].

-   *Surface roughness*[5]

-   *Chemical contamination*[5]

-   *Solutes in the liquid (surfactant, polymers, etc…) may deposit a film on the solid surface, and the presence or absence of the film, once formed is stuck on the solid surface (Chappuis,1984)*

The presence of contamination is definitely a contributing factor, but it is by no means the only one. Therefore, even with carefully purified material, both advancing and receding contact angles should be measured.

3   Surface free energy of solids

Surface tension is a force that operates on a surface and acts perpendicular and inward from the boundaries of the surface, tending to decrease the area of the interface. A simple apparatus based on this notion may be used to measure surface tension (Fig.6). The figure represents a loop of wire with one movable side on which a film could be formed by dipping the frame into a liquid.
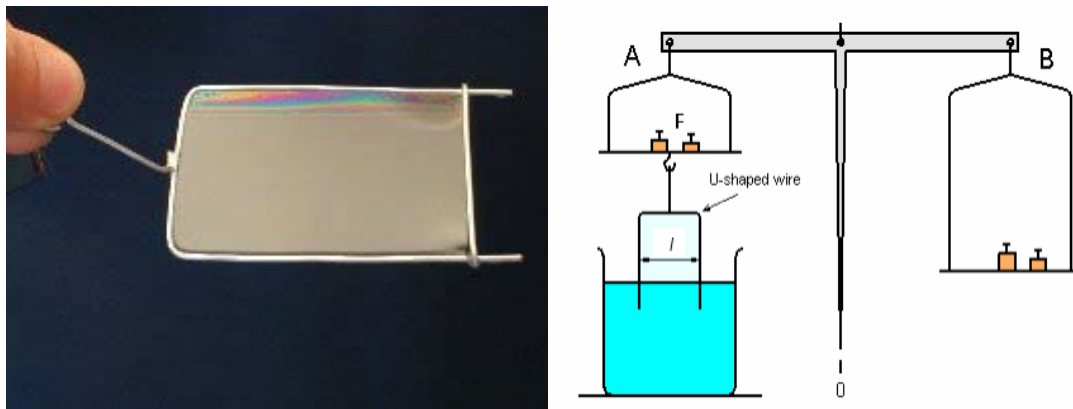

Fig 6 – experimental device to measure the surface tension of a liquid

The surface tension of a stretched film in the loop will cause the slide wire to move in the direction of decreasing film area unless an opposing force F is applied. In actual apparatus, the friction of the slide wire may be sufficient for this. In an idealized, frictionless apparatus the force opposing γ could be measured. Since the film has two sides, the surface tension as measured by this apparatus equals:

$$\gamma = F/2\ell$$

The above equation defines the units of surface tension to be those of force per length (Nm^{-1} in SI).

Surface tension may be defined also in a different way: it equals the work per unit area required to produce a new surface. The equation that relates γ to the work required to increase the area of the surface is

$$work = Fdx = \gamma 2ldx = \gamma dA$$

Therefore, there are two equivalent interpretations of γ: force per unit length of boundary of the surface and energy per unit area of surface. In terms of this last definition, the units of γ are energy per area (Jm^{-2} in SI)[3]

The surface tension (or surface free energy) γ_s, as obtained from contact angle measurements, is one-half the free energy of cohesion ΔG^C, of the solid with respect to the plane that constitutes the surface[1]

$$\gamma_S = G^\sigma = \frac{\Delta G^C}{2}$$

$$= \left(\frac{\partial G^C}{\partial A} \right)_{T,P,n_i} \tag{1}$$

where G is the Gibbs free energy and A is area. (See Good et al.[8-10] for a more extensive thermodynamic discussion).

As a quantitative measure of surface properties, γ_S is related to an important qualitative criterion for classifying solids. Thus, solids may be characterized as "high-energy" or "low-energy" on the basis of whether or not

liquids with relatively high surface tension, such as water, spread with zero contact angle on the solids.

Hard solids, characterized by covalent, ionic, or metallic bonding, have "high-energy surfaces" ($\gamma_{S0} \sim 500$ to 5000 ergs/cm^2) while molecular solids (and also molecular liquids) bound by van der Waals forces, or in some special cases, by hydrogen bonds have "low-energy surface" ($\gamma_{S0} \sim 50$ ergs/cm^2)[3].

Low-energy surfaces can give rise to partial ($\theta \neq 0$) or to complete wetting ($\theta = 0$), depending on the liquid chosen. A useful way to present these results with a series of homologous liquids is to plot $\cos\theta$ vs. surface tension γ of the liquids (Zisman plots). Although, in many cases we never reach $\cos\theta = 1$ (i.e. the complete wetting), we can extrapolate the plot down to a value $\gamma = \gamma_C$ which would correspond to $\cos\theta = 1$.

In general we would expect γ_C to depend on the solid S, but to depend also on the liquid series L. However when dealing with simple molecular liquids (where van der Waals forces are dominant), Ziesman observed that γ_C is essentially independent of the nature of the liquid, and is a characteristic of the solid alone.

If we want to find a molecular liquid that wets completely a given low-energy surface, we must choose a liquid of surface tension $\gamma < \gamma_C$. Thus γ_C may be called "critical surface tension" and is clearly the essential parameter for many practical applications[4].

Various authors tried to relate γ_C to some simple physical parameters of the solids (see text below, Girifalco and Good, 1957; Fowkes, 1962; Good, 1964).

For curved surface with radii R_1 and R_2, the surface tension is expressed by the relationship

$$\Delta p = \gamma \left(\frac{1}{R_1} + \frac{1}{R_2} \right) \tag{2}$$

due to the pressure difference across a curved interface. This expression is known as ***Laplace equation*** and was derived in 1805[†].

[†] for further discussion see **Hiemenz Paul C., Rajagopalan Raj** "Principles of colloid and surface chemistry" New York: Marcel Dekker Inc, 1997 pg 257-259

For spherical surface, $RB_1 = R_2 = R_s$, therefore $\Delta p = 2\gamma/R_s$ (3)

For cylindrical surface, $R_1 \rightarrow \infty$, therefore $\Delta p = \gamma/R_2$ (4)

For planar surface, $R_1 = R_2 \rightarrow \infty$, therefore $\Delta p = 0$ (5)

An important consequence of the pressure associated with the curvature is the effect it has on thermodynamic activity of substances: phase equilibria (including dissolution of chemical species in the different phases) are affected by the presence of interfaces.

The influence of curvature on phase equilibria is most readily understood for liquids, for which the activity is measured by the vapor pressure of the liquid. We consider the process of transferring molecules of a liquid from a bulk phase with a vast horizontal surface to a small spherical drop of radius R_s. According to equation (5) no pressure difference exists across a plane surface; the pressure is simply p_0, the vapor pressure. However, a pressure difference given by equation (3) exists across a spherical surface. Therefore, for liquid vapor equilibrium at a spherical surface, both the liquid and the vapor must be brought to the same pressure $p_0 + \Delta p$. Assuming the liquid to be incompressible and the vapor to be ideal, ΔG for the process of increasing the pressure from p_0 to $p_0 + \Delta p$ may be written for the liquid and the vapor phase. When the liquid and the vapor are at equilibrium, these two values of ΔG are equal:

$$RT\ln\left(\frac{p}{p_0}\right) = 2\frac{V_L\gamma}{Rs} = 2\frac{M\gamma}{\rho \cdot Rs} \tag{6}$$

with the volume per mole $V_L = M/\rho$ with M molecular weight and ρ density of the liquid. This expression, known as **Kelvin equation**† enables us to evaluate the actual pressure above a spherical surface and not just the pressure difference across the interface (Laplace equation).

The Kelvin equation may also be applied to the equilibrium solubility of a solid in a liquid. In this case the ratio $p/p0$ in equation (6) is replaced by the ratio *a/a0* (a is the activity of dissolved solute in equilibrium with a flat surface,

and a is the analogous quantity for a spherical surface. For a ionic compound having the general formula M_mX_n, the activity of a diluted solution is related to the molar solubility S as follows:

$$a = (mS)^m (nS)^n$$

Therefore for a solid sphere

$$2\frac{M\gamma}{\rho Rs} = RT\ln\left(\frac{a}{a_0}\right) = (m+n)RT\ln\left(\frac{S}{S_0}\right) \tag{7}$$

where S and S_0 are the solubilities of the spherical and flat particles, respectively.

Equation (7) provides a thermodynamically valid way to determine γ for an interface involving a solid. The thermodynamic approach makes it clear that curvature has an effect on activity for any curved surface. The surface free energy interpretation of γ is more plausible for solids than the surface tension interpretation, which is so useful for liquid surfaces. Either interpretation is valid in both cases, and there are situations in which both are useful.

Although the increase in solubility of small particles is unquestionably a real effect, using it quantitatively as means of evaluating γ_{SL} is quite difficult:

the difference in solubility between a small particle and a larger one will probably be less than 10%. Since a phase boundary exist at all, the solubility is probably low to begin, so there may be some difficulty in determining the experimental solubilities accurately

solid particles are not likely to be uniform spheres, even if the sample is carefully fractionated; rather, they will be irregularly shaped and polydisperse, although the particle size distribution may be narrow. The smallest particles will have the largest effect on solubility, but they may be the hardest to measure.

The radius curvature of sharp points or protuberances on the particles has a larger effect on the solubility of irregular particles than the equivalent radius of the particles themselves.

4 Relationship between surface tension and contact angle

Suppose a drop of liquid is placed on a perfectly smooth surface, and these phases are allowed to come to equilibrium with the surrounding vapor phase. Viewing the surface tension as force acting along the perimeter of the drop enables us to write immediately an equation that describes the equilibrium force balance in the horizontal direction[9,11,12]:

$$\gamma_{LV}\cos\theta = \gamma_{SV} - \gamma_{SL} \tag{8}$$

where γ_{SV} is the solid-vapor interfacial free energy, γ_{SL} the solid-liquid interfacial free energy, γ_{LV} the liquid-vapor interfacial tension, and ϑ_e the equilibrium contact angle.
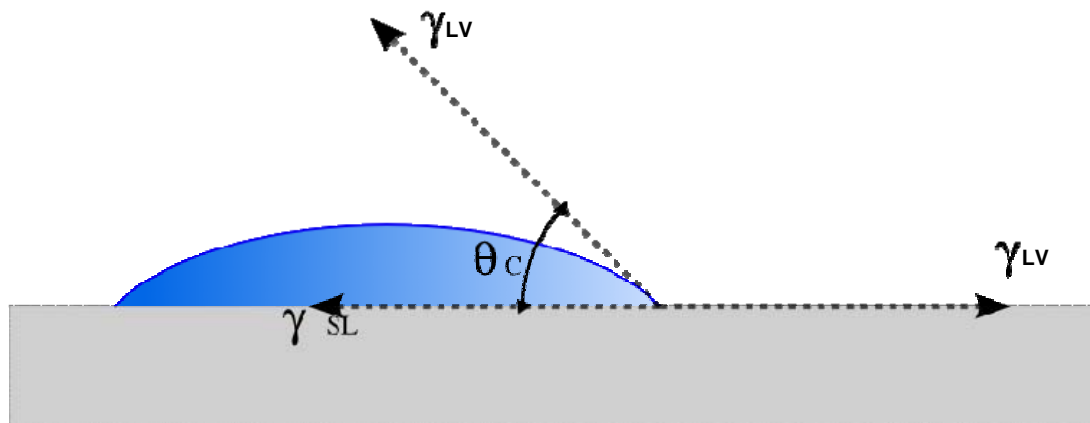
Fig.7

This Equation was qualitatively proposed by Thomas Young in 1805 and is generally known as ***Young's equation***. Young's equation is a plausible, widely used result, but its apparent simplicity is highly deceptive. The two terms that involve the interface between the solid and other phases cannot be measured independently, so experimental verification is difficult, although a variety of experiments have been directed along these lines.

There are also a number of objection to Young's Equation, classifiable into two main categories:

- the noncompliance of the experimental system to the assumptions in the derivation

- the assumption of thermodynamic equilibrium in the solid

4.1 Thermodynamic theory of equilibrium contact angles on ideal solids[1]

On a smooth, homogeneous rigid, isotropic solid surface, the equilibrium contact angle of a pure liquid is a unique quantity[8]. Young's equation obeyed.

$$\gamma_{SV} - \gamma_{SL} = \gamma_{LV} \cos \vartheta_e$$

where γ_{SV} is the solid-vapor interfacial free energy, γ_{SL} the solid-liquid interfacial free energy, γ_{LV} the liquid-vapor interfacial tension, and ϑ_e the equilibrium contact angle.

The term $\gamma_{LV} \cos \vartheta_e$ has, in the past be referred to as the "wetting tension" or "adhesion tension". In terms of γ_S, Young's equation is written

$$\gamma_S = \gamma_{LV} \cos \vartheta_e + \gamma_{SL} + \pi_e \qquad (9)$$

$$\pi_e \equiv \gamma_S - \gamma_{SV} \qquad (10)$$

with π_e film pressure. On non-homogeneous surfaces and on rough solids, it is expected that π_e will often be appreciable, even when the average surface energy is low.

After Young's equation, the most fundamental equation for the treatment of contact angle data is [6,7] (**Girifalco – Good equation**):

$$\gamma_{SL} = \gamma_S + \gamma_L - 2\Phi\left(\gamma_S \gamma_L\right)^{1/2} \qquad (11)$$

where Φ is an interaction parameter that will be discussed below.

Combining this with Young's equation to eliminate γ_{SL}, the following equations are obtained:

$$\cos \vartheta_e = -1 + 2\Phi_{SL}\left(\frac{\gamma_S}{\gamma_{LV}}\right)^{1/2} - \frac{\pi_e}{\gamma_{LV}} \qquad (12)$$

$$\approx -1 + 2\Phi_{SL}\left(\frac{\gamma_S}{\gamma_{LV}}\right)^{1/2}$$

$$\gamma_S = \frac{\left[\gamma_{LV}(1 + \cos \vartheta_e) + \pi_e\right]^2}{4\Phi^2 \gamma_{LV}} \qquad (13)$$

$$\approx \frac{\gamma_{LV}(1 + \cos \vartheta_e)^2}{4\Phi^2}$$

$$\gamma_{SL} \approx \gamma_{LV}\left[\frac{(1 + \cos \vartheta_e)^2}{4\Phi_{SL}^2} - \cos \vartheta_e\right] \qquad (14)$$

π_e may be neglected since $\pi_e \ll \gamma_{LV}$. Φ_{SL} is a function of the molecular properties of the liquid and the solid, and it can easily be computed from readily accessible data. For non polar liquids on non-polar solids $\Phi \approx 1$.

More generally, Φ_{SL} lies between about 0.5 and 1.0 for common systems in which contact angles are observed. Equation (15) is the expression for Φ_{SL}[7]

$$\Phi_{SL} = \frac{\frac{3}{4}\alpha_S\alpha_L\left[2I_S I_L/(I_S + I_L)\right] + \left[\left(\alpha_S\mu_L^2 + \alpha_L\mu_S^2\right)/2\right] + \mu_S^2\mu_L^2/3kT}{\left[\left(3\alpha_S^2 I_S/4 + \alpha_S\mu_S^2 + \mu_S^4/3kT\right)\left(3\alpha_L^2 I_L/4 + \alpha_L\mu_L^2 + \mu_L^4/3kT\right)\right]^{1/2}} \qquad (15)$$

where α is the molecular polarizability, μ the dipole moment, and I the ionization energy of the molecules.

If either component is polymeric, these molecular properties are the properties of groups, e.g., the (CH_2CHCl) group in the polyvinyl chloride.

If the component is a copolymer, an appropriate weighting must be given for the relative concentrations of the different kinds of groups.

If preferred orientations of unsymmetrical groups are present, that must be taken into account in an "a priori" computation of Φ.

Φ, as calculated by equation (15), is related to the fractional polarities [13] of the two components. For component *i*,

$$D_i^p \equiv \frac{C_i^p}{C_i^L + C_i^i + C_i^p} = \frac{C_i^p}{C_i} \tag{16}$$

$$D_i^L \equiv \frac{C_i^L}{C_i^L + C_i^i + C_i^p} = \frac{C_i^L}{C_i} \tag{17}$$

$$D_i^i \equiv \frac{C_i^i}{C_i^L + C_i^i + C_i^p} = \frac{C_i^i}{C_i} \tag{18}$$

$$C_i^p \equiv \frac{\mu_i^4}{3kT} \tag{19a}$$

$$C_i^L \equiv \frac{3}{4}\alpha_i^2 I_i \tag{20a}$$

$$C_i^i \equiv \alpha_i \mu_i^2 \tag{21a}$$

$$C_i \equiv C_i^p + C_i^L + C_i^i \tag{22a}$$

where D_i^p, D_i^L and D_i^i are, respectively, the fractional polar contribution, the fractional London (dispersion) force contribution, and the fractional induction force contribution, to intermolecular forces. If these three kinds of force account for all the intermolecular forces in the system, then $D_i^p + D_i^L + D_i^i = 1$.

The force components for unlike substances can likewise be written in the form:

$$C_{SL}^p \equiv \frac{\mu_S^2 \mu_L^2}{3kT} \tag{19b}$$

$$C_{SL}^L \equiv \frac{3}{4}\alpha_S \alpha_L \frac{2I_S I_L}{I_S + I_L} \tag{20b}$$

$$C_{SL}^i = \frac{\alpha_S \mu_L^2 + \alpha_L \mu_S^2}{2} \tag{21b}$$

$$C_{SL} = C_{SL}^L + C_{SL}^i + C_{SL}^p \tag{22b}$$

combining equations (15)-(22), we obtain

$$\Phi_{SL} = \frac{C_{SL}}{\left(C_S C_L\right)^{1/2}} \tag{23}$$

For the polar component, equation (19a) and (19b) are valid provided the dipoles are not too large (about 2-2.5 Debyes is the limit of validity[7])

Therefore, we can write

$$D_{SL}^{p} = \left(D_{S}^{p} D_{L}^{p} \right)^{1/2} \tag{24}$$

This will break down if one of the dipoles is large enough that its rotation is restricted, in the pure compound, and the other is not, or if motion is restricted for any reason. We can also write, provided IS and IL are not very different (and this is frequently true),

$$D_{SL}^{L} \approx \left(D_{S}^{L} D_{L}^{L} \right)^{1/2} \tag{25}$$

Also if $\alpha_{S}\mu_{S}^{2}$ and $\alpha_{L}\mu_{L}^{2}$ are not too different,

$$D_{SL}^{i} \approx \left(D_{S}^{i} D_{L}^{i} \right)^{1/2} \tag{26}$$

The approximation, equation (26), gives little trouble, because the induction term is relatively small compared to the other two terms in equation (22a) and (22b). Finally, we obtain the expression for Φ in terms of the fractional polarities of the two components:

$$\Phi_{SL} \approx \left(D_{S}^{L} D_{L}^{L} \right)^{1/2} + \left(D_{S}^{i} D_{L}^{i} \right)^{1/2} + \left(D_{S}^{p} D_{L}^{p} \right)^{1/2} \tag{27}$$

This expression shows that Φ is close to unity when there is a close match between the force components (expressed on a fractional basis) of the two substances, and is less than unity when there is a mismatch [13].

4.2 Contact angles on non-ideal surfaces

Real solid surfaces may be quite different from the idealized one in the above derivation.

The non-ideality of common surfaces may arise from at least three distinct causes[1]. The first is that matter has different chemical composition. For

example, micrographs of steel reveal striations due to lamellae of Fe_3C in a matrix of α-Fe. A second component of a solid surface may be an essential component of the material (as in the case of steel) or it may be an impurity. A surface impurity may be present as a distinct phase or as an adsorbed film that may not be identifiable as a phase; it may be present as discrete molecules or atoms, uniformly or randomly distributed, or in clusters. With respect to contact angle and surface energy, the types of heterogeneity that are of interest are those in which patches or bands exist, with local variation of γ_s over the surface.

The second cause of heterogeneous surfaces is the presence of different crystallographic faces on a chemically homogeneous solid. The difference in density of atom packing in different planes lead to different energies of cohesion. In addition, there may be different kinds of molecular groups exposed in different planes. Adam and Jessop [13] observed that the contact angle of water on crystalline stearic acid that had been cut through with a knife was variable, and lower than on a stearic acid surface formed by solidifying in contact with air. They attributed this result to the exposure of the edges of sheets of carboxyl groups in the cut crystal, that were buried, in the case of a crystal solidified in air.

A third cause of heterogeneity is the existence of grain boundaries, crystal edges and corners,or steps. Dislocations give rise to high-energy sites where they intersect a surface. A solid surface may be in a dynamic equilibrium condition, particularly if the temperature is high. A surface that is in dynamic equilibrium and has a steady-state distribution of adatoms, steps, ledges, etc., would be considered uniform; but a heterogeneous surface is, in general, not in a condition of thermodynamic equilibrium. It is, of course, not always safe to assume that the structure of a solid surface remains the same when the solid is in vacuum as when it is in contact with a liquid, even if no chemical reaction or chemisorption occurs.

The energy density of line defects, such as the intersection of a grain boundary with an external surface, has the dimensionality of energy per unit length, as opposed to γ_s having dimensions of energy per unit area. For point defects, The energy density has the dimension of energy per point. The contribution of line and point defect energies to γ_s can be treated in terms of the defect energies only if the number of such defects per unit area is known.

As a measure of γ_s, the contact angle of a liquid does not directly distinguish the structural features (such as defects) that cause the average γ_s to have any particular value, when there is a distribution of γ_s values over the surface.

4.2.1   Rough surface: Wenzel equations

Roughness, as a departure from ideality in a surface, cannot be sharply separated from heterogeneity. Configurations such as ledges, crystal edges, corners, etc. can be considered both as line or point defects (high-energy sites) and as parts of ridges, hills, etc., as topographic features. For our present purposes, we can imagine a rough surface that is energetically homogeneous. Indeed, it is not difficult to prepare real surfaces where the microscale roughness has a far greater effect on contact angle than does heterogeneity. The simplest parameter for describing roughness is the roughness ratio

$$r \equiv \frac{A}{a} \tag{28}$$

where A is the true area and a is the projected area on a plane parallel to the apparent surface.

The basic effect of surface structure is so easy to describe by the **Wenzel equation** [15,16] which states that the apparent contact angle ϑ^* of the drop on the rough surface is related to Young's intrinsic angle ϑ on the smooth surface by

$$\cos\vartheta^* = r \cdot \cos\vartheta \tag{29}$$

This equation indicates that the surface roughness enhances the hydrophilicity of hydrophilic surfaces (and also the hydrophobicity of hydrophobic ones) because r is always larger than 1.

4.2.2   Heterogeneous surface: Cassie-Baxter equation

Cassie[16,17] proposed an equation describing the contact angle ϑ' at a heterogeneous surface composed of two different materials. When a unit area of the surface has a surface fraction f_1 with a contact angle ϑ_1 and an area

fraction f_2 with a contact angle ϑ_2, the contact angle on the surface can be expressed by the equation:

$$\cos \vartheta' = f_1 \cos \vartheta_1 + f_2 \cos \vartheta_2 \tag{30}$$

When f_2 represents the area fraction of trapped air, equation (30) can be modified as follows

$$\cos \vartheta' = f \cos \vartheta + (1 - f) \cos 180^\circ = f \cos \vartheta + f - 1 \tag{31}$$

Where f is the remaining area fraction, i.e., liquid-solid interface.

REFERENCES

[1] **R.J.Good, R.R.Stromberg** *Surface and Colloid Science,* Plenum press, New York and London
[2] **D.Myers** *Surfaces, Interfaces, and Colloids: Principles and Applications,* John Wiley & Sons Inc Second Edition (1999) - Chapter 17
[3] **P.C.Hiemenz, R.Rajagopalan,** *Principles of colloid and surface chemistry*, Marcel Dekker Inc. (1997)

[4] **P.G. de Gennes** *Wetting: statics and dynamics* Review of Modern Phisics, Vol.57, No.3 Part 1, July 1985

[5] **R.E. Johnson, R.H. Dettre** *Adv. Chem. Ser.* **43,**112 (1963)

[6] **R.J.Good, L.A.Girifalco**, *J.Phys.Chem* **64**, 561 (1960)

[7] **R.J. Good**, *J.Colloid Interface Sci.* **59**, 368 (1977)

[8] **A.W.Neumann, R.J.Good**, *J.Colloid Interface Sci.* **38**, 341 (1972)

[9] **J.D.Eick, R.J.Good, A.W.Neumann**, *J.Colloid Interface Sci.* **53**, 235 (1975)

[10] **R.J.Good***, J.Phys. Chem.* **74**, 5041 (1953)

[11] **R.E.Johnson** *J.Phys. Chem.* **63**, 1655 (1959)

[12] **A.W.Newmann** *Advan. Colloid Interface Sci.* **4**, 105 (1975)

[13] **J.L Gardon,** *Encyclopedia of Polymer Science and Technology***,** Mark Gaylord and Bikales eds. Interscience New York (1965)

[14] **N.K. Adam, G.Jessop**, *J. Chem. Soc* **1925**, 1863 (1925)

[15] **Wenzel R.N.** *Ind.Eng.Chem* **28**, 988-994 (1936)

[16] **Miwa, Nakajima, Fujishima, Hashimoto, Wanatabe** *Langmuir* **16**, 5754-5760 (2000)

[17] **A.B.D Cassie, S**.**Baxter**, *Trans.Faraday Soc.* **40**, 546-551 (1944)

For further reading

[18] **J.Bico, C.Marzolin, D.Quéré,** *Europhys. Lett.,* **47,** 220 (1999)

[19] **J.Bico, C.Tordeux, D.Quéré,** *Europhys. Lett.,* **55,** 214 (2001)

[20] **C.Yang, U.Tartaglino, B.N.J.Persson**., *Phys. Rev. Lett.*, **97**, 116103 (2006)

[21] **E.Chibowski,** *Advan. Colloid Interface Sci.,* Volume 133, Issue 1, 51 (2007)

[22] **F.M. Fowkes** *J.Phys.Chem.*, **66**, 382 (1962)